Scoping Studies for the Layout of INTOR

K. Borrass
R. Buende

IPP 4/178 May 1979

MAX-PLANCK-INSTITUT FÜR PLASMAPHYSIK

8046 GARCHING BEI MÜNCHEN

MAX-PLANCK-INSTITUT FÜR PLASMAPHYSIK

GARCHING BEI MÜNCHEN

Scoping Studies for the Layout of INTOR

K. Borrass

R. Buende

IPP 4/178 May 1979

Die nachstehende Arbeit wurde im Rahmen des Vertrages zwischen dem Max-Planck-Institut für Plasmaphysik und der Europäischen Atomgemeinschaft über die Zusammenarbeit auf dem Gebiete der Plasmaphysik durchgeführt.

IPP 4/178

Scoping Studies for the Layout of INTOR

K. Borrass
R. Buende

May 1979

Abstract

A reference system layout for an INTOR-like device is performed on the basis of a zero-dimensional, time-dependent tokamak model. Emphasis is placed on the description of the complete, reactor--relevant burn cycle. Novel results on dynamic burn control by cyclic major radius compression and decompression are reported. The temporal behaviour of all key quantities of the reference system is given for various assumptions on impurity behaviour.

Sensitivity studies are performed in two steps. The first is the calculation of all data that characterize the operation of all components of the plant at a reference layout point. The second step is to calculate the influence exerted by the variation of uncertain parameters on the operation of the plant, assuming that the plant has already been built according to the reference layout.

CONTENTS

References are listed at the end of each chapter.

1. Introduction

This paper reports the scoping studies for an INTOR device conducted by the IPP systems study group. It consists of essentially three parts.

The first part (Section 2) specifies a reference system on the basis of the INTOR workshop guiding data.

In the second part (Sections 3 and 4) special topics related to the reference system layout are studied in greater detail.

The third part (Section 5) deals with the sensitivity of the system's performance to variations of the key parameters.

In specifying the details of the reference system, emphasis was placed on the reactor relevance of all concepts under consideration. In the first step of a general layout this means essentially that the proposed concepts must be compatible with a reasonable overall energy balance. This criterion is taken as a basis to propose a burn cycle involving low-density start-up to minimize heating energy requirements, and dynamic control of beta during the burn phase to keep the power density at its highest possible value.

The system is assumed to burn at the lower, unstable burn point. Novel results on dynamic burn control by cyclic major radius compression and decompression are reported. It is shown that this control scheme, unlike, for instance, control by additional heating, practically does not affect the overall energy balance of the system.

Controlled refuelling is considered an inevitable tool in ignited systems. Central refuelling, by, for instance, pellet injection, is probably the only scheme of performing it on a sufficiently fast time scale. Such a refuelling scheme is therefore tacitly assumed. Accordingly, the density profiles are relatively peaked.

The burn scenario proposed here is not claimed to be unique. However, it is in a certain sense complete and self-consistent.

The studies on start-up and burn control are performed by the NUDIPLAS[+)] code, a time-dependent zero-dimensional code for the description of tokamak reactor plasmas. This plasma code is integrated in the SISYFUS[++)] code, a mathematical model for a fusion power plant.

Such a mathematical model is necessary to perform sensitivity analyses in a sufficiently detailed form. These analyses have to be made in order to allow for later determining a layout point which is as insensitive as possible to the uncertainties of assumed parameters. Parameters which are largely uncertain because of the still prevalent lack of knowledge are, for example, the achievable ß value, the amount of impurity influx into the plasma, and, in addition, it is not known today how the α-particles will behave in the plasma, i.e. whether they will accumulate or not. In spite of these uncertainties the layout of fusion reactor power plants must be such that the risk of failure because of deviations from assumptions is minimized.

+) Nulldimensionales Plasmamodell

++) Simulation model for systematic analyses of fusion power plants

2. Reference System Layout

2.1 Global Parameters and Assumptions

The global data of the system are chosen close to the INTOR reference data determined at the first session of the INTOR workshop, namely:

major radius	(R)	480 cm
minor radius	(a)	120 cm
elongation	(s)	1.5
safety factor	(q(a))	3
maximum toroid. beta (vol. average)	($\bar{\beta}_T$)	0.06
toroidal field (on axis)	(B_T)	40 kG

The value for B_T is considerably lower than the INTOR guiding value. The value chosen here is closer to the values of B_T determined self-consistently within the SISYFUS-T plant model (see below).

All calculations presented here are made with a time dependent, 0-d tokamak transport model /1/, /2/. In this model profiles for densities and temperatures can be prescribed. If not otherwise stated the following spatial distributions will be taken for all temperatures and densities, respectively:

$$T = T_o \left[0.9 \left(1 - \left(\frac{r}{a}\right)^{1,8\ 2,5}\right) + 0,1\right], \tag{2.1}$$

$$n = n_o \left[0,9 \left(1 - \left(\frac{r}{a}\right)^{1,5\ 4}\right) + 0,1\right] . \tag{2.2}$$

The following transport model has been applied in agreement with the INTOR group recommendations

$$\kappa_e(r) = 5 \cdot 10^{17} \frac{1}{n_e(r)} \ \text{cm}^2\ \text{sec}^{-1}, \tag{2.3}$$

$$\kappa_i(r) = 3\, \kappa_i^{\text{neocl.}}(r)\ \text{cm}^2\ \text{sec}^{-1}, \tag{2.4}$$

$$D(r) = 0.4\, \kappa_e(r) \quad \text{cm}^2\ \text{sec}^{-1}. \tag{2.5}$$

Here χ_e, χ_i are the electron and ion thermal conductivities, and D is the hydrogen diffusion coefficient. Estimation of the average transport losses on the basis of these space dependent coefficients was made according to Ref. /1/.

The profiles as given by eqs. (2.1) and (2.2) are rather peaked. Since the main losses strongly increase with r, they are considered to be a reasonable guess, provided that refuelling is performed through a real volume source (such as injected pellets). The opposite case, where refuelling is performed through a surface source (such as recycling from the wall in a system whose minor radius is large compared with the penetration length of neutrals) quite generally results in flat density profiles with steep gradients near the boundary. This rather extreme case, which results from straightforward extrapolation of the boundary condition in small experiments to large systems, is considered to be rather unrealistic for a reactor-like system.

To specify the parameters not yet determined, the details of the burn scenario have to be prescribed.

2.2 Description of the Burn Cycle

The plasma temporal behaviour can, in principle, be influenced by several methods, such as

- controlling the source terms in the energy and particle balance (add. heating, refuelling, compression, etc.),
- controlling the losses (enhanced radiation by impurity influx, enhanced transport by ripple production or exitation of instabilities, etc.),
- controlling of α-heating (control of fast α-losses, etc.).

In this study we confine ourselves to additional heating by neutral beam injection, cold refuelling (such as pellet injection) and compression. Beam heating and compression, if applied to a TNS requires relatively modest extrapolation from present knowledge. Controlled refuelling seems to be inevitable in any reactor-like device.

In this context the following conditions for a reasonable burn cycle are imposed by the requirement of high energy amplification and low capital costs:

- $\bar{\beta}_T$ should be kept at its maximum permissible value as long as possible during a burn cycle;
- the energy required for heating the system should be as low as possible;
- the beam energy and beam power should be as low as possible;
- the power and energy for burn control should be as low as possible.

The power requirements for density control are considered to be negligible throughout.

To meet these demands at least partly, the following burn cycle, consisting of 4 phases, has been chosen:

Heat-up phase (I)

All calculations start with a fully developed, ohmically heated plasma with full current and q(a) having its design value. In this first phase the plasma is heated to ignition. The density is kept fixed by controlled refuelling. The beam energy is chosen in such a way that full penetration is achieved for the given density. Obviously the aim of this procedure is to minimize the beam particle energy requirements by choosing the density in this phase as low as possible. The possibility of reducing the beam energy requirement further by starting with an even lower density which is raised at the end of the heat-up phase, when α-heating becomes relevant, has not been considered here. A 1-d treatment is more adequate to study this topic.

The following data are chosen in the reference system:

beam power	(P_{inj})	50 MW,
beam energy	(E_o)	200 keV.

The corresponding density is slightly above the lowest value that is compatible with ignition (see Sec. 3).

Fuelling phase (II)

The beta value at the ignition point is typically lower than the desired value. After reaching ignition, the system is kept slightly above ignition by controlling the refuelling rate. Since the energy balance is positive, beta increases. This phase terminates when beta has reached its final value. No additional energy requirements arise from this procedure.

Burn phase (III)

At the end of phase II the system has reached its final beta value, being ignited at the lower, unstable burn point. In this study we decide to operate at this lower burn point. Two modes of burn control are considered, namely controlled additional heating and stabilization by cyclic major radius compression and decompression. A more detailed discussion will be presented in Sec. 4.2. Within the context of sensitivity studies an ideal control procedure is applied for simplicity, the effect of which on the overall energy balance can be neglected.

The main reason for considering burn at the lower, unstable burn point is that it requires only relatively modest extrapolation beyond densities and temperatures of near-term experiments.

The upper burn point, on the other hand, is characterized by low densities and high temperatures. Hence, as it is situated in a much more collisionless regime enhanced transport is likely. Furthermore, at these high temperatures the rather ambiguous cyclotron losses can no longer be neglected. Furthermore the contribution to beta by fast α-particles is smaller at the lower burn point. Finally, the system being more radiation dominated, distributes power on the relatively large wall surface and thus weakens the problem of heat removal.

During the burn phase the system may change slowly as a result of, for instance, the accumulation of α-particles or wall impurities. To keep beta at its maximum value despite these disturbances, the refuelling rate is appropriately controlled.

The time scale of these disturbances is of the order of the burn time (typically $\gtrsim$ 10 sec). The characteristic time for the development of the burn instability is much smaller (typically $\lesssim$ 1 sec). This difference in order of magnitude considerably facilitates simultaneous control of burn and beta.

Shut down phase (IV)

We shall treat clean systems resulting in stationary solutions and systems whose burn terminates by α-particle or wall impurity accumulation. Once ignited performance is no longer possible these systems cool down owing to radiation and transport losses. Effects such as transformation of poloidal field energy into internal energy are not taken into account. This would call for a selfconsistent treatment of the plasma and pulsed coil system /3/. This will be studied in a subsequent paper. However, these effects which may strongly affect the design of the pulsed coil system and its power supply, only weakly influence the burn times. Hence we can neglect these details in this study, where emphasis is laid on the overall energy and particle balance of the system.

2.3 Summary of the Reference System Layout Data

We shall consider essentially three reference cases which are identical, except for the assumptions as to impurity behaviour. The clean case (A); (Z_{eff} = 1), the case of wall impurity accumulation and anomalous α-particle diffusion (B) and the case of α-particle accumulation with complete wall impurity control (C) will be considered as natural limiting cases.

The complete set of input data for these cases is summarized in Table 1.

TABLE 1

		A	B	C
major radius	(R)	480 cm	-	-
minor radius	(a)	120 cm	-	-
elongation	(s)	1.5	-	-
safety factor	(q(a))	3	-	-
maximum toroid. beta (vol.aver.)	($\bar{\beta}_T$)	0.06	-	-
toroid. field on axis	(B_T)	40 kG	-	-
beam energy	(E_o)	200 keV	-	-
beam power	(P_{inj})	50 MW	-	-
beam comp.		deuterium	-	-
heating time	(τ_h)	1,23 sec	1,28 sec	1,23 sec

reflux coefficient	(γ)		0	$2 \cdot 10^{-4}$	0
α-accumulation			no	no	yes
initial density	($n_o^e = n_o^i$)	3.8	10^{-14} cm^{-3}	-	-
plasma-first wall dist.	(1)		12 cm	-	-

The relation between peak values and average values is as follows:
($\bar{}$ denotes a volume average)

$\bar{n}/n_o = 0{,}2202$

$\overline{nT}/n_o T_o = 0{,}1178$

As noted above the same profiles have been used for all densities and temperatures respectively.

The reflux coefficient γ is defined as

γ = impurity inward flux/fuel outward flux

and characterizes the plasma wall region /4/. In this study iron is taken as the dominant wall impurity.

The temporal behaviour of the most interesting quantities is given by Figs. 1 to 21 for the three cases A-C. In case A (clean case) the computation is terminated once the stationary burn phase is reached. Thus, phases I and II of the burn cycle, which are essentially identical in cases A-C, feature in greater detail in the plots. Figures 1 to 21 are self-explainatory, but some features are worth mentioning:

The temperatures show characteristic behaviour which is determined by the specific scaling of the empirical transport law. At the end of phase I the losses are dominated by transport owing to the relatively low density and the system ignites at a rather high temperature (Figs. 1, 8, 15). At the end of phase II the density has considerably increased (Figs. 4, 10, 17). Confinement has now improved so much that radiation is the dominant loss mechanism (Figs. 6, 13, 20). In this early stage the impurity content is so low that bremsstrahlung dominates. Hence the system burns near the ideal

ignition temperature. In cases B and C the temperatures increase owing to enhanced radiation losses. In this part of the cycle the transport losses increase, too, as a consequence of the decreasing density, but the system remains radiation dominated till the burn terminates.

In case B the power density slightly increases with time during the burn phase (Fig. 12). This is a consequence of the increase of T_o^i in this phase (Fig. 8) and the increase of power density for fixed beta in this temperature regime. In case C this effect is compensated by fuel replacement due to accumulated α-particles and the power density happens to be essentially constant during the burn phase (Fig. 19).

The total wall loading has the guiding value 1 to 2 MW/m^2 despite the relatively low toroidal field at axis (Figs. 7, 14, 21).

References

/1/ K. Borrass, A Zero-Dimensional Tokamak Transport Model. Part I: General Description. Max-Planck-Institut für Plasmaphysik Report IPP 4/146, August 1977.

/2/ K. Borrass, A Zero-Dimensional Tokamak Transport Model for Systems of Time Dependent Size and Position, Max-Planck-Institut für Plasmaphysik Report, in preparation.

/3/ J. Raeder, A mathematical model of the pulsed coil system of a tokamak reactor, Max-Planck-Institut für Plasmaphysik Report IPP 4/174, January 1979.

/4/ See for instance ref. /1/ and the literature cited there.

3. Studies on Start-Up

In this section some additional calculations on phase I of the burn cycle are presented.
The beam energy that is required for full penetration is determined by the relation

$$E_o = 4.5 \times 10^{-15} \; n_o^e \; a \; Z_{eff} \qquad (3.1)$$
$$(keV) \qquad (cm^{-3}) \; (cm)$$

The values for the coefficient in eq. (3.1) given in the literature differ within a factor of about two. The value chosen here lies at the lower end of the spectrum. This is considered to be consistent with the relatively peaked density profiles being used. They facilitate penetration. On the other hand, the initial impurity concentration was set equal to zero in all our calculations, which is a rather optimistic assumption. However, once full penetration is assumed the power and energy requirements for start-up only weakly depend on E_o.

In Table 2 the time τ_h and energy E_h that are necessary to heat the system to the ignition point are given for several fuel densities n_o^f. The injection power was 50 MW in all cases.

TABLE 2

$n_o^f(0)$	3.8	3.6	3.5	3.4	$\times 10^{14}$ cm^{-3}
τ_h	1.30	1.43	1.55	1.79	sec
E_h	64.99	71.49	77.49	89.48	MJ

For densities below $n_o^f = 3.4 \times 10^{14}$ ignition was no longer possible. Near this limit E_h strongly increases with decreasing density. The value $n_o^f = 3.8 \times 10^{14}$ was therefore chosen for the reference case. It requires only slightly higher beam energy but considerably lower heat-up energy than the limiting value.
For the fixed density value $n_o^f = 3.8 \times 10^{14}$ the heating time τ_h and heating energy E_h were calculated for various injection powers P_{inj}. The result is summarized in Table 3.

TABLE 3

P_{inj} (MW)	τ_h (sec)	E_h (MJ)
75	0.7940	59.55
70	0.8599	60.19
65	0.9359	60.84
60	1.028	61.68
55	1.140	62.69
50	1.280	63.99
45	1.462	65.78
40	1.708	68.31
35	2.058	72.02
30	2.599	77.98
25	3.559	88.98

For injection powers below 25 MW ignition cannot be achieved. E_h is essentially constant apart from very low injection powers. The reason is that for these low values of P_{inj} τ_h becomes comparable with the energy confinement time. ($\tau_E \approx 1.6$ sec in phase I of the reference system.) Hence part of the injected energy is lost during the heating phase owing to transport.

The reference value P_{inj} = 50 MW is situated at the beginning of the regime where E_h as a function of P_{inj} saturates.

The values for τ_h and E_h obtained here are, at first glance, surprisingly low. These favourable results are essentially a consequence of the peaked profiles. Indeed, the energy confinement time τ_E, if computed for these peaked profiles on the bases of the space dependent transport coefficients according to Ref. /1/, essentially agree with usual estimates of τ_E for less peaked profiles. On the other hand, the α-heating, for fixed density, increases with peakedness of the density and temperature /2/. Ignition is thus facilitated by peaked profiles. Refuelling techniques and boundary conditions resulting in peaked profiles thus seem to lower the start-up energy requirements.

/1/ K. Borrass, A Zero-Dimensional Tokamak Transport Model, Part I: General Description, Max-Planck-Institut für Plasmaphysik Report IPP 4/146, August 1977.

/2/ K. Borrass, The Influence of the Radial Density and Temperature Profiles on the Mean Power Density in a Tokamak, Max-Planck-Institut für Plasmaphysik Report IPP 4/140, June 1976.

4. Studies on Burn Control

Up to now we have considered ignited systems in which either the density or $\bar{\beta}_T$ is kept fixed. As is well known, in such systems, if ignition can be achieved at all, there exist two burn points, the one with the lower temperature being unstable with respect to temperature excursions. We now discuss stabilization of this thermal instability by means of controlled reheating and cyclic major radius compression and decompression. Both schemes are non wattless. The power that is required for an effective control depends, of course, on the accuracy with which deviations from equilibrium can be measured. In what follows we shall assume that the ratio $\bar{Q}/\bar{Q}_N$ can be measured with accuracy ε, where $\bar{Q}_N$ is the volume averaged total α-power density and $\bar{Q}$ the volume averaged right-hand side of the total (sum over all species) energy balance in the absence of control terms. $\varepsilon = 0.05$ will be taken as a reasonable value.

In the following discussion, emphasis is laid on the following problems, the relevance of which is obvious:

- Is effective control possible at all and under which conditions?
- What are the power and energy requirements and how do they affect the overall energy balance of the system?

4.1 Burn Control by Additional Heating

The density $\bar{Q}_H$ of the heating power is always positive. Hence $\bar{Q} < 0$ is a necessary condition in the case of burn control by additional heating. In the case of finite accuracy even $\bar{Q} \leq -\varepsilon \bar{Q}_N$ must be fulfilled. If this control scheme is applied, the system thus turns out to be a driven one.

Obviously $\varepsilon \bar{Q}_N V$ is the minimum power that has to be fed into the system for control. In the reference system $\varepsilon \bar{Q}_N V \approx 4$ MW.

The impact on the overall energy balance can be conveniently characterized by an ideal energy amplification factor

$$Q_{ideal} = \frac{5 \bar{Q}_N V \tau_b}{E_H + \varepsilon \bar{Q}_N V \tau_b} \quad , \tag{4.1}$$

where τ_b is the burn time and E_H the energy to heat up the system. In writing Q_{ideal} in this way, we have tacitly assumed that $\bar{Q}_N \approx$ const during most of the burn cycle. This assumption is in good agreement with what we have found for reference cases A-C.

For large values of τ_b one gets $Q_{ideal} \longrightarrow 5/\varepsilon$. Hence in this limit Q_{ideal} is purely determined by the accuracy. Taking the reference case data we have with $\varepsilon = 0.05$

$$Q_{ideal} = \frac{400\,\tau_b}{61+4\cdot\tau_b} \qquad (4.2)$$

In this case for burn times $\tau_b \gtrsim 15$ sec Q_{ideal} is thus determined by the power requirements for control and restricted to the rather low value $Q_{ideal} = 100$.

The situation will be even more unfavourable if, for instance, the heating power can attain discrete values only so that in the time average $\bar{Q} < \varepsilon\,\bar{Q}_N$.

4.2 Burn Control by Cyclic Major Radius Compression and Decompression

A second way of influencing the energy balance is by major radius compression and decompression respectively. It gives rise to additional terms in the energy balance equations and changes the transport losses through their radial dependence. We study its application to burn control within the framework of a 0-d transport model /1/ that has been extended to plasmas of variable size and position /2/. This scheme has also been proposed by K. Lackner /3/.

As we shall see below for effective control compression generally needs not be adiabatic. In this case the results largely depend on the relative positioning of the limiter to the plasma centre. The effect of various limiter options on the control problem will be studied in a subsequent paper. In this study we confine ourselves to a limiter which is always in contact with the same toroidal flux surface. A typical example is the so-called rail limiter (Fig. 22).

In this case, if the compression or decompression is adiabatic, the total particle number N is constant. In the following treatment, refuelling is assumed to occur in such a way that this condition holds in the non-adiabatic case too.

With these constraints the full nonlinear model is treated numerically. By assuming in addition $T_e=T_i=T$ and $n_e=n_i=n$ the following set of equations results, a linearized version of which has been used for an analytical treatment of the control problem:

$$3\frac{d}{dt}\,nT = \bar{Q} - 2\,\overline{nT}\left(\frac{7}{2}\frac{1}{R}\frac{d}{dt}R + 3\frac{1}{a}\frac{d}{dt}a\right) \qquad (4.3)$$

$$\bar{Q} = \bar{Q}_N - \bar{Q}_T - \bar{Q}_R$$

$$\bar{Q}_N \sim \bar{n}^2\,\overline{\langle\sigma v\rangle}$$

$$\bar{Q}_T \sim \frac{\overline{nT}}{\tau_E} \sim \frac{\bar{T}}{a^2} \quad \text{(empirical scaling)} \ ,$$

$$\bar{Q}_R \sim \bar{T}^{1/2}\,\bar{n}^2 \quad \text{(bremsstrahlung)} \ ,$$

$$\frac{d}{dt}\bar{n} = -\bar{n}\left(2\frac{1}{a}\frac{da}{dt} + \frac{1}{R}\frac{d}{dt}R\right) \ , \qquad (4.4)$$

$$\frac{d}{dt}a = \frac{a}{2}\,\frac{1}{R}\,\frac{d}{dt}R \ , \qquad (4.5)$$

$$\frac{d}{dt}q(a) = q(a)\left(\frac{2}{a}\,\frac{d}{dt}a - \frac{1}{R}\,\frac{d}{dt}R\right) \ . \qquad (4.6)$$

$\bar{\ }$ denotes a volume average except for temperatures where $\bar{T} = \overline{n\cdot T}/\bar{n}$. Eq. (4.5) is a special version of a more general equation /2/ exhibiting the special limiter option. The absence of source terms and diffusion loss terms in eq. (4.4) stems from the refuelling condition N = const. In eq. (4.6) skin penetration terms are omitted. It is easy to verify from eqs. (4.3) to (4.6) the usual scaling laws of adiabatic compression.

From eqs. (4.3), (4.4) and (4.5) we get

$$3\,\bar{n}\,\frac{d}{dt}\,\bar{T} = \bar{Q} - 4\,\bar{n}\,\bar{T}\,\frac{1}{R}\,\frac{d}{dt}\,R \qquad (4.7)$$

The following discussion is simplified by noting that the system under consideration is completely characterized by the two variables R and T. Now a reasonable control scheme naturally implies that the variation δR and δT during the time development of the system should be small relative to the equilibrium values R_o, T_o:

$$\left|\frac{\delta R}{R_o}\right|, \left|\frac{\delta T}{T_o}\right| \ll 1 \qquad (4.8)$$

From eq. (4.7) we get by integration

$$\left(1 + \frac{\delta R}{R_o}\right)^2 \left(1 + \frac{\delta T}{T_o}\right)^{3/2} = e^{\int_o^t \frac{\bar{Q}}{2\bar{n}\bar{T}}\,dt'} \qquad (4.9)$$

To meet condition (4.8), it must hold that

$$\int_o^t dt' \frac{\bar{Q}}{2\,\bar{n}\bar{T}} \approx 1 \qquad (4.10)$$

Now, as noted above, $\bar{Q} \approx \varepsilon\ \bar{Q}_N$ and hence

$$\left|\frac{\bar{Q}}{2\,\bar{n}\bar{T}}\right| \approx \left|\frac{\varepsilon\ \bar{Q}_N}{2\,\bar{n}\bar{T}}\right| \approx \frac{\varepsilon}{\tau_s}\,, \qquad (4.11)$$

where τ_s is the e-folding time of α-heating. Typically, one has $\tau_s \approx 1/3$ sec and $\tau_b \gg \tau_s/\varepsilon$. To meet condition (4.10) $\bar{Q}$ must thus change sign during burn with a period length τ_o such that $\tau_o \lesssim \tau_s/\varepsilon$.

The change of sign of $\bar{Q}$ can be achieved by a sufficiently fast compression or decompression respectively.

The fact that deviations from equilibrium can only be measured with finite accuracy thus essentially implies the system to run through a cycle being periodically ignited and non ignited. No other means of influencing the energy balance being provided, the change of sign has to be achieved by periodically compressing or decompressing the system.

Obviously, many cycles meet these demands. The one we have used here is conveniently visualized by Fig. 23. In that figure the equilibrium points are given by the curve $\bar{Q} = 0$. The four segments of the cycle are characterized as follows:

(1) $\quad \bar{Q} = \varepsilon \bar{Q}_N$

(1) $\longrightarrow$ (2) $\dot{R} = 0$, self-heating

(2) $\quad \bar{Q} = m \varepsilon \bar{Q}_N$

(2) $\longrightarrow$ (3) $\dot{R} > 0$, decompression

(3) $\quad \bar{Q} = - \varepsilon \bar{Q}_N$

(3) $\longrightarrow$ (4) $\dot{R} = 0$, self-cooling

(4) $\quad \bar{Q} = - m' \varepsilon \bar{Q}_N$

(4) $\longrightarrow$ (1) $\dot{R} < 0$, compression

A similar cycle has been studied by E. Minardi with respect to the problem of direct energy conversion /4/.
In all specific calculations $\varepsilon = 0.05$ and $m = 2$ will be used.

m' is determined by the requirement that the cycle be closed. Closure of the cycle avoids drifting of the major radius. In the numerical model m' is determined by a feedback control keeping for instance $R_{(2)}$ or $R_{(1)}$ at a desired value. In the linearized model to lowest order closure is automatically given. Indeed deviations from closure are a higher-order effect, so that $m \approx m'$ in practice.

The choice of m is to a certain degree arbitrary. Enlarging m enlarges the cycle duration, which is favourable, but enlarges the energy that has to be transferred per cycle,too, which is unfavourable. In practice, the optimum value of m will strongly depend on the specific design of the power supply (switches, sources etc.). We have therefore not pursued this question further. It is clear from what follows that the results presented here do not qualitatively depend on the choice of m.

For simplicity dR/dt was kept fixed during compression and decompression. Hence the compression velocity is conveniently characterized by $\tau_R = R/|dR/dt|$. Another quantity of interest is the change of R: $\Delta R = R_{(2)} - R_{(1)} = R_{(3)} - R_{(4)}$.

In Figures 24 and 25 the time dependence of temperatures, major radius and minor radius is given for a clean INTOR-like system with $\tau_R = 3$.

We now summarize some results that have been obtained for this type of control. The details will be presented elsewhere /5/. All specific statements apply to a clean INTOR plasma (type A) in phase III of the burn cycle. As noted previously, m = 2 and $\varepsilon = 0.05$ are used throughout.

Linearizing eqs. (4.3), (4.4), (4.5) with respect to the relative vatiations $\delta T/T_0$, $\delta n/n_0$, $\delta R/R_0$ .... and the small quantity ε and applying it to the cycle under consideration results in the following relation between τ_R and ΔR

$$3(m+1)\,\varepsilon\,\frac{R_0}{\Delta R} + (2\gamma - \alpha - 1)\frac{\tau_R}{\tau_N} = 2\left(2\gamma + \frac{7}{2}\alpha - 1\right) \qquad (4.12)$$

Here $\tau_N = \dfrac{\tau_s}{m\varepsilon}$

$$\alpha = \frac{\bar{Q}_{T(1)}}{\bar{Q}_N(1)}$$

$$\gamma = \frac{\partial\, \mathrm{en}\, \bar{Q}_N(1)}{\partial\, \mathrm{en}\, \bar{T}(1)}$$

(γ here not to be confused with the reflux coefficient of section 3). α determines whether the system is radiation dominated ($\alpha = 0$) or transport dominated ($\alpha = 1$). The first case is typically given in large, reactor-like systems; the latter case prevails in small ignition experiments.

γ characterizes the temperature dependence of the fusion power density in the vicinity of the equilibrium point.

In the special example under consideration $\tau_N = 9.25$ sec; $\alpha = 0.26$; $\gamma = 3.31$.

All terms being positive in eq. (4.12) implies the existence of an upper limit for τ_R:

$$\left.\frac{\tau_R}{\tau_N}\right|_{max} \leq 2\,\frac{2\gamma + \frac{7}{2}\alpha - 1}{2\gamma - \alpha - 1} \qquad (4.13)$$

The $\Delta R/R$ dependence on τ_R/τ_N as given by numerical calculations with the full nonlinear model (———) and by eq. (4.12) (-----) is plotted in Figure 26 for the special system under consideration. A vertical line marks the two stability limits resulting from eq. (4.13) and numerical calculations, respectively. There is good agreement between analytical and numerical results except near $\tau_R/\tau_N \approx 1$, where the linearization breaks down.

The major radius compression is essentially achieved by variation of the vertical field. The power and energy that is required for control has to be fed into the pulsed coil system (OH-transformer, vertical field coil) as electric power (and energy). To compute them, a slightly simplified model of the pulsed coil system being proposed by K. Lackner /6/ has been coupled to the plasma model. In this model skin penetration through the vacuum vessel and ohmic losses in the coils are neglected. Coupling to a more involved model is under preparation /7/.

For an otherwise fixed system, it follows from this model that

$$P_m \sim 1/\tau_R \qquad (4.14)$$

and

$$E_c \sim \Delta R \quad , \qquad (4.15)$$

where P_m is the maximum power that has to be fed into the coils during compression, and E_c the energy that is transferred to the coil system during the compression phase.

From the above-mentioned results one immediately concludes that there is a lower limit for P_m to achieve effective control and E_c only weakly depends on the speed of compression.

For the special example the dependence of P_m and E_c on τ_R as resulting from numerical calculations is plotted in Figs. 27 and 28.

As can be seen from Fig. 27, the minimum power P_m that is required for control is of the same order as the additional power that was estimated in the case of control by additional heating.

However, there is a principal difference. In Figs. 29 and 30 the electric power P and energy E that are fed into the coil system are plotted as a function of time for the special example. Comparison with 25 shows that essentially the same power and energy that is fed into the system in the compression phase is delivered back in the decompression phase. The average power that is transferred is more than an order of magnitude smaller than P_m. Hence, unlike in control by additional heating the overall energy balance in this case is practically not affected by the power requirements for control. Moreover, from Figure 30 it is seen that the average power is even negative, indicating that, in the average, power is delivered from the plasma to the outer circuit.

References

/1/ K. Borrass, A Zero-Dimensional Tokamak Transport Model, Part I: General Description. Max-Planck-Institut für Plasmaphysik Report IPP 4/146, August 1977.

/2/ K. Borrass, A Zero-Dimensional Tokamak Transport Model for Systems of Time Dependent Size and Position, Max-Planck-Institut für Plasmaphysik Report, in preparation.

/3/ K. Lackner, Annual Controlled Fusion Theory Conference, Gatlinburg, 1978.

/4/ E. Minardi, private communication.

/5/ K. Borrass, K. Lackner, under preparation.

/6/ K. Lackner, private communication.

/7/ J. Raeder, A mathematical model of the pulsed coil system of a tokamak reactor, Max-Planck-Institut für Plasmaphysik Report IPP 4/174, January 1979.

5. Plant Sensitivity Studies

5.1 Scope

In the foregoing sections the behaviour and control of the plasma during its operational phases has been considered in detail. These considerations are based on many assumptions, most of which were made as far as possible according to the guidelines of the Vienna Workshop (Session I). Three reference cases for the layout were thus considered, case C of which corresponds most closely to the recommendations. However, these three cases do not cover all the areas of uncertainties of the assumptions. It is therefore necessary to ask what would happen if these assumptions cannot be realized.

This question can be delt with in two ways. The first assumes that the machine has already been built. It thus has to be calculated in what way operation changes if one of several of the values assumed for layout cannot be met in reality. Starting from a reference layout with a consequently constant geometry, we calculate the sensitivity of the operational parameters as a function of the layout parameters. By means of this kind of analysis it is possible to find out, for example, whether and to what extent an experimental device might meet its objectives.

The second kind of analysis is characterized by the following procedure: At first a special desired value is fixed as a constraint which has to be met in any case, e.g. the net electric output power of the plant or the wall load of the reactor. Assuming a set of additional parameters, the necessary size of the torus, e.g. expressed by the minor plasma radius at constant aspect ratio, is determined so that the constraint is met. Varying the assumptions leads to a set of different torus sizes. The dependence of the torus size on these variations is a measure of the sensitivity of the layout. The most insensitive layout is found when the freely choosable parameters are arranged in such a way that the variation of the uncertain parameters has the least bearing on the torus size.

However, this second kind of analysis requires a detailed definition of constraints being not available at this early stage of work on INTOR. Therefore the scope of the sensitivity analyses had to be restricted to the first kind of analysis, the sensitivity of operation.

The complexity of a power plant makes it necessary to represent all the interactions of the plant components in a mathematical model. Such a model has been developed in the Systems Studies Project at IPP Garching.

5.2 The SISYFUS Code

5.2.1 General Description

A simulation model for systematic analysis of fusion power plants, called SISYFUS, is being developed at IPP. Its overall structure is shown in Fig. 31. The main components of the model are ENERGY BALANCE, MATERIALS BALANCE, COSTS, IMPACT ON ENVIRONMENT, and BENEFIT. Of these the ENERGY BALANCE is sufficiently complete for sensitivity studies in the operational and the layout sense, as was pointed out before. The structure of the ENERGY BALANCE of a fusion power plant with a tokamak reactor, called SISYFUS-TE (T = Tokamak, E = Energy Balance), is represented in Fig. 32. It allows for the calculation of all flows of energies and fuel related materials and includes a one-dimensional time-dependent plasma model. A description of the code is given in /1/ and /2/. However, several important improvements and extensions have been made since then: Besides the trapped-ion mode the empirical scaling has been included as an option in the plasma model as well as the control of the burn phase in the vicinity of the ignition point. The step towards elliptical cross-sections of the plasma, first wall, blanket and shielding has been accomplished and includes the possibility of a variable blanket thickness along the small circumference of the torus. The number of toroidal coils is determined according to a given ripple coefficient for the magnetic field. The maximum magnetic field at the superconductor is calculated according to the kind of conductor materials and cooling temperature, and the thickness of the constant-tension D-shaped coils is adjusted so that a given value for the strain in the conductor is utilized but not exceeded (for details see /3/).

5.2.2 Application to INTOR

The Vienna Workshop's information on data to be achieved and constraints were transferred as far as possible into the data set necessary for the application of SISYFUS-TE. These data and additional necessary assumptions resulted in an arrangement, shown in Fig. 33, which is largely correct in scale. The corresponding geometric data are listed in Tab. 1. Of course, these data may be changed during future steps of the iterative INTOR layout and design procedure.

However, as the SISYFUS code includes not only the reactor with its auxiliary systems but also the balance of plant, additional assumptions and data are required. These are listed in Tab. 2. Of special importance is the assumption of liquid lithium as breeding material and coolant with a maximum coolant temperature of 525^{o} C, thus allowing for a live steam temperature of 500^{o} C at the entrance of the steam turbine, as assumed for energy conversion. Since a 100 % blanket was assumed, the amount of electricity calculated will have to be adjusted according to the Vienna Workshop's recommendation to use only 10 % of the torus' surface area for a real blanket, thus probably requiring a reduction of the assumed maximum coolant temperature. For these first calculations a full-scale balance of plant was nevertheless assumed in order to give an impression of what a real power plant based on INTOR would look like. However, as mentioned before, also these assumptions may be changed rather freely.

Besides being set out in a detailed list, the output of a computer run of SISYFUS-TE is represented in a plot that comprises the main data of plant components and the overall plant energy balance. For the reference case C which has already been defined and considered in the foregoing sections, and which is the nearest to the Vienna Workshop's recommendations such a plot is shown in Fig. 34. By means of the detailed legend and together with Fig. 35, which explains the designations of diagrams and the respective scales, Fig. 34 can be understood without any further comment. It represents the scope of information that can be handled by SISYFUS-TE. The net electric power

output from this plant (with a 100 % blanket) would be 120 MWe, the net electric efficiency 28.1 %. The latter, rather low, value is mainly due to the fact that nearly one-quarter of the plasma power output has to be removed from the shielding because of the thin blanket. A thicker blanket is therefore recommended for future work.

Figure 34 was valid for reference case C, which is mainly characterized by the assumptions that the α-particles will accumulate in the plasma whereas the impurities from the wall will not do so. Since, however, these assumptions have not yet been verified by experiments, two other reference cases, A and B, have already been defined. For these two cases the SISYFUS-TE plots are shown in Figs. 36 and 37 respectively, the explanations being given in Figs. 34 and 35. In case A (Fig. 36) no accumulation of α-particles and impurities from the wall is taken into account, thus leading to a burn time which is limited only from the outside, e.g. by the transformer flux swing. In Fig. 36 this limit was arbitrarily chosen to be 5 min. Figure 37 - case B - is based on the assumption that a certain amount of impurities emitted by the wall will accumulate within the plasma, but that α-particles will leave the plasma owing to anomalous outward diffusion.

As far as the plasma data are concerned, the absolute values in Figs. 34, 36 and 37 deviate somewhat from the results in the foregoing sections. The reason is that the earlier calculations were made for a magnetic field of B = 4.0 T at the plasma centre, while the subsequent calculations with SISYFUS-TE used a value of about 4.5 T, which is a result of the more detailed specification of the geometry of the INTOR arrangement (see Fig. 33 and Tab. 1).

5.3 Ranges of Parameter Variations

The changes of assumptions between the three reference cases, however, do not cover all the uncertainties of the assumed values. Besides the fact that the behaviour of the α-particles in the plasma is not yet known, the rate of impurity accumulation in the plasma is absolutely uncertain (for Fig. 37 an arbitrary value of $f = 2 \times 10^{-4}$ was chosen). The value of f thus has to be varied in wide ranges:

$0 \leq \varepsilon \leq 5 \times 10^{-4}$. The upper value will be discussed in connection with the results.

Another uncertain parameter is the toroidal β_T that can be achieved. The value of $\beta_T = 6$ %, on which the reference cases were based (in accordance with the Vienna Workshop's recommendations), is therefore varied in both directions: $4.5\ \% \leq \beta_T \leq 9\ \%$, the lower value being necessary to get ignition in this scenario and the upper value being due to some optimism.

An additional range of uncertainty is given by the transport coefficients. However, up to now these could not be varied within the SISYFUS-code for lack of time. This work will be started soon so that information about the sensitivity of INTOR to this uncertainty will be available for the next step of iteration of the layout.

Up to now the maximum magnetic field at the superconductor (B_{max} = 8,46 T for Nb Ti)has not been varied either, in spite of the fact that this is possible. This will only be done if it turns out to be necessary for any reason.

As was pointed out in Sec. 5.1, the sensitivity of operation and of layout will be determined for the variation of ε and β_T in the cases of α-particle accumulation and anomalous outward diffusion of α-particles.

5.4 Sensitivity of Operation

According to Sec. 5.1 this kind of study assumes the reactor to be already built, i.e. the geometry of the reactor will not be changed during calculation, and the question is how the operation of the

plant varies with varying values of the uncertain parameters. Now that the ranges of parameter variation have been defined in the subsection immediately preceding, those quantities have to be specified which describe the operation of the plant or which may have a special importance with respect to the sensitivity of layout to be considered later on. Five quantities have thus been chosen for this purpose

- the wall load $\bar{q}^{b}_{tot}$ averaged over the burn time
- the burn time t_b
- the wall load $\bar{q}^{c}_{tot}$ averaged over the cycle time (cycle time = burn time + idle time t_{id})
- the usable thermal power output $\bar{P}^{c}_{th}$ averaged over the cycle time (thermal power from blanket plus divertor).
- net electric power output $P_{e,n}$.

For both cases separated - without and with α-particle accumulation - these five magnitudes are represented as functions of δ^* with β_T as parameter in Figs. 38 - 42 and Figs. 43 - 46 and 48 respectively.

5.4.1 Anomalous Outward Diffusion of α-Particles

In Figs. 38 - 41 the reference cases A and B are designated by circles on the curves for β_T = 6 % at δ^* = 0 and $\delta^* = 2 \times 10^{-4}$. In Figs. 38, 40 and 41 each curve for β_T = constant consists of two ranges. Considering such a curve starting at $\delta^* = 5 \times 10^{-4}$ and proceeding to lower δ^*-values leads via point B to a point at which the curve splits into two branches. Just at this point the burn time has increased up to 300 s (see Fig. 39, β_T = 6 % curve). Keeping this value constant while further decreasing δ^*-values means that the burn phase is limited from outside but would have been longer from the point of view of plasma burn conditions. In this case the wall load decreases with decreasing δ^*-values, reaching point A for δ^* = 0. This decrease of the wall load is due to the fact that at a constant δ^*-value the time-dependent wall load increases during the burning phase (e.g. see Fig. 37, third diagram on the left-hand side), so that limiting the burn phase from outside cuts off a time range of increasing wall load, thus reducing the average value. In the case of the burn phase not being limited to 300 s the original trend of the curve with point B on

it continues to lower f_e-values. If the burn phase is terminated at, for example, 25 min (see Fig. 41, dashed curve), the decreasing branch of the curve begins just at $f_e = 5 \times 10^{-6}$, dropping to intersect with the ordinate slightly above point A because of the now higher ratio between the burn time and cycle time (the idle time is constant at $t_{id} = 30$ s). In principle, the shapes of the curves in Figs. 38, 40, and 41 are identical and the absolute values are the higher the higher β_T is. This is also true of the burn time represented in Fig. 39.

In evaluating now the sensitivity of operation on f_e it can be said that the influence of increasing f_e is the lower the higher the absolute value of f_e is. This holds mainly for the burn time averaged wall load (Fig. 38), whereas by means of the strong influence of f_e on the burn time (Fig. 39) the cycle time averaged wall load (Fig. 40) and, consequently, the thermal reactor power (Fig.41) are slightly more affected. Nevertheless comparing, for example, the reference cases A and B leads to the conclusion that the uncertainty of f_e will have no dramatic impact on the energetics of the reactor itself but strongly affects the burn time if values of $f_e \lesssim 1$ to 2×10^{-4} are assumed as reference values. A value of $f_e \geq 2 \times 10^{-4}$ should therefore be recommended as a basis for the layout so that burn times of $t_b \lesssim 60$ s will have to be taken into account for the design.

It was said that the influence of the amount of the impurity influx on the power output of the reactor was not as dramatic as its influence on the burn time. However, it has to be borne in mind that the decreasing burn time leads to a relative increase of the power requirement of the auxiliary systems, e.g. heating system, pulsed coils, and the cooling system of the superconducting magnets, thus impairing the energy balance of the total power plant. For this reason the net electric output power of the plant is shown in Fig.42 again as a function of f_e with β_T as a parameter. A comparison with the curves of Fig. 41 shows that this adverse effect is the higher the lower β_T is.

5.4.2 Accumulation of α-Particles

In Figs. 43 - 46 the same quantities as in Figs. 38 - 41 are shown as functions of f^* with β_T as a parameter assuming now, however, that the α-particles will accumulate in the plasma. As can be seen from Fig. 44, a burn time of 300 s, which was used as limitation from outside, was never reached. The curves for the wall load and thermal power therefore are not split. Reference case C is denoted by a circle in all diagrams.

In general, the influence of the variation of f^* is not as strong as in the case without α-particle accumulation. Again it is true that the influence of f^* on the burn time is stronger than that on the wall load and the thermal output power of the reactor. In the range of small f^*-values the absolute values for the burn times, wall load and thermal reactor power are considerably less than in the case of no accumulation of α-particles.

For a better comparison the data of Figs. 40 and 45 are represented in a three-dimensional diagram (Fig. 47). This clearly shows that at low β_T-values there is only a small difference between the two cases of behaviour of the α-particles especially if a higher amount of influx of impurities into the plasma is assumed. With increasing β_T the absolute differences between the two areas increase, the ratio of these values, however, does not change very much.

Comparing the burn times of both cases (Figs. 39 and 44) the difference by a factor of 5 (or even more) at $f^* = 0$ decreases to a factor of 2 at $f^* = 2 \times 10^{-4}$ and remains in this range even for higher f^*-values. It should, therefore, be recommended that the design point be chosen at $f^* = 2 \times 10^{-4}$, which is not far from the most favoured reference point C.

Even in this case there is yet an electric net power output of nearly 100 MWe (Fig. 48) in the 100 % blanket case. If one sticks to using only 10 % of the torus surface area for a real blanket part, the thickness of the blanket should be increased as pointed out before, so that the demonstrative coupling of an energy conversion part makes sense.

5.5 Conclusions of the Sensitivity Studies

To sum up the outcome of studying the sensitivity of operation, it should be recommended that a layout point be chosen on the assumption of α-particle accumulation and, in addition, an impurity reflux coefficient of $\gamma = 2 \times 10^{-4}$ because such a plant would not be dramatically affected by any deviations of $\beta_T \neq 6\ \%$, $\gamma > 2 \times 10^{-4}$ and the behaviour of the α-particles. In addition, possible variations of the design should be provided in order to cope easily with the results of experiments to be done before INTOR is built.

ACKNOWLEDGEMENT

The authors gratefully acknowledge the contributions from W. Daenner to the blanket programme and M. Soell to the toroidal magnets programme, the stimulating discussions with J. Raeder and especially the tremendous amount of programming and calculating done by H. Gorenflo.

REFERENCES FOR SECTION 5

/1/ Borrass, K., R. Buende, W. Daenner: First results with the SISYFUS code: The influence of plasma impurities of the performance of Tokamak power plants. 3rd Topical Meeting on the Technology of Controlled Thermonuclear Fusion. Santa Fé, N.M., 1978

/2/ Borrass,K., R. Buende, W. Daenner: SISYFUS - A simulation model for systematic analyses of fusion power plants. 10th Symposium of Fusion Technology, Padova, Italy, 1978

/3/ Soell, M.: Maximum attainable toroidal magnetic fields for Tokamaks. IEEE Transactions on Magnetics, Vol. MAG-15, No. 1, January 1979.

TABLE 1 Geometric data for INTOR arrangement

a_1	minor seminaxis of plasma	1,2 m
a_2	major seminaxis of plasma	1,8 m
b	distance plasma - 1^{st} wall	0,12 m
c	1^{st} wall thickness	0,01 m
d	outer blanket thickness	0,22 m
e	last wall thickness	0,02 m
f	c + e (no inside blanket)	0,03 m
g	shielding thickness	0,75 m
h	horizontal gap	1,05 m
j	thermal insulation thickness	0,15 m
k	coil thickness	0,60 m
l	distance coil-central support cylinder	0,07 m
m	thickness of the wall of the central support cylinder	0,20 m
R	major plasma radius	4,80 m

TABLE 2 Additional assumptions and data

PLASMA:	
empirical scaling	
operation at ignition point	
for data see the foregoing sections	
BLANKET:	
coolant and breeding material	liquid lithium
structure and wall material	stainless steel
max. coolant temperature	525^{o} C = 798 K
lithium pressure drop	40 bar = 4 MPa
HEATING SYSTEM:	
neutral injection	
electric power input	50 MWe
efficiency of device	50 %
TOROIDAL MAGNETS:	
superconductor material	Nb Ti
maximum operation temperature (4.2 K+ΔT)	5 K
ripple coefficient	1 %
strain at superconductor	0,1 %
HEAT TRANSPORT SYSTEM:	
no intermediate loop	
temperature difference coolant-live steam (energy storage included)	25 K
ENERGY CONVERSION SYSTEM:	
steam turbine cycle	
thermal efficiency (gross)	39,6 %

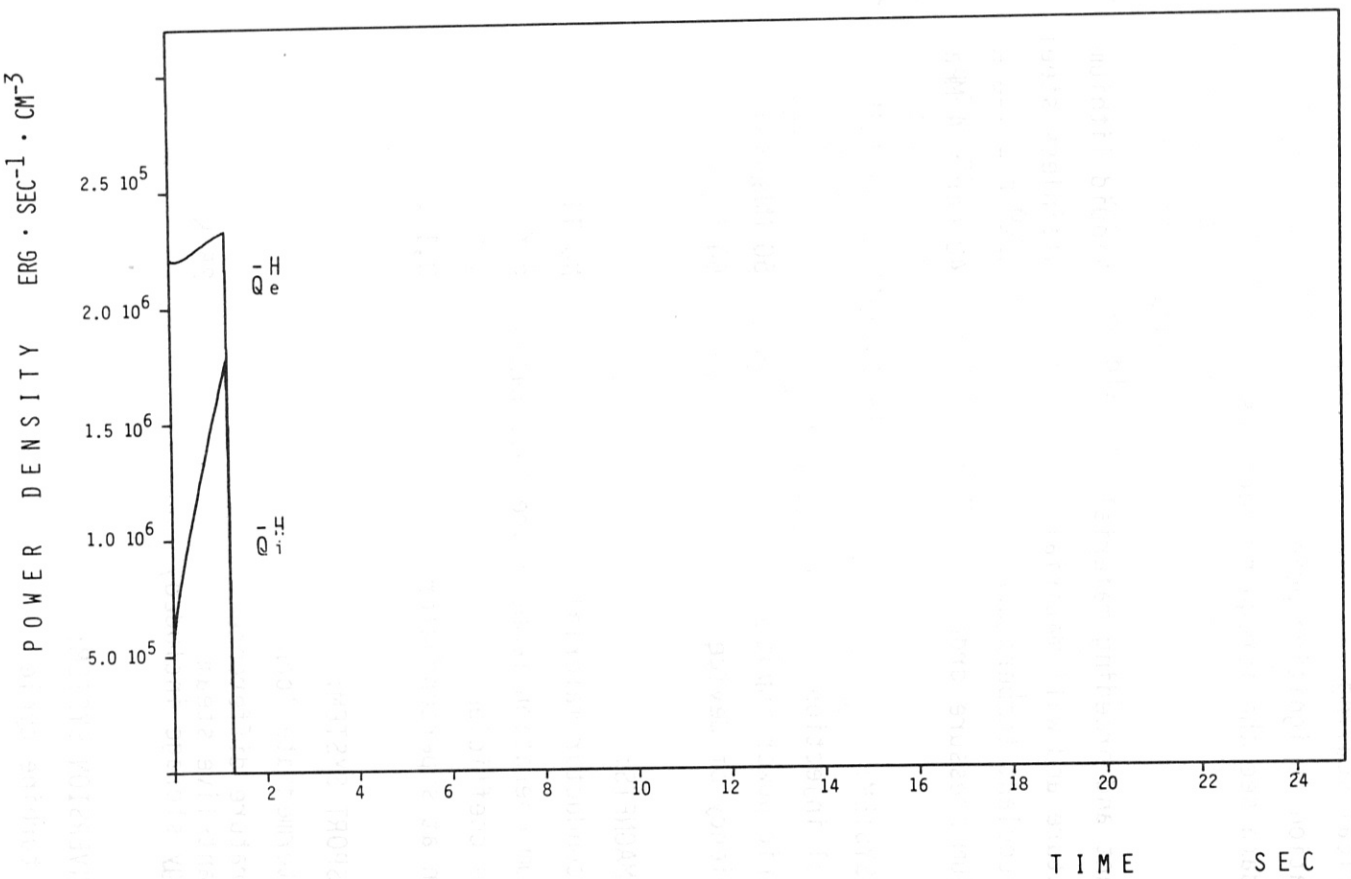

FIGURE 1

Reference case A. Heating power density going to electrons ($\bar{Q}_e^H$) and ions ($\bar{Q}_i^H$). Contributions by beam fusion reactions are included.

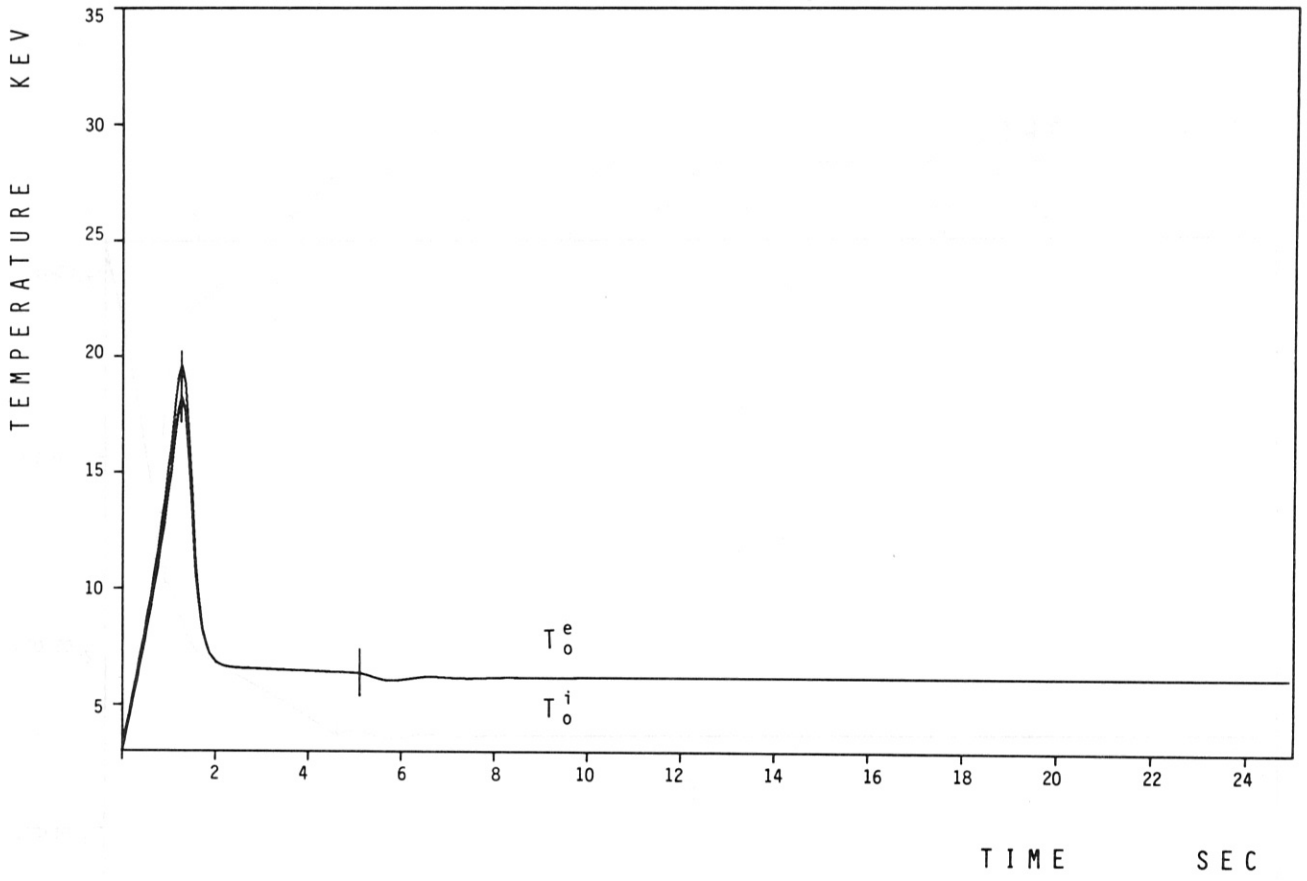

FIGURE 2

Reference case A. Time dependence of electron peak temperature (T_o^e) and ion peak temperature (T_o^i).

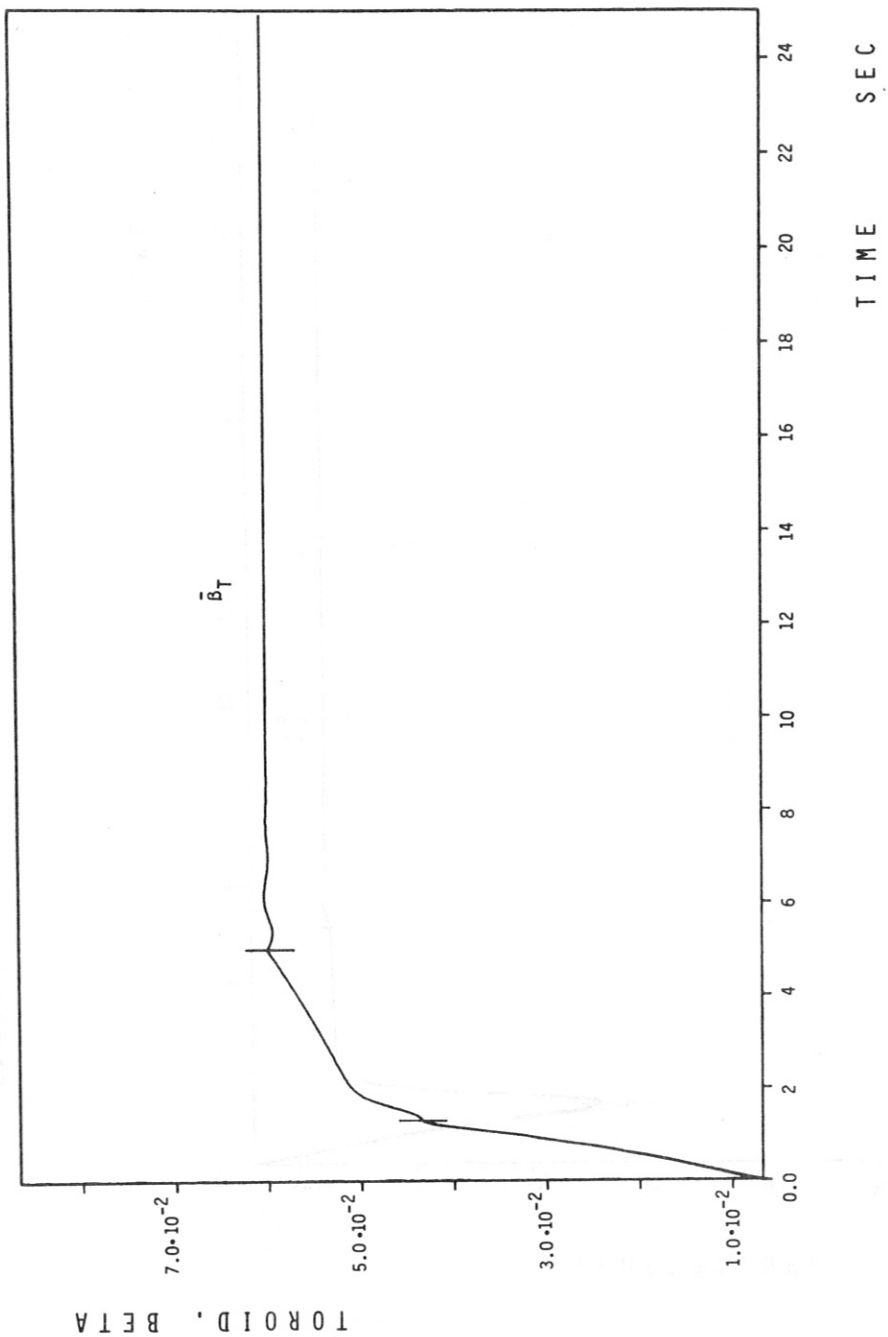

FIGURE 3

Reference case A. Time dependence of toroidal beta.

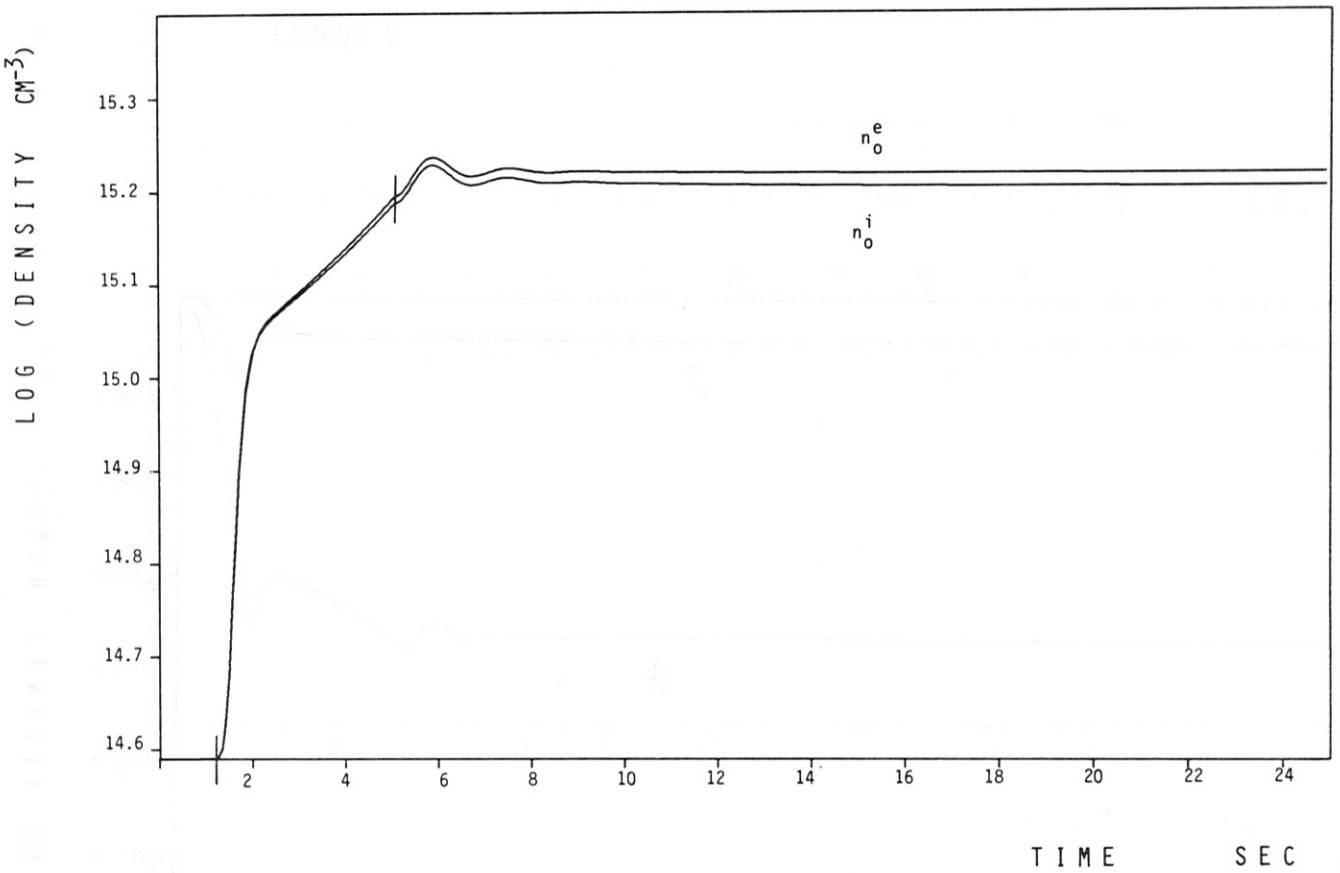

FIGURE 4

Reference case A. Time dependence of peak electron density (n_o^e) and peak ion density (n_o^i).

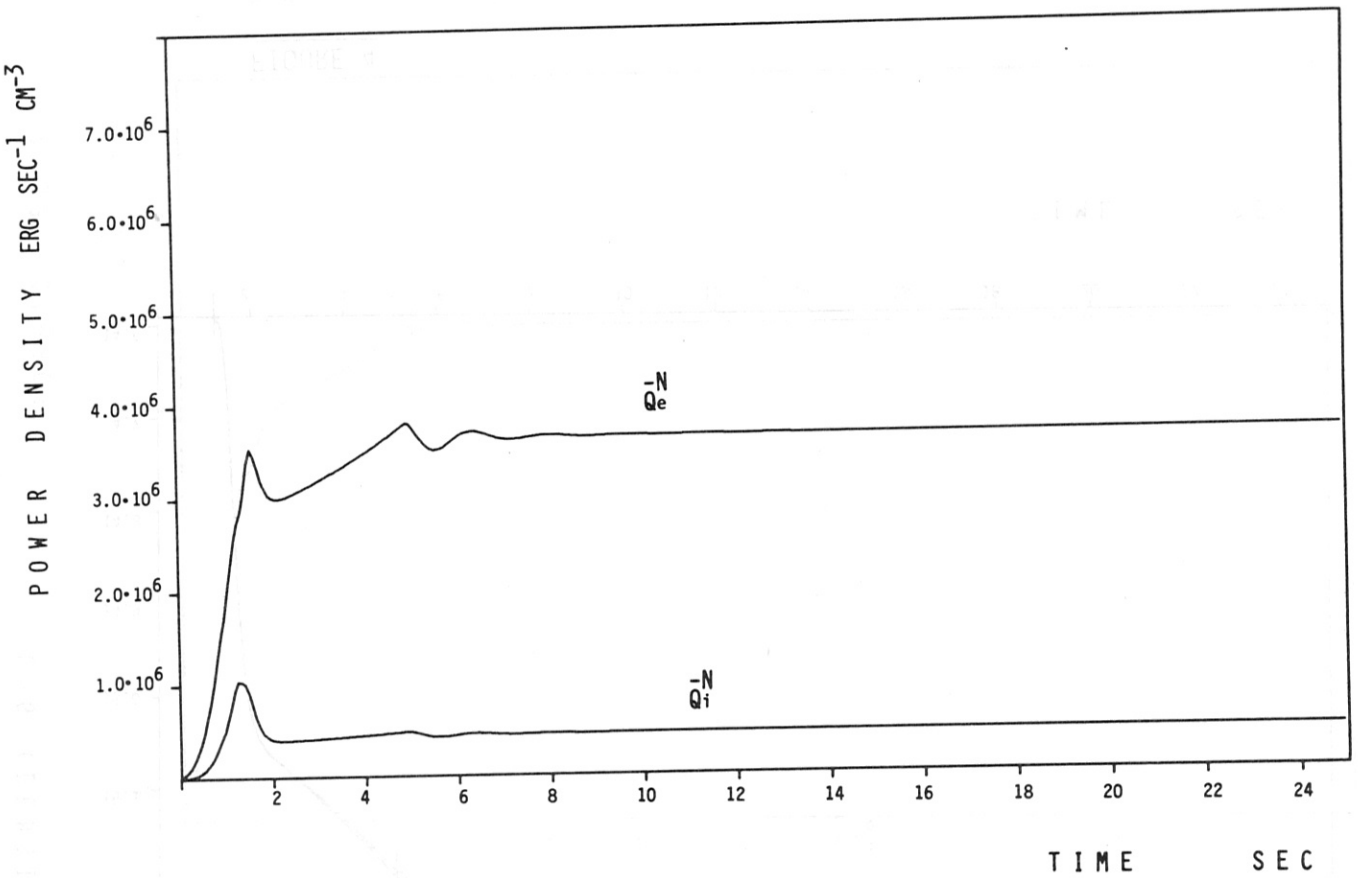

FIGURE 5

Reference case A. Time dependence of fusion power density going to electrons ($\bar{Q}_e^N$) and ions ($\bar{Q}_i^N$) respectively.

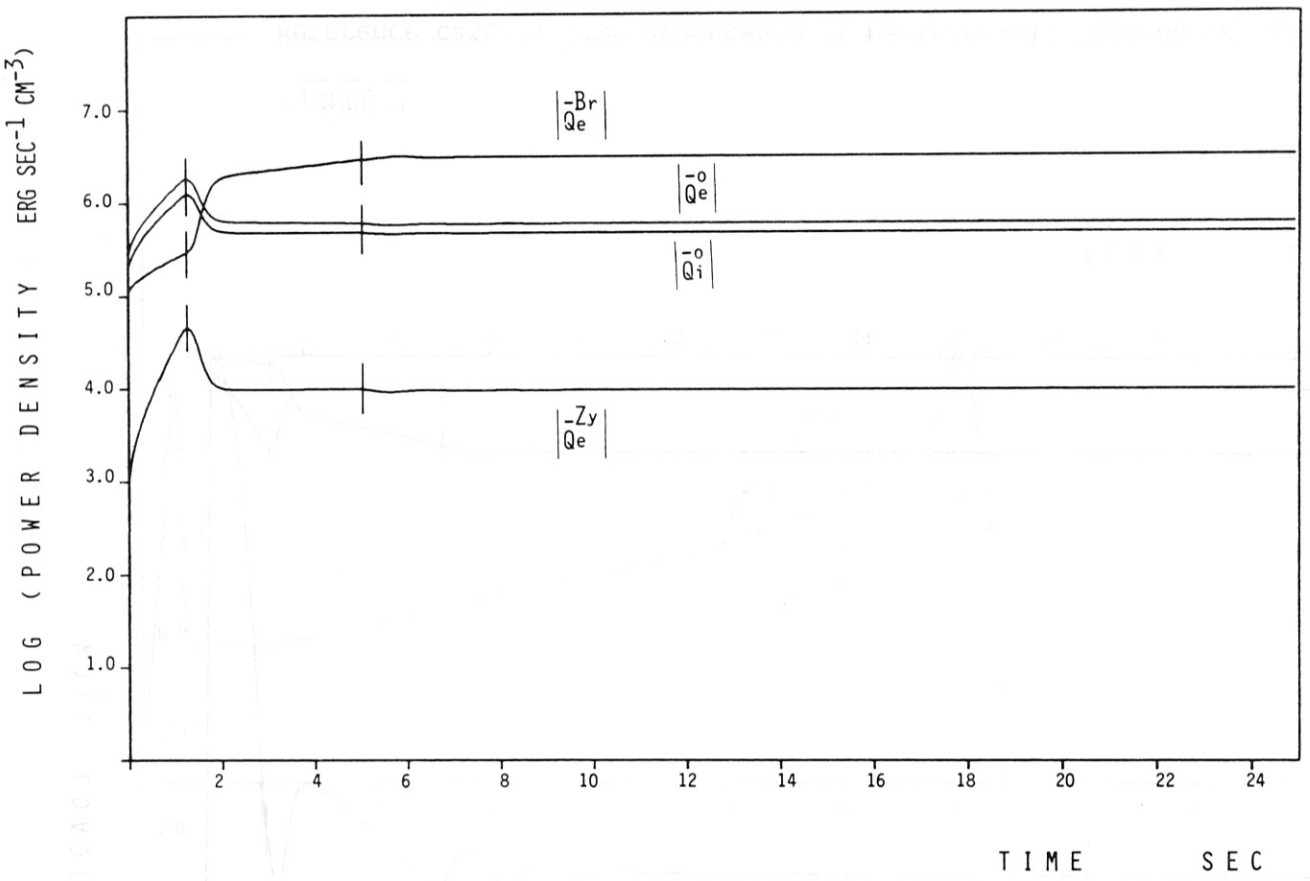

FIGURE 6

Reference case A. Time dependence of absolute value of bremsstrahlung losses ($/\bar{Q}_e^{Br}/$), transport losses ($/\bar{Q}_e^{o}/$, $/\bar{Q}_i^{o}/$) and cyclotron radiation losses $/\bar{Q}_e^{zy}/$.

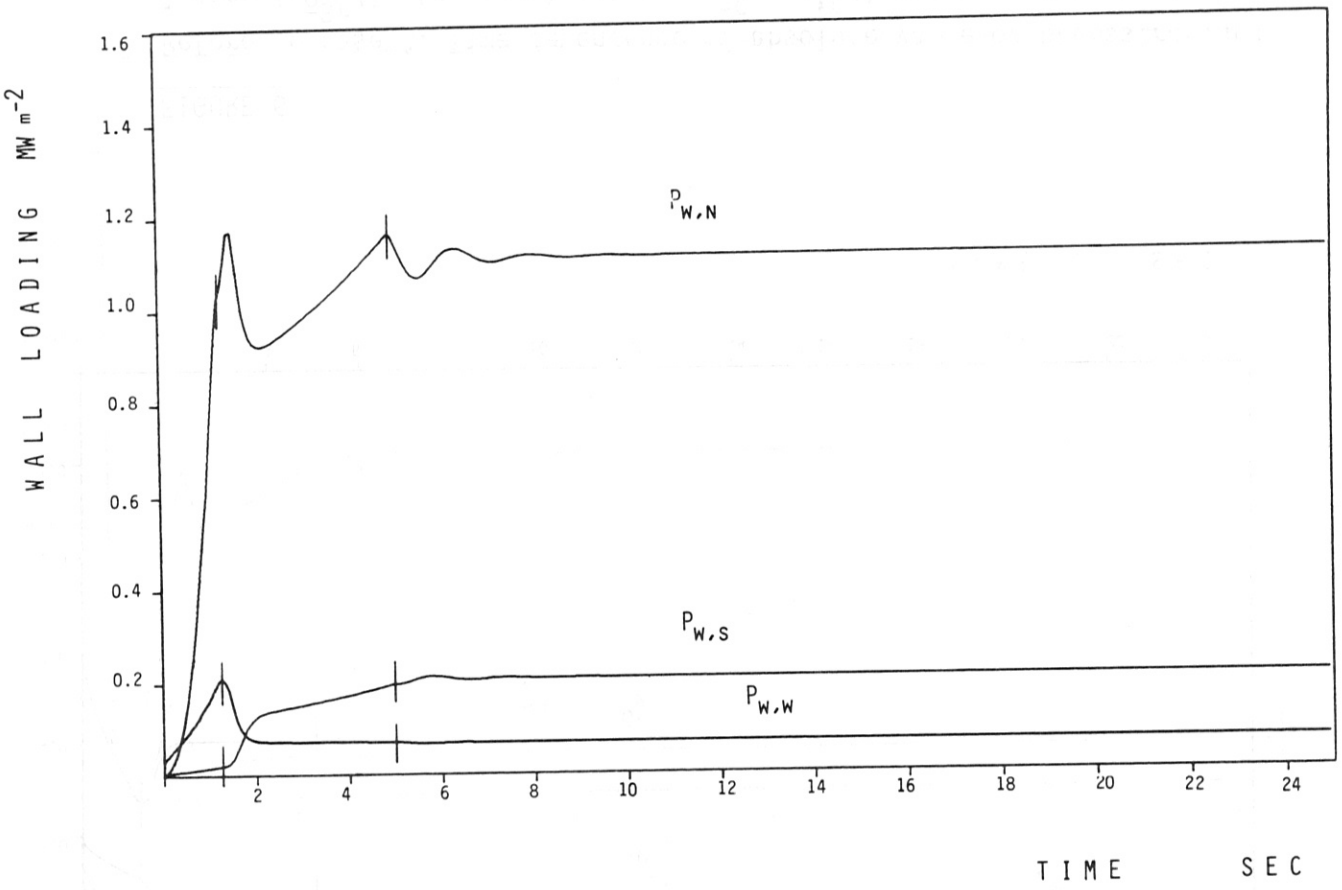

FIGURE 7

Reference case A. Time dependence of neutron wall loading ($P_{W,N}$), total radiation wall loading ($P_{W,S}$) and energy flow density due to transport, normalized to wall surface ($P_{W,W}$).

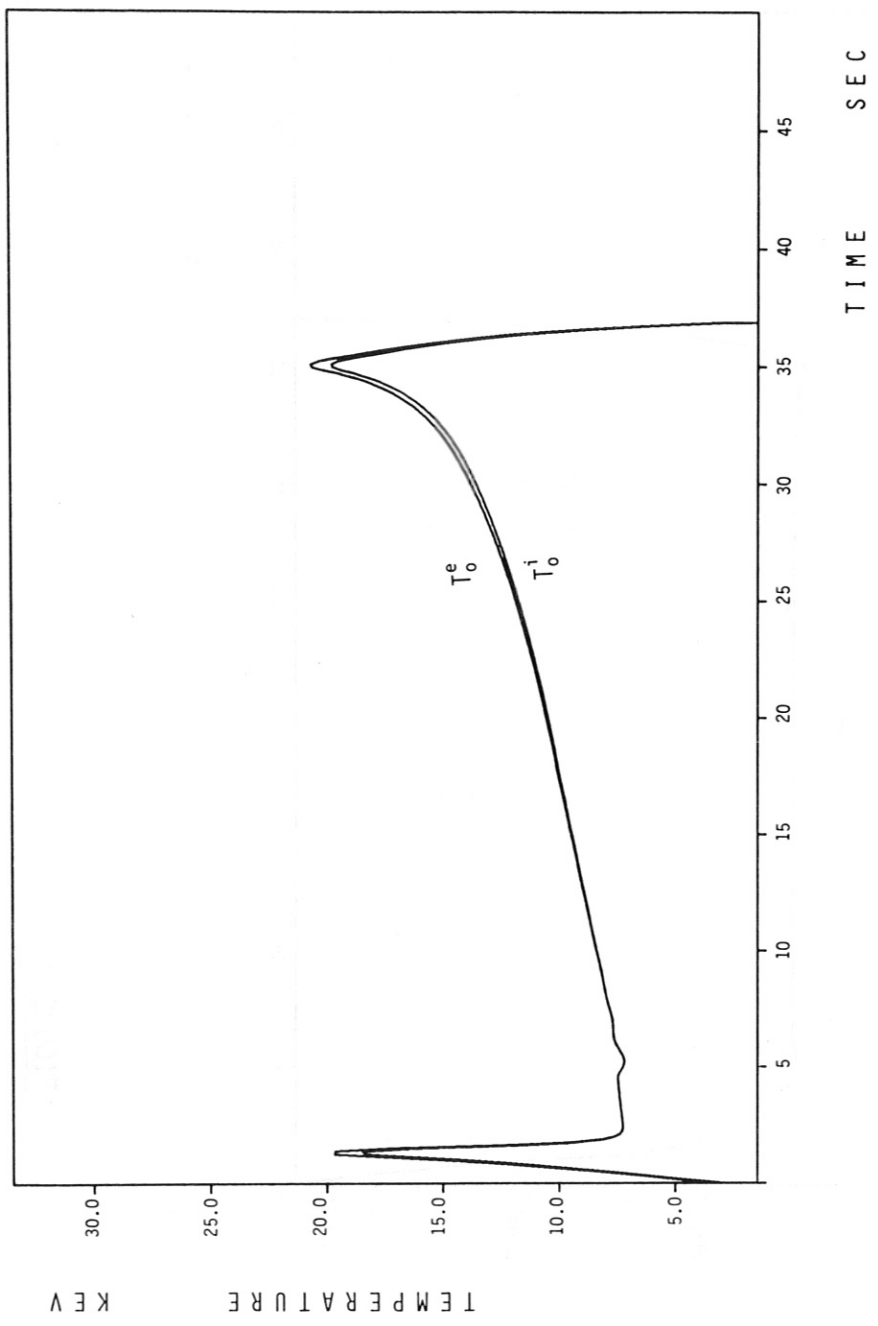

FIGURE 8

Reference case B. Time dependence of electron peak temperature (T_o^e) and ion peak temperature (T_o^i).

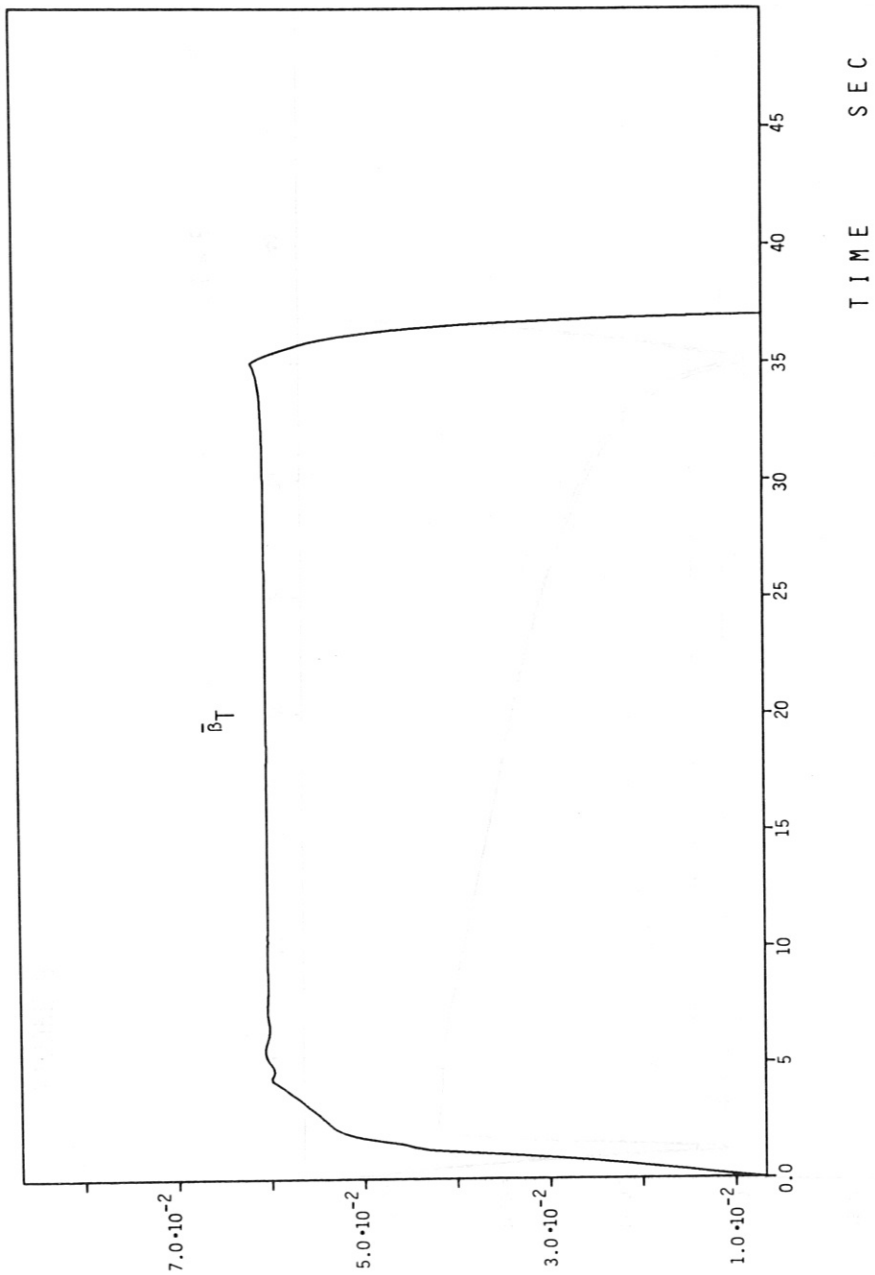

FIGURE 9

Reference case B. Time dependence of toroidal beta.

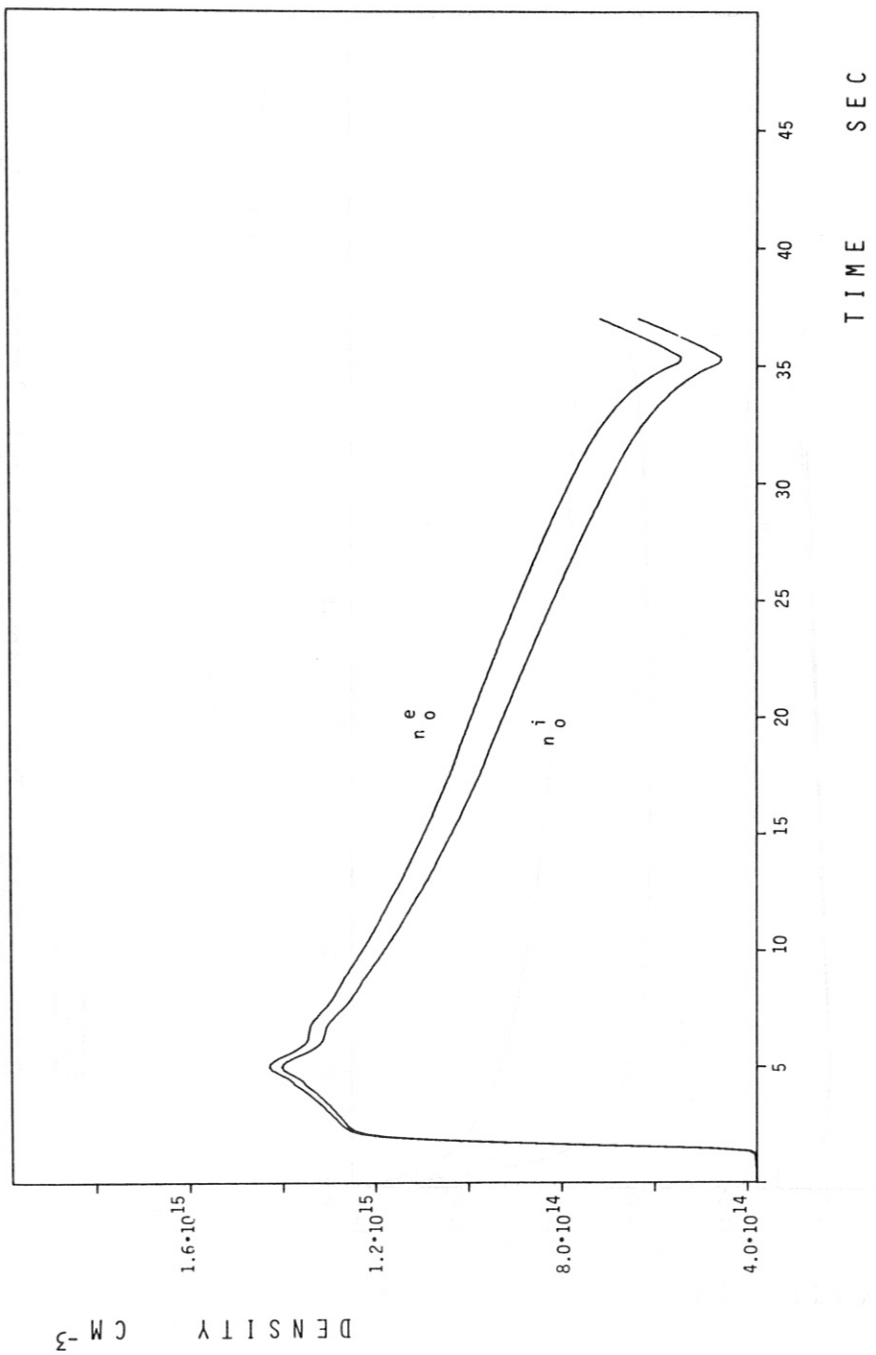

FIGURE 10

Reference case B. Time dependence of peak electron density (n_o^e) and peak fuel ion density (n_o^i).

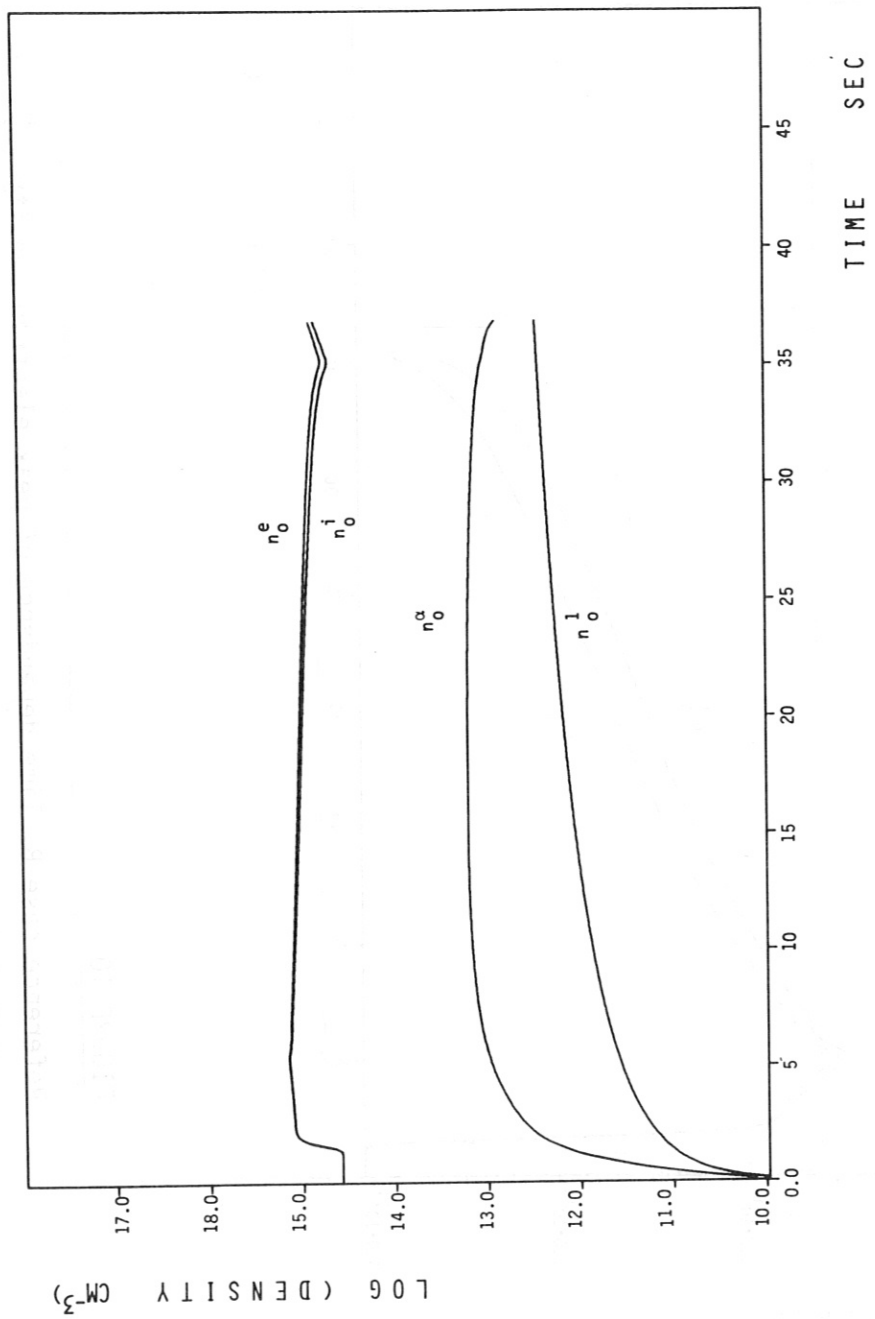

FIGURE 11

Reference case B. Time dependence of peak electron density (n_o^e), peak fuel ion density (n_o^i), peak α-density (n_o^α) and peak iron density (n_o^1)

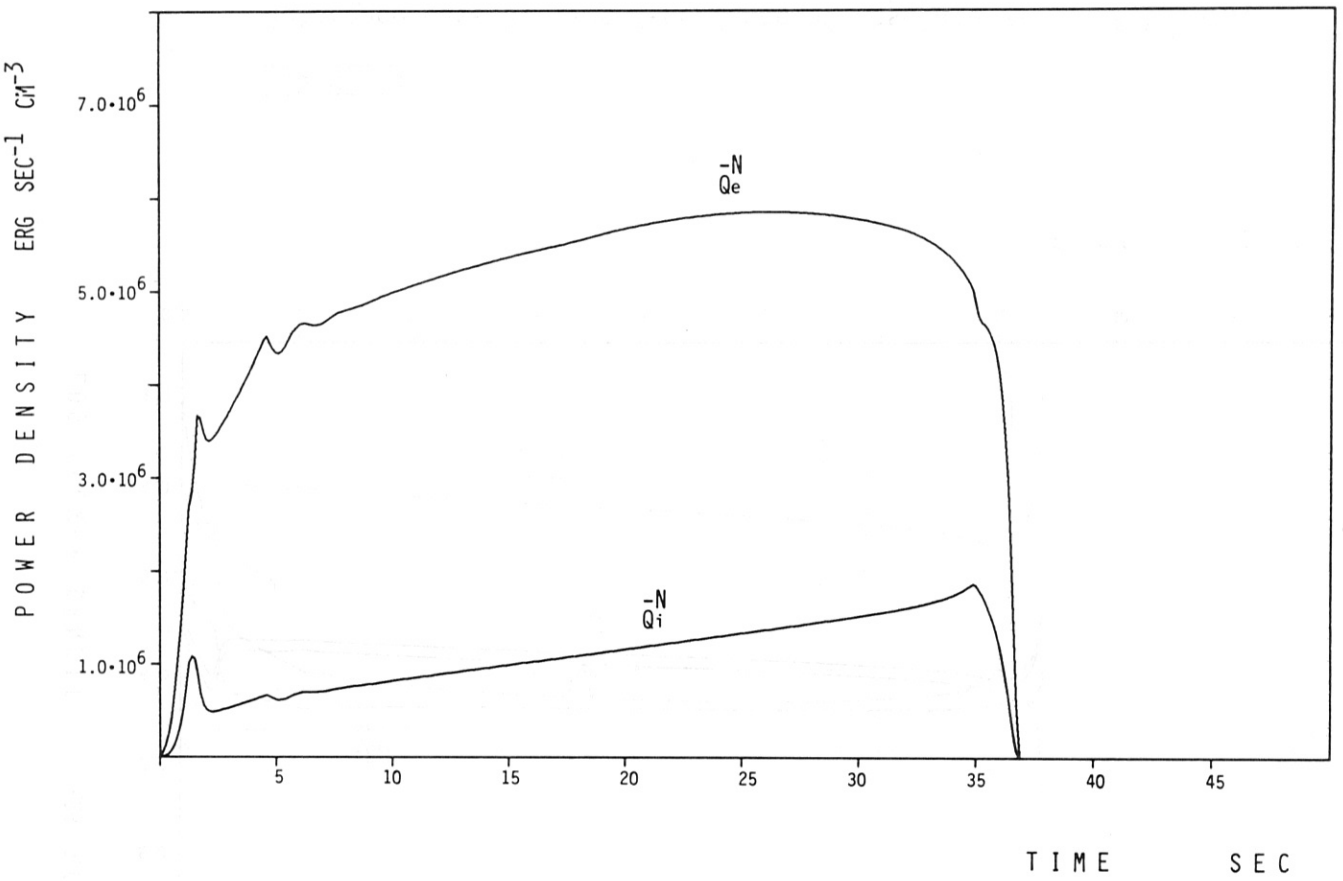

FIGURE 12

Reference case B. Time dependence of fusion power density going to electrons ($\bar{Q}_e^N$) and ions ($\bar{Q}_i^N$) respectively.

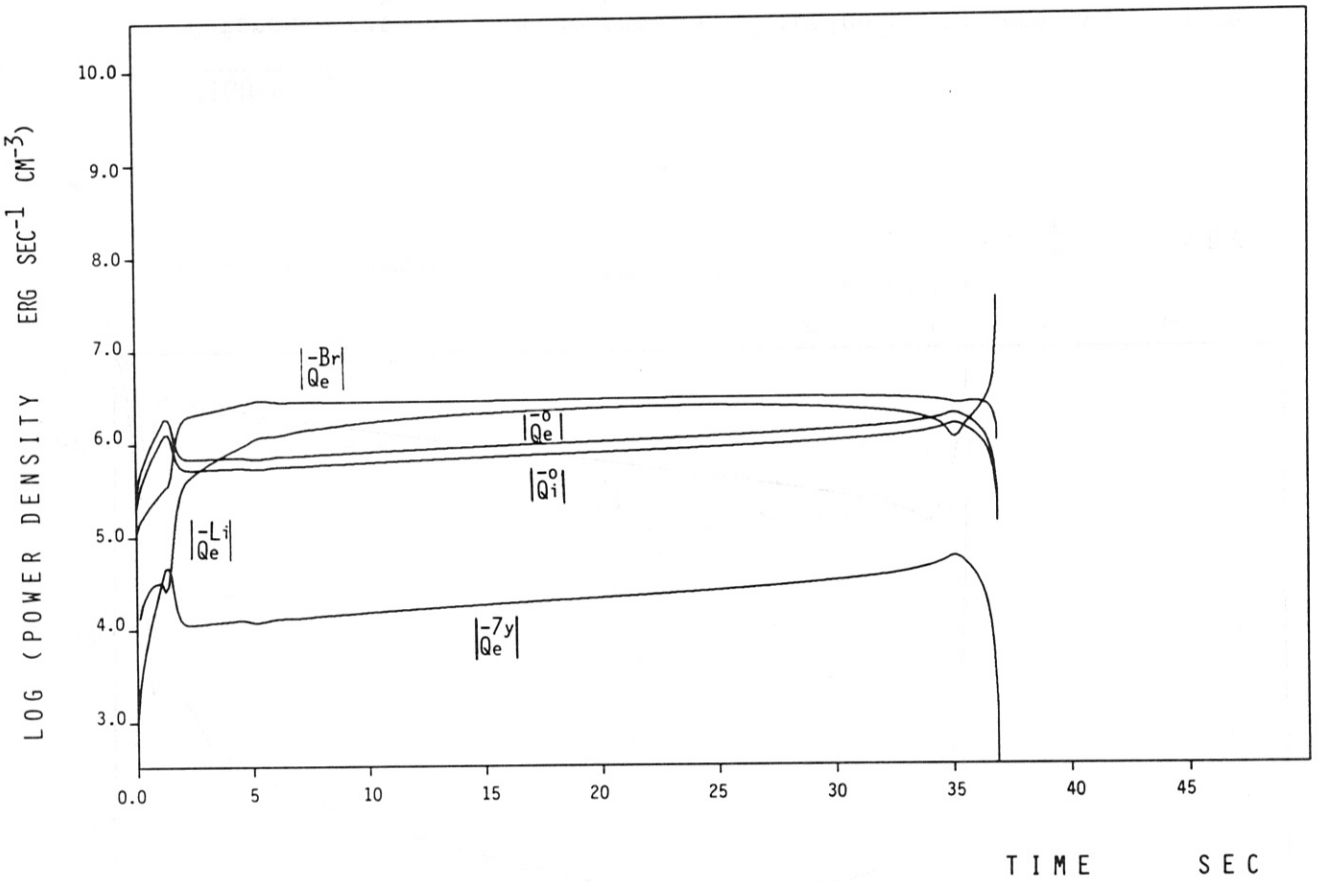

FIGURE 13

Reference case B. Time dependence of absolute value of bremsstrahlung losses ($/\bar{Q}_e^{Br}/$), line radiation losses ($/\bar{Q}_e^{Li}/$), transport losses ($/\bar{Q}_e^{o}/$, $/\bar{Q}_i^{o}/$) and cyclotron radiation losses ($/\bar{Q}_e^{Zy}/$).

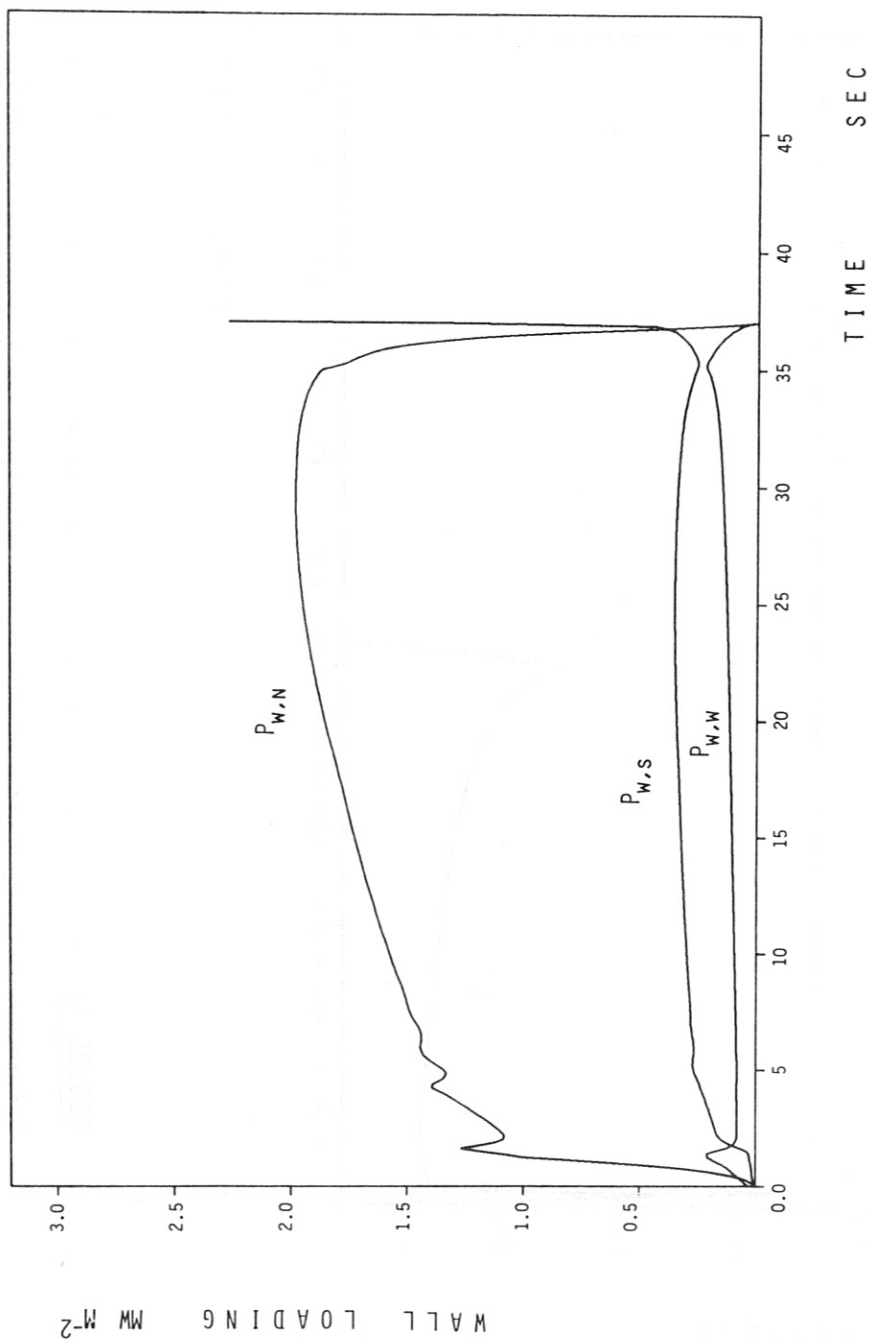

FIGURE 14

Reference case B. Time dependence of neutron wall loading ($P_{W,N}$), total radiation wall loading ($P_{W,S}$) and energy flow density due to transport, normalized to wall surface ($P_{W,W}$).

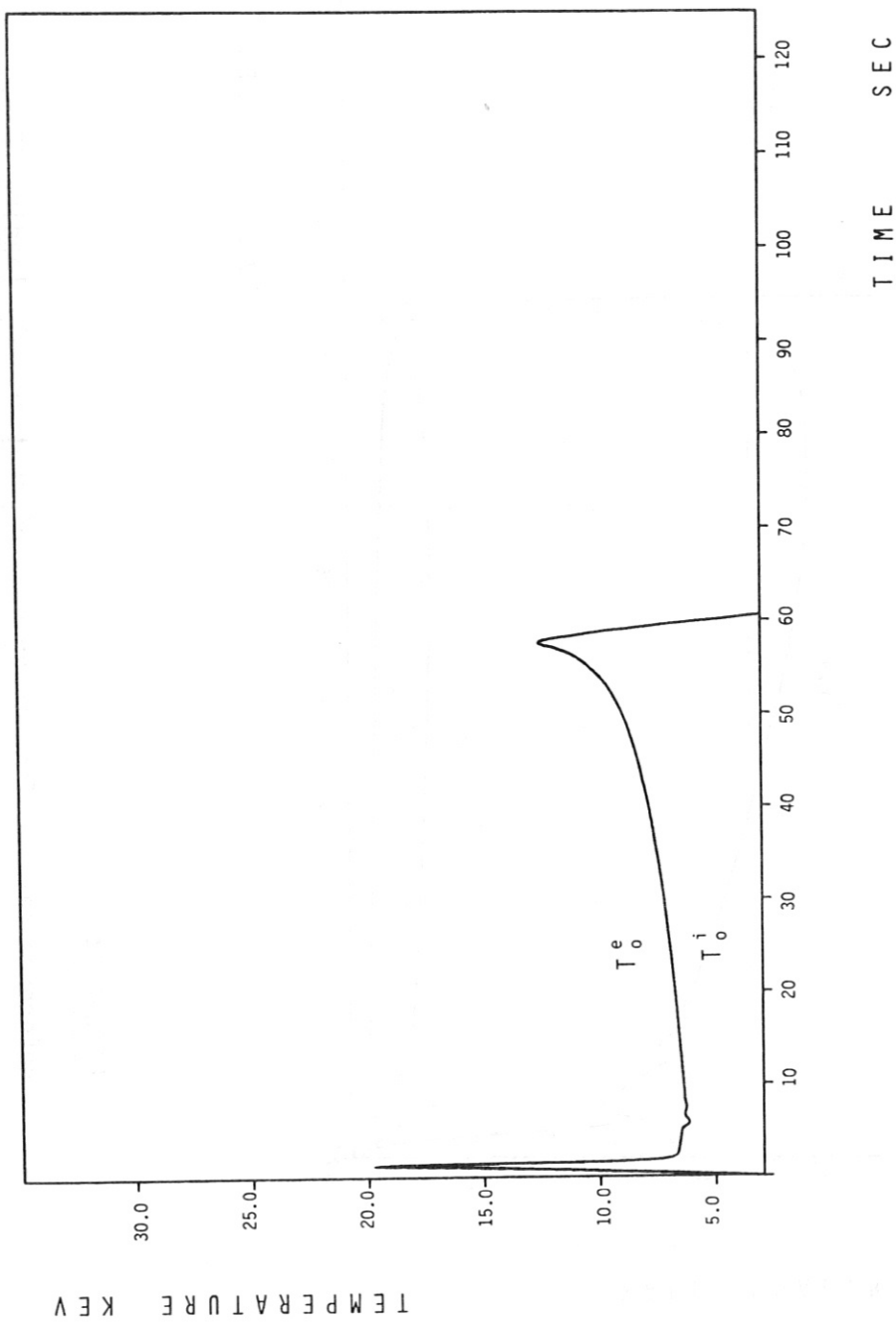

FIGURE 15

Reference case C. Time dependence of electron peak temperature (T_o^e) and ion peak temperature (T_o^i).

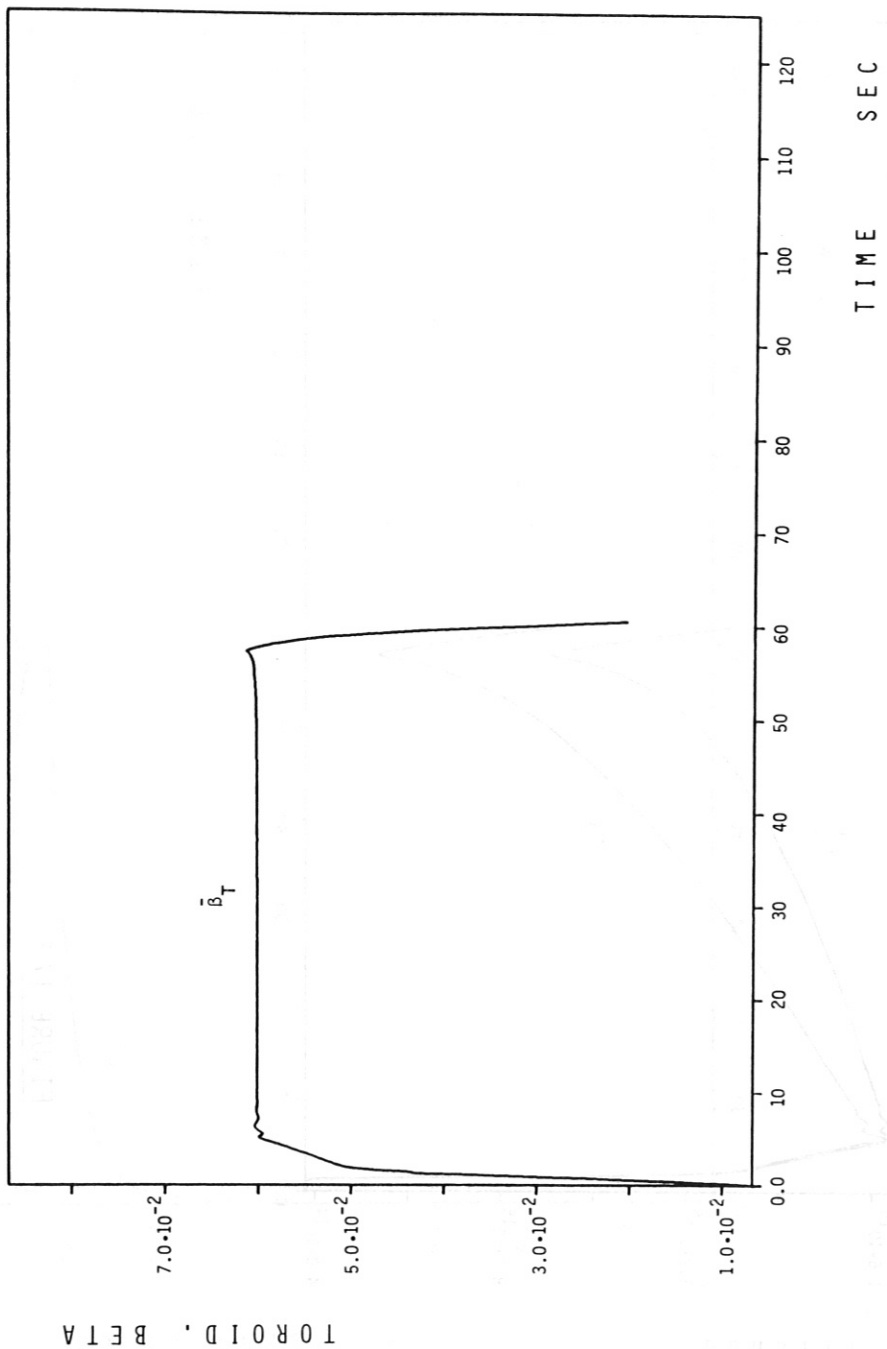

FIGURE 16

Reference case C. Time dependence of toroidal beta.

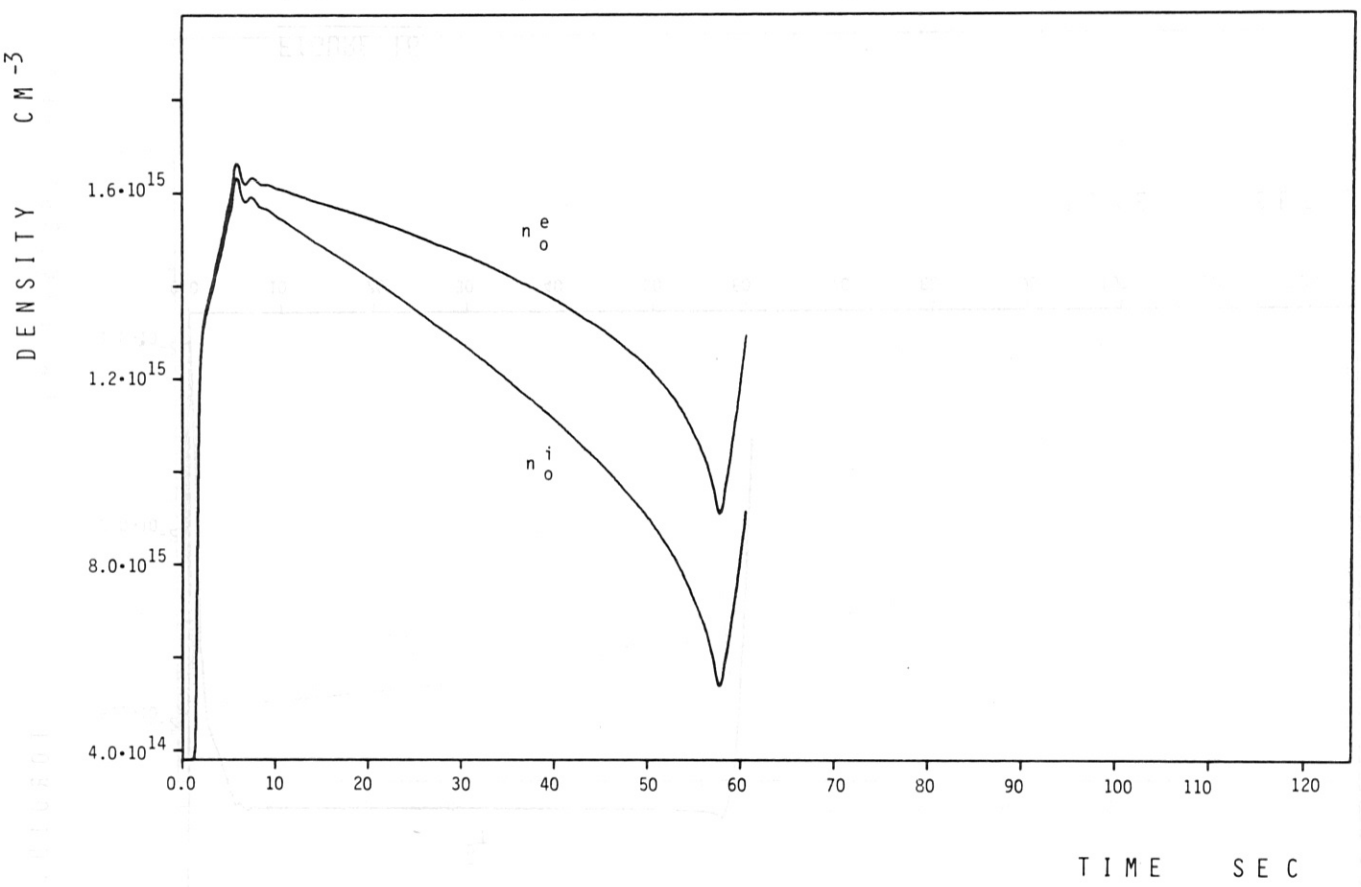

FIGURE 17

Reference case C. Time dependence of peak electron density (n_o^e) and peak fuel ion density (n_o^i).

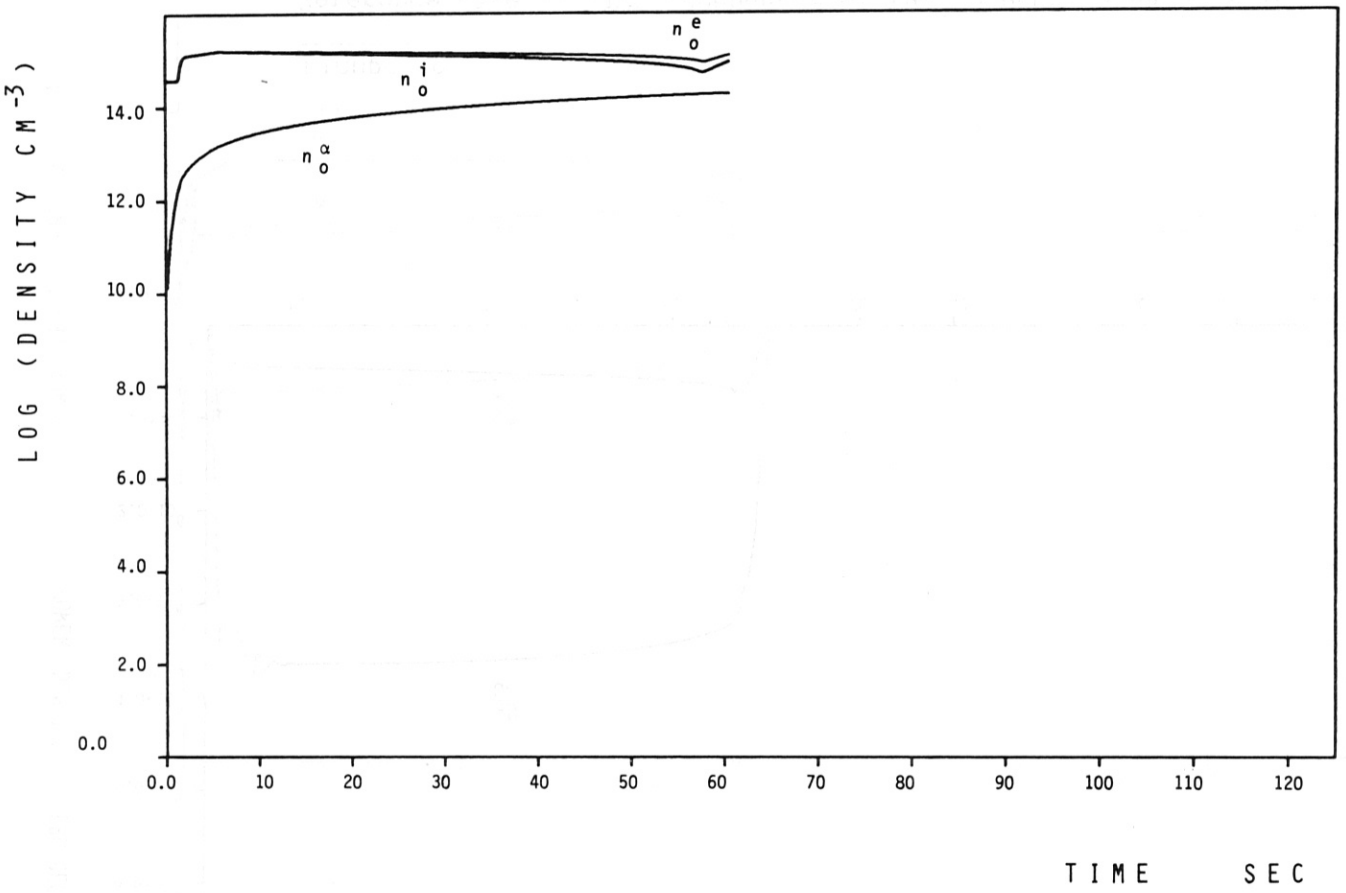

FIGURE 18

Reference case C. Time dependence of peak electron density (n_o^e), peak fuel ion density (n_o^i) and peak α-particle density (n_o^α).

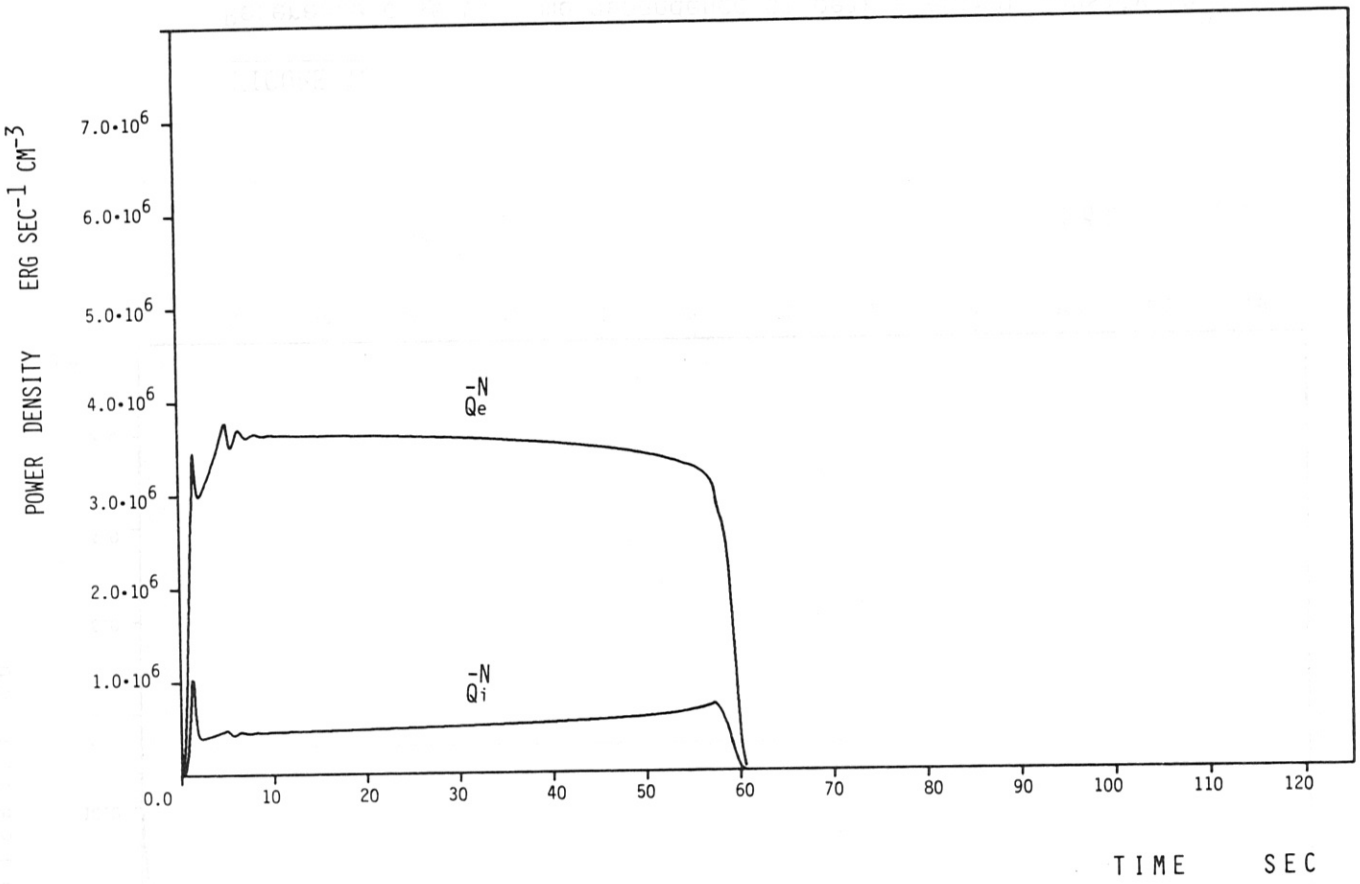

FIGURE 19

Reference case C. Time dependence of fusion power density going to electrons ($\bar{Q}_e^N$) and ions ($\bar{Q}_i^N$) respectively.

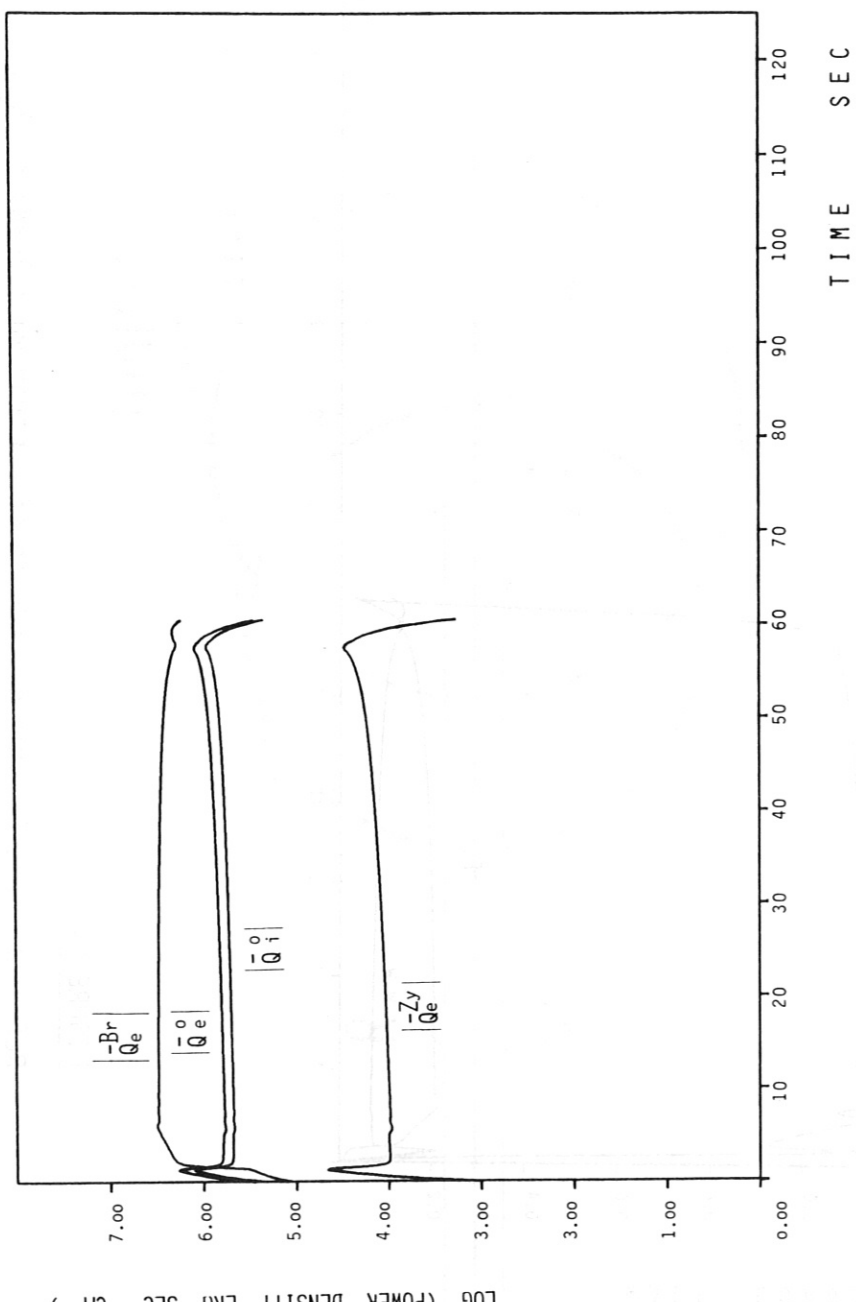

FIGURE 20

Reference case C. Time dependence of absolute value of bremsstrahlung losses ($/\bar{Q}_e^{Br}/$, transport losses ($/\bar{Q}_e^o/$, $/\bar{Q}_i^o/$) and cyclotron radiation ($/\bar{Q}_e^{Zy}/$).

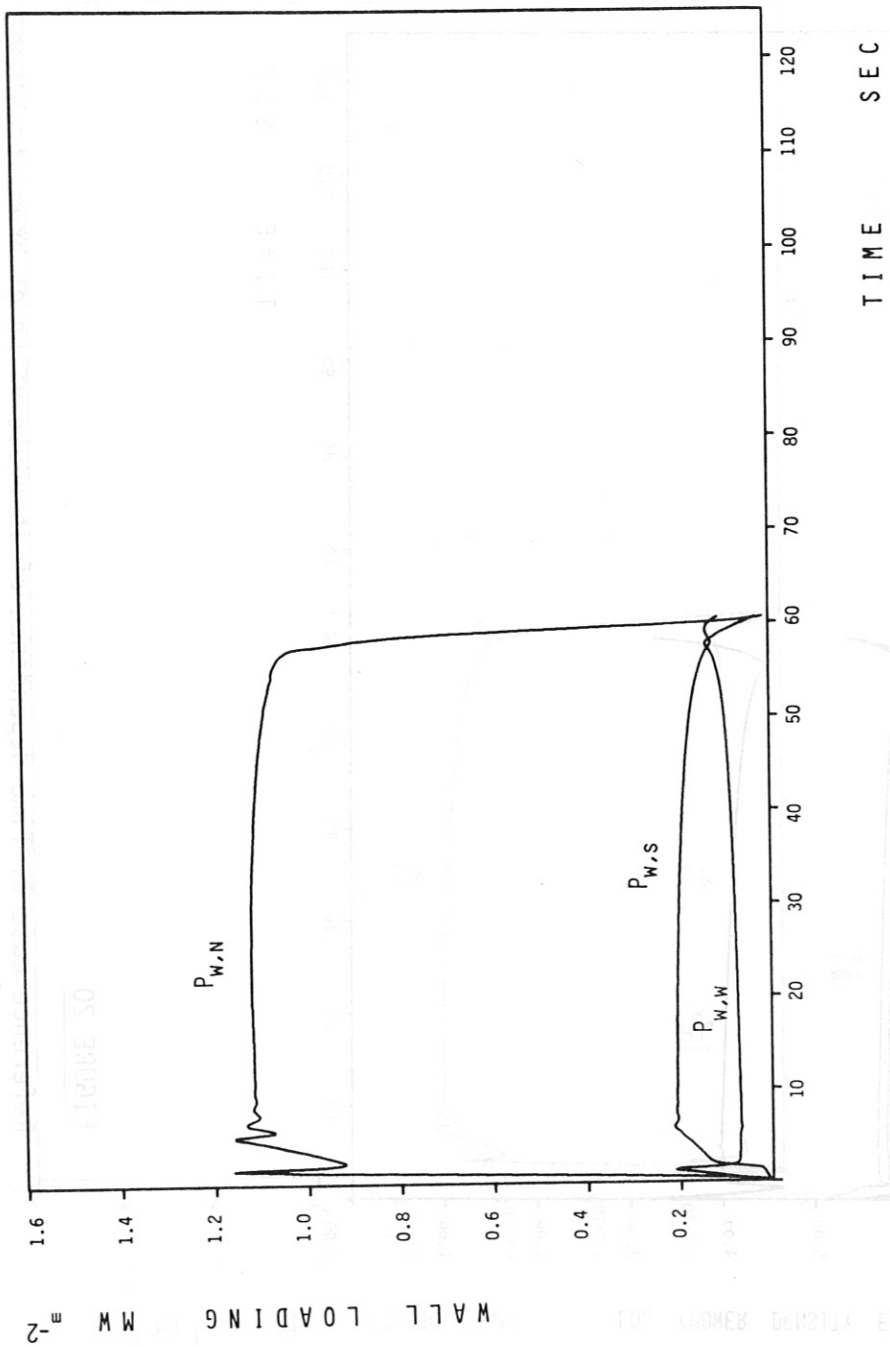

FIGURE 21

Reference case C. Time dependence of neutron wall loading ($P_{W,N}$), total radiation wall loading ($P_{W,S}$) and energy flow density due to transport, normalized to wall surface ($P_{W,W}$).

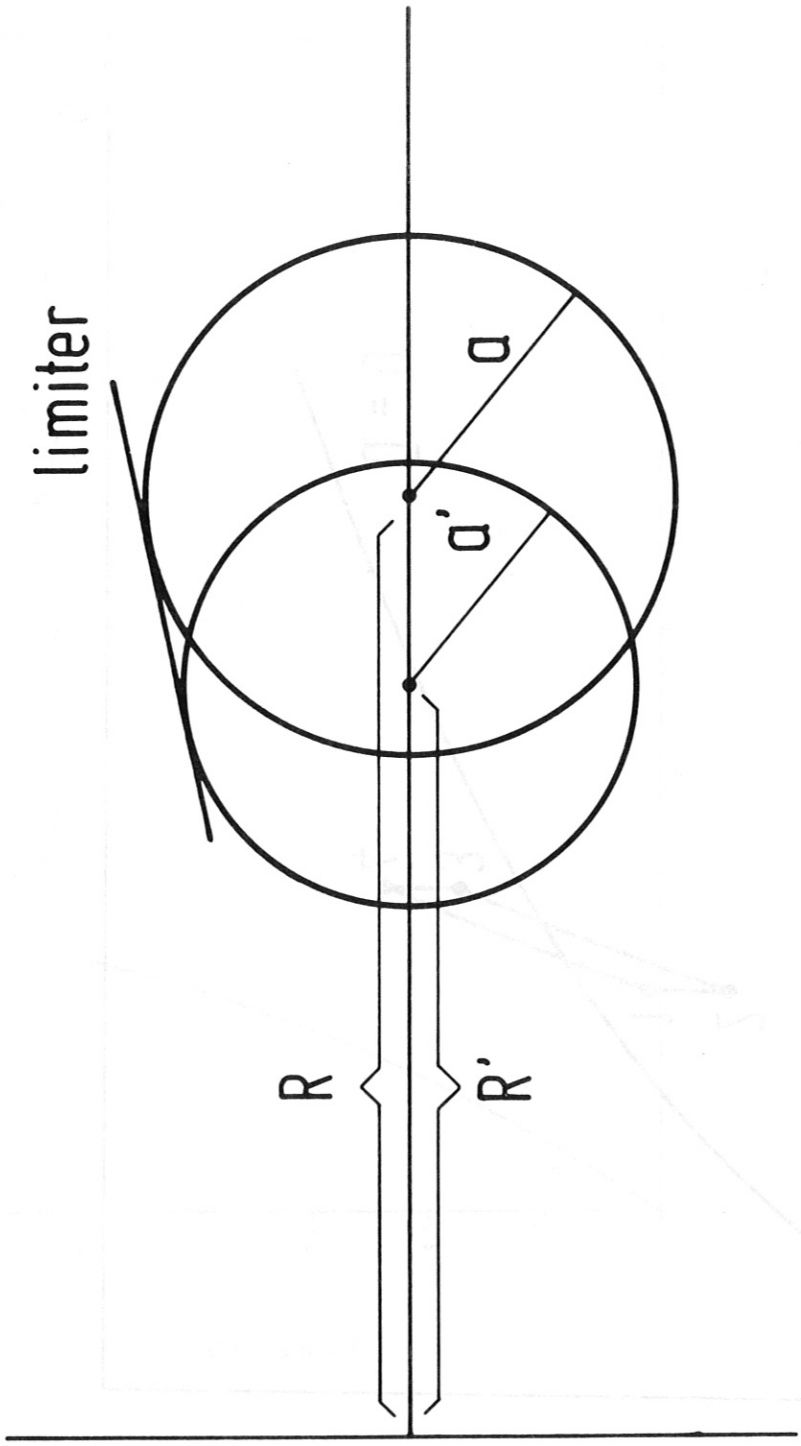

FIGURE 22

Schematic limiter configuration used in the compression-decompression control scheme.

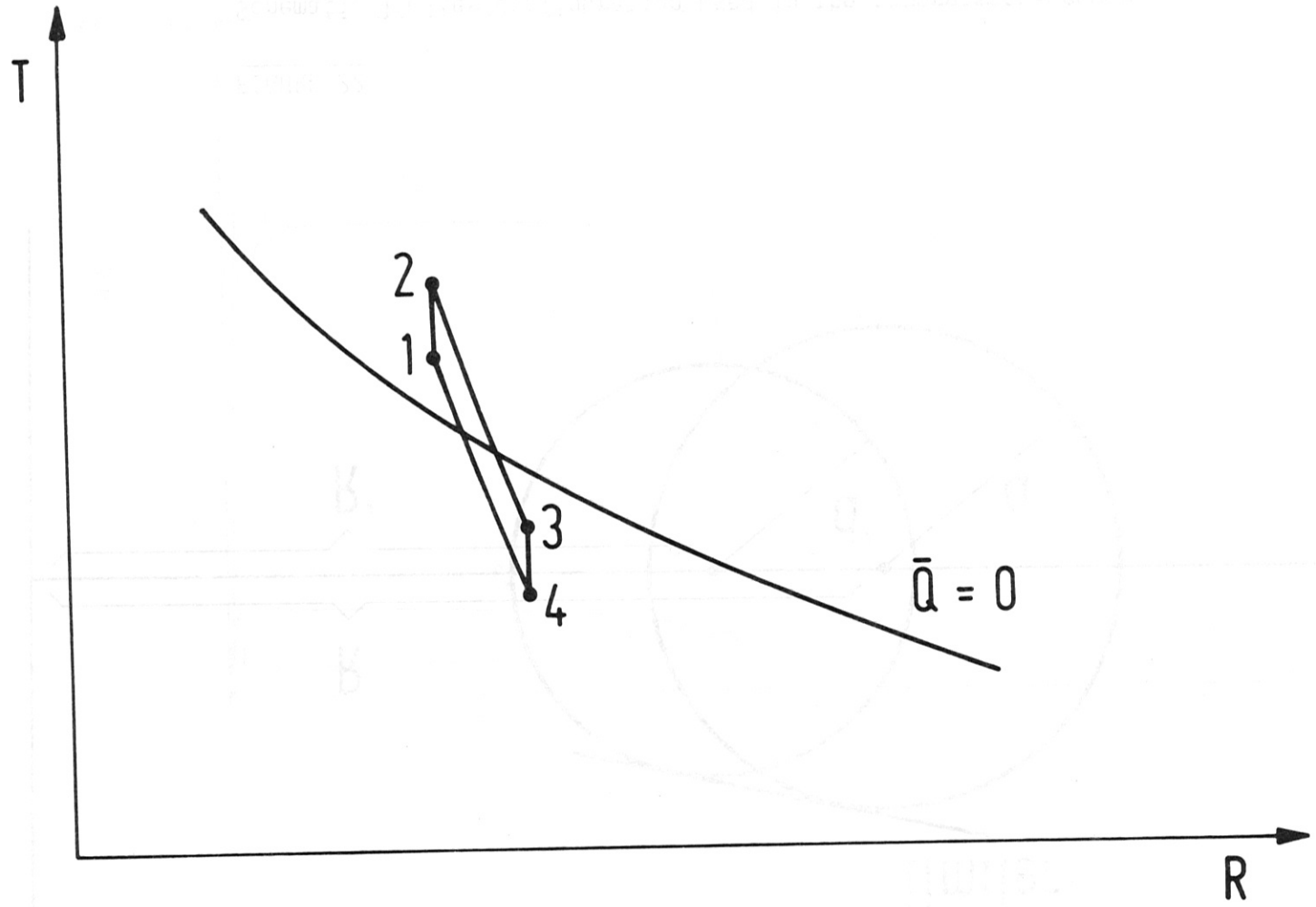

FIGURE 23

Schematic description of the control cycle used in the compression--decompression control scheme.

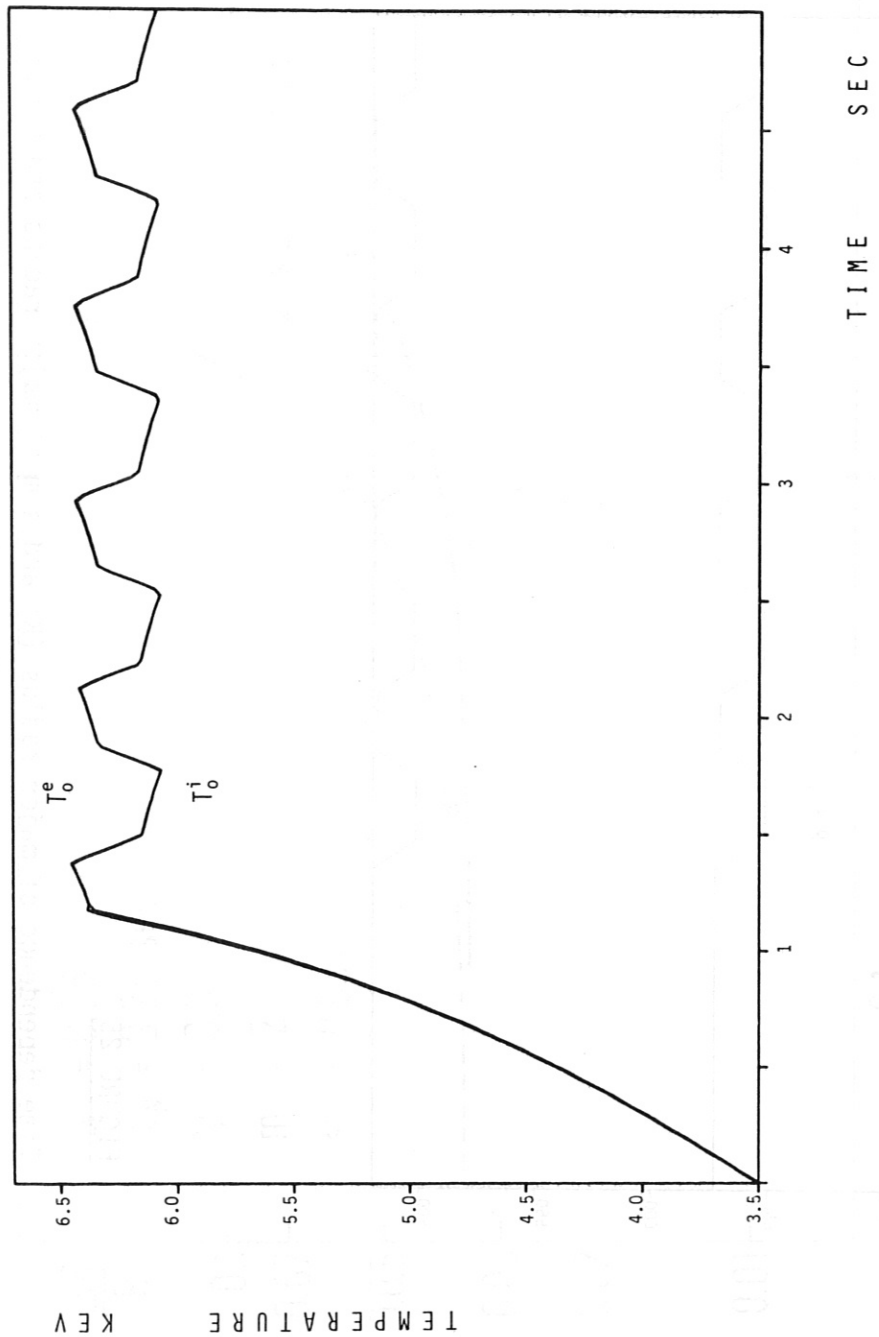

FIGURE 24

Time dependence of peak electron temperature (T_o^e) and peak ion temperature (T_o^i) in an INTOR-like system with burn control by cyclic major radius compression and decompression. τ_R = 3 sec.

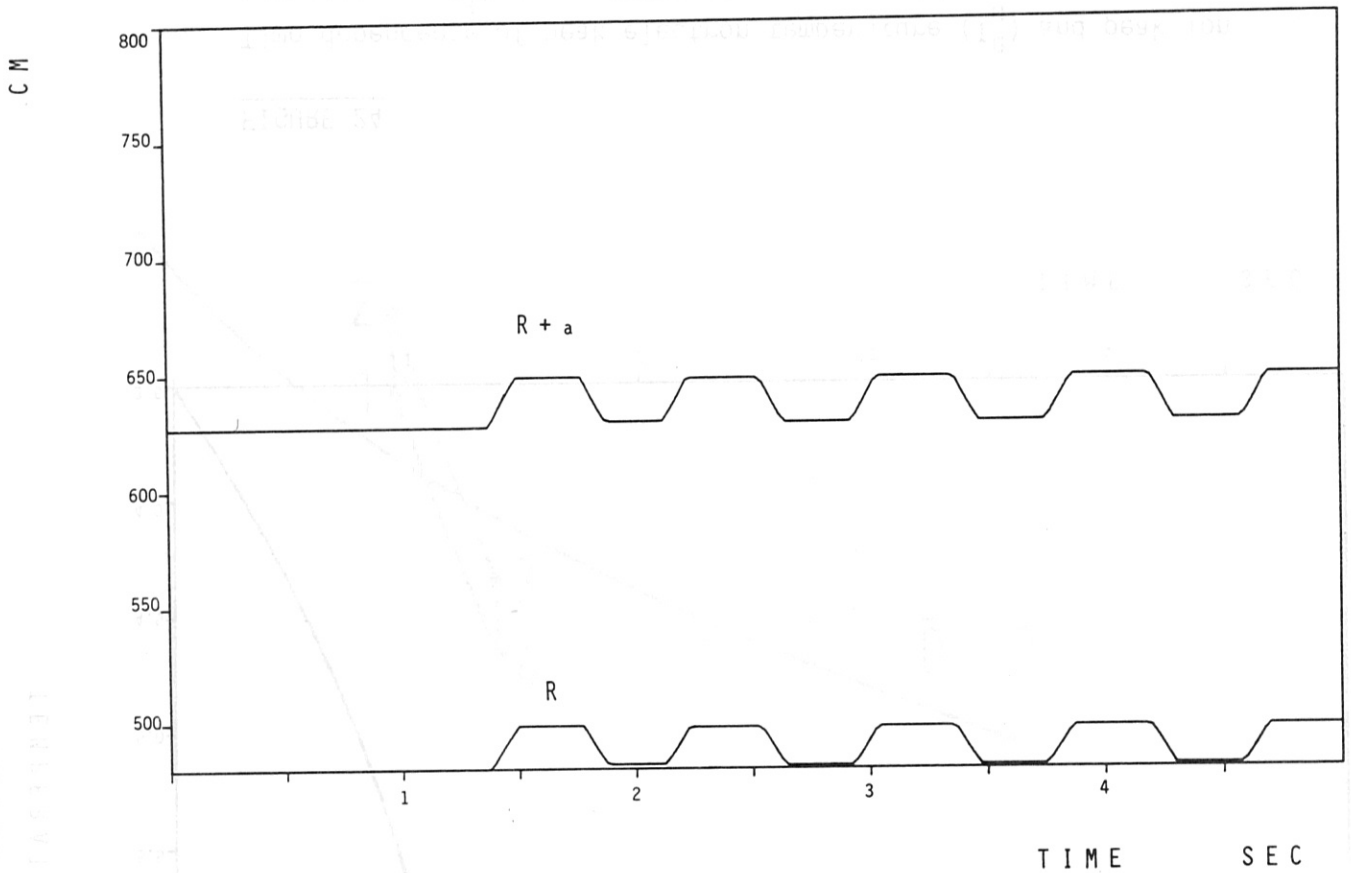

FIGURE 25

Time dependence of major radius (R) and sum of major radius and minor radius (R+a) in the system of figure 24.

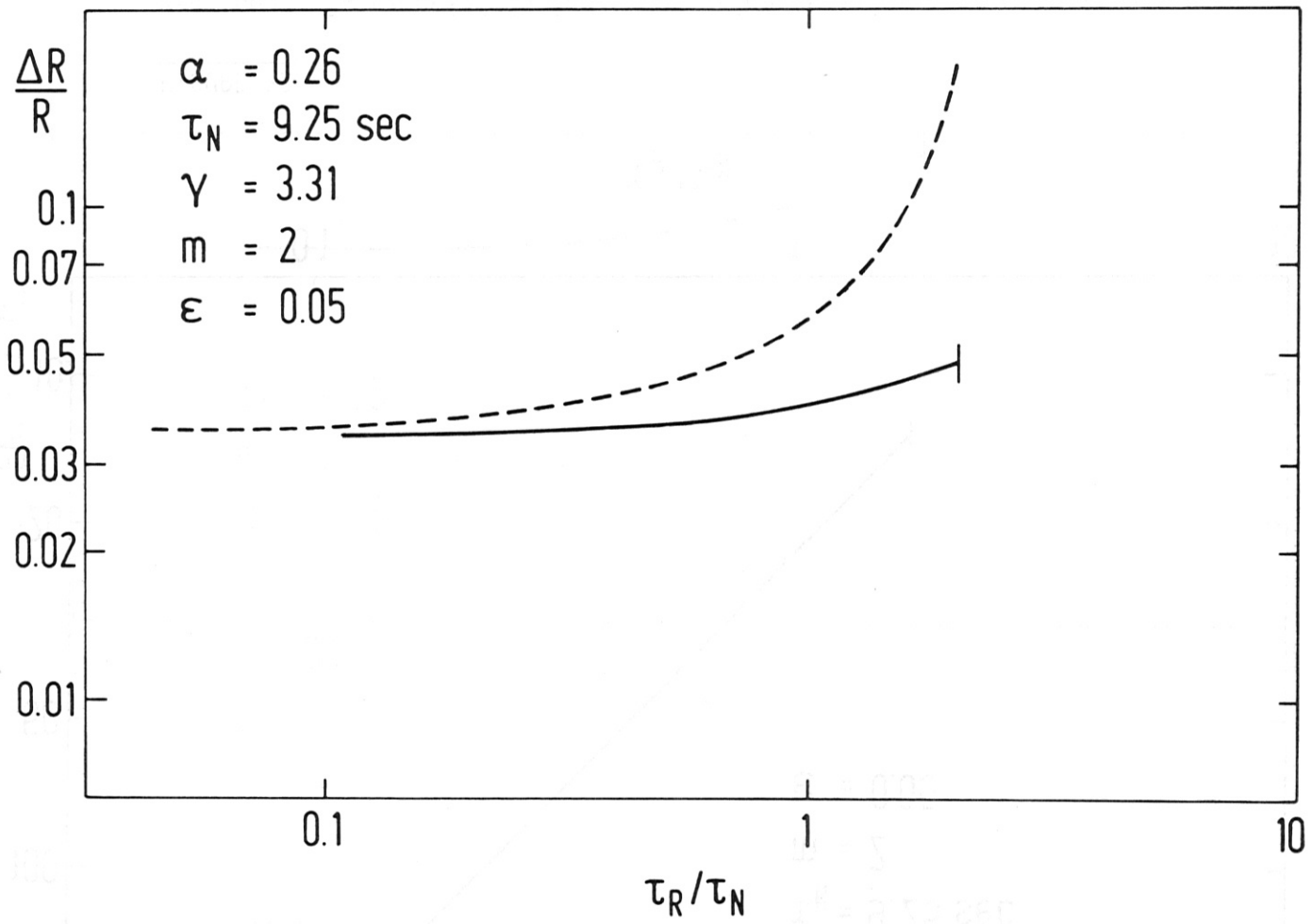

FIGURE 26

ΔR/R as a function of τ_R/τ_N.— numerical result. ---- analytical result. | marks the stability limit.

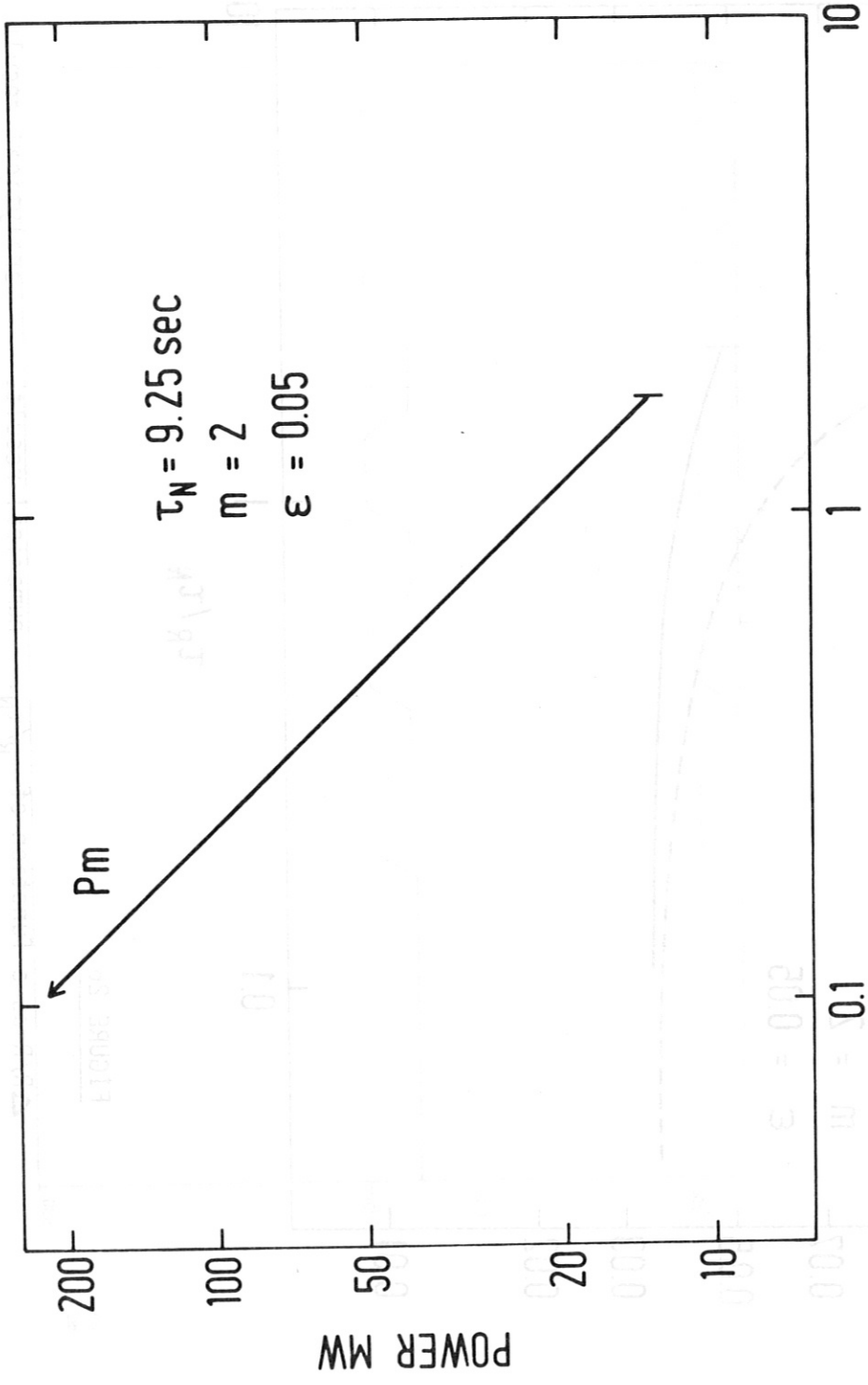

FIGURE 27

Peak power P_m requried during compression as a function of compression velocity. | marks the stability limit.

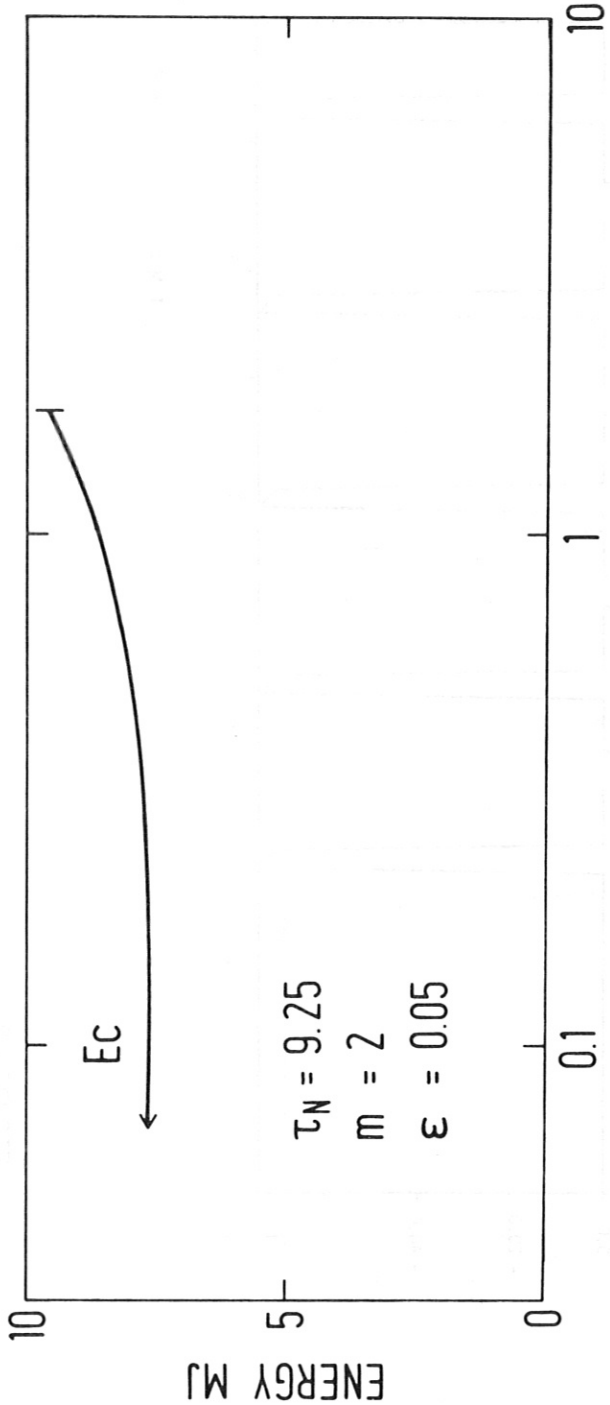

FIGURE 28

Energy E_c transferred in the compression phase as a function of the compression velocity. | marks the stability limit.

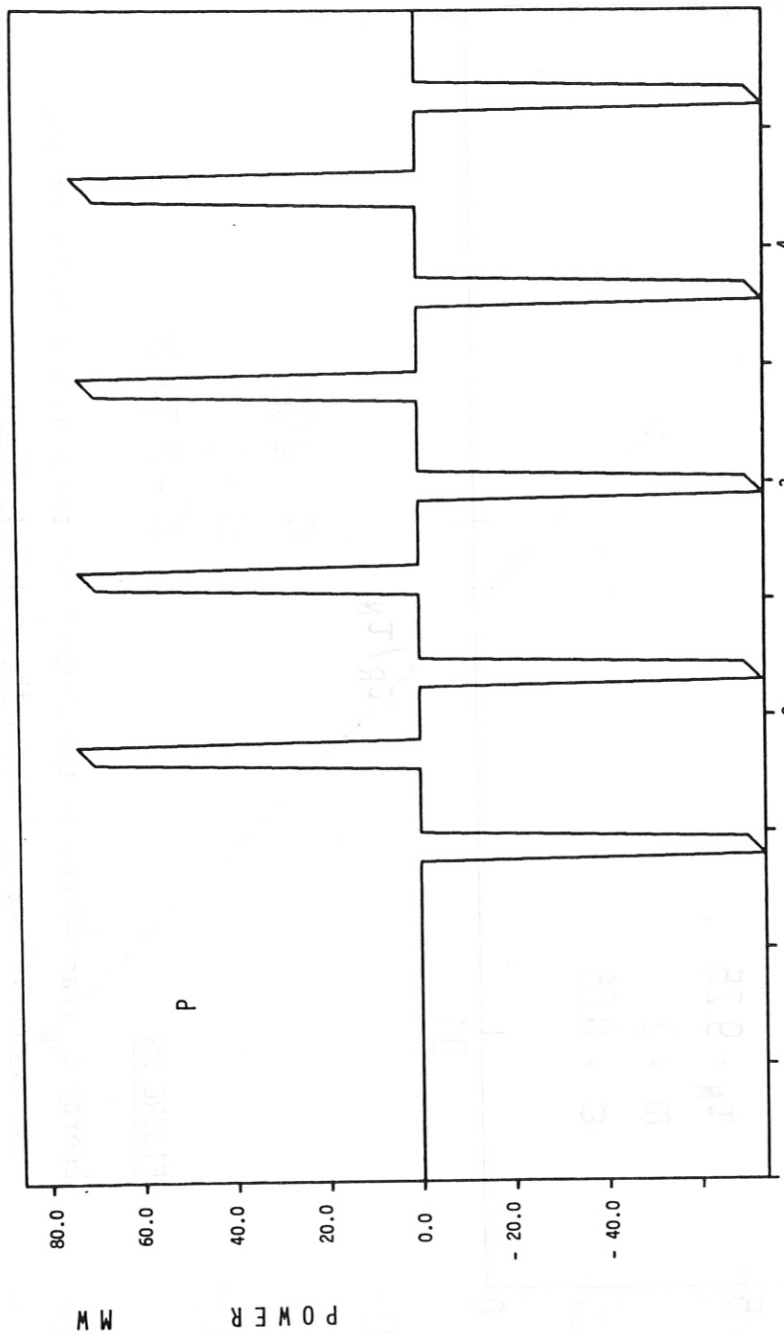

FIGURE 29

Time dependence of electric power P required for compression-decompression control.

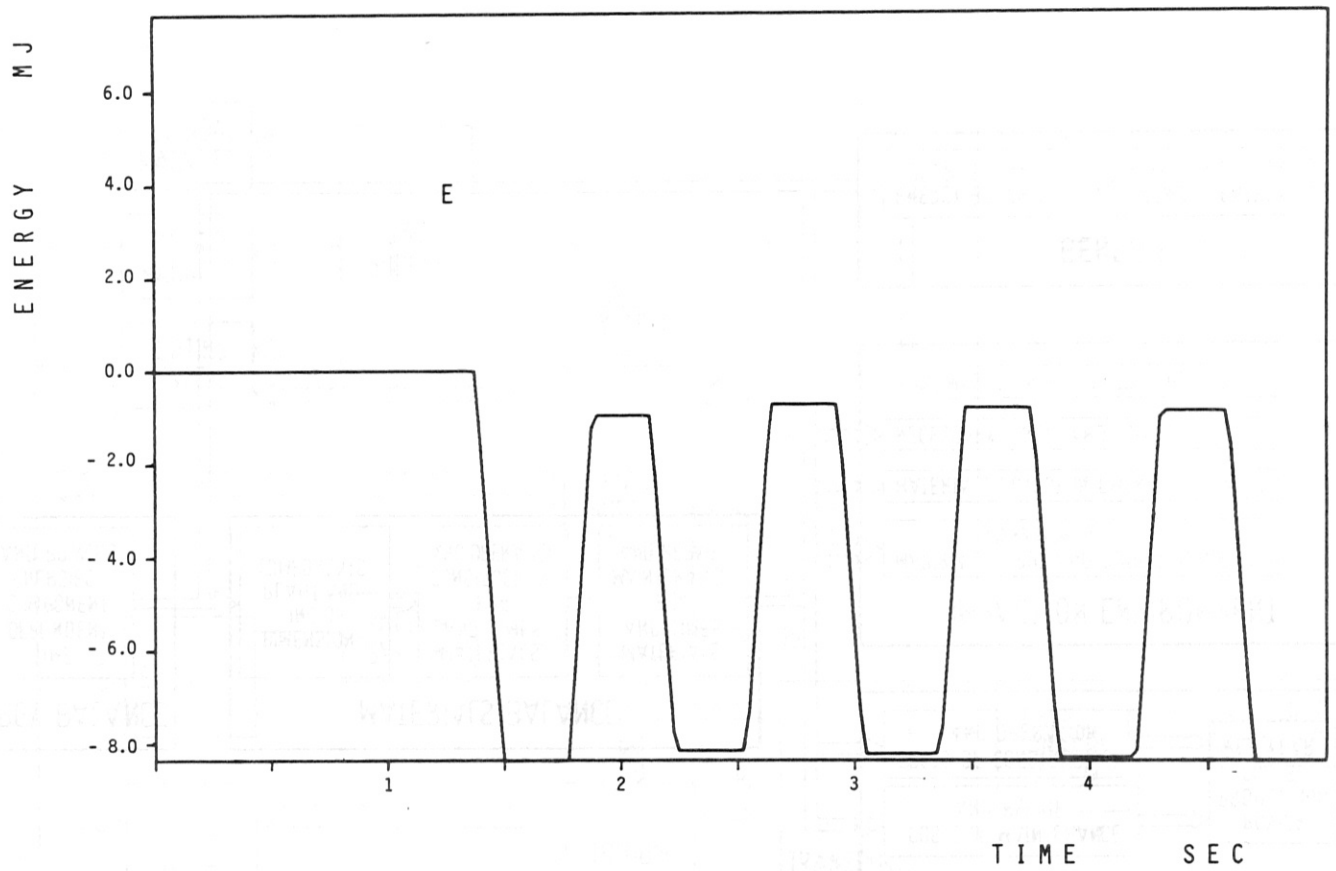

FIGURE 30

Time dependence of electric energy required for compression-decompression control.

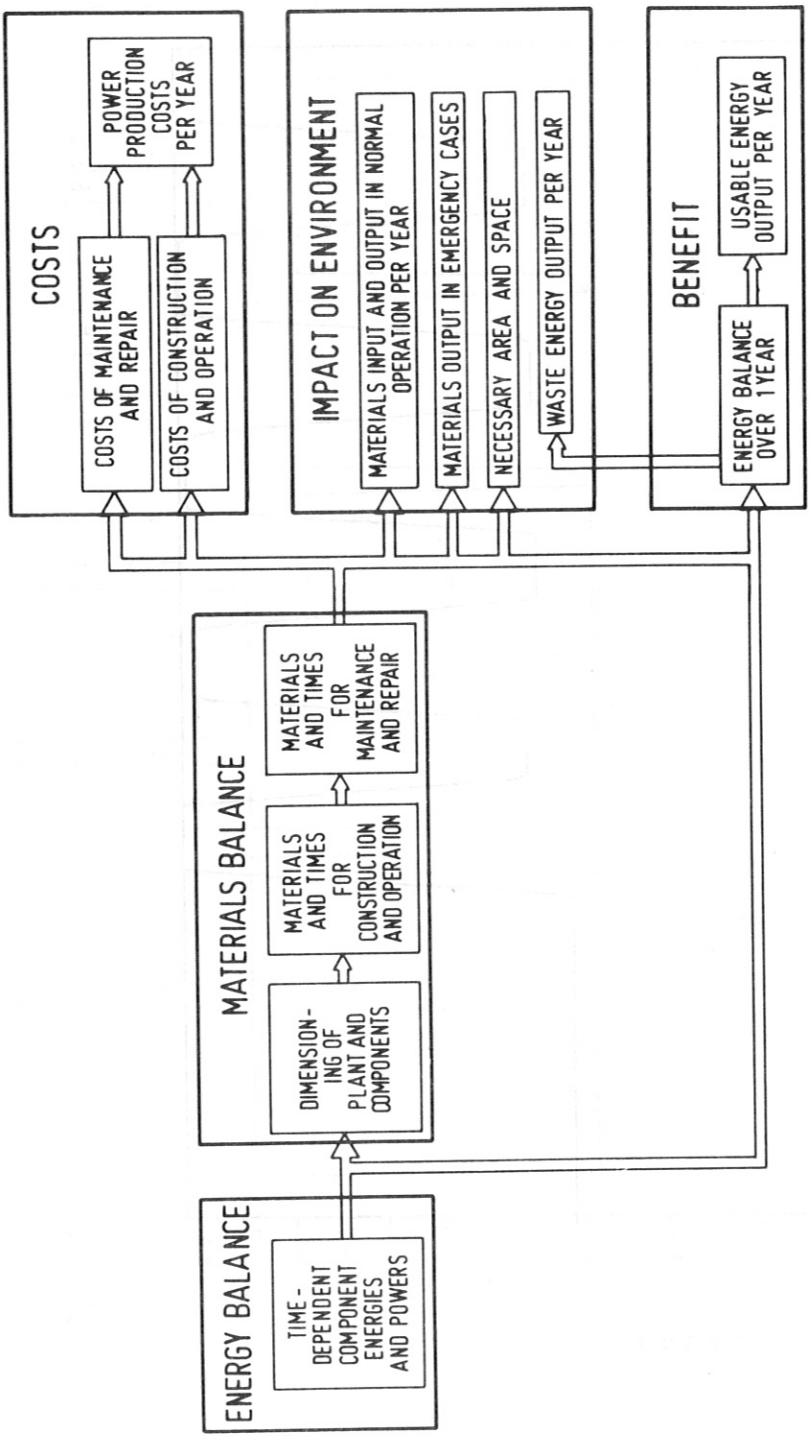

FIGURE 31 Structure of the SISYFUS code

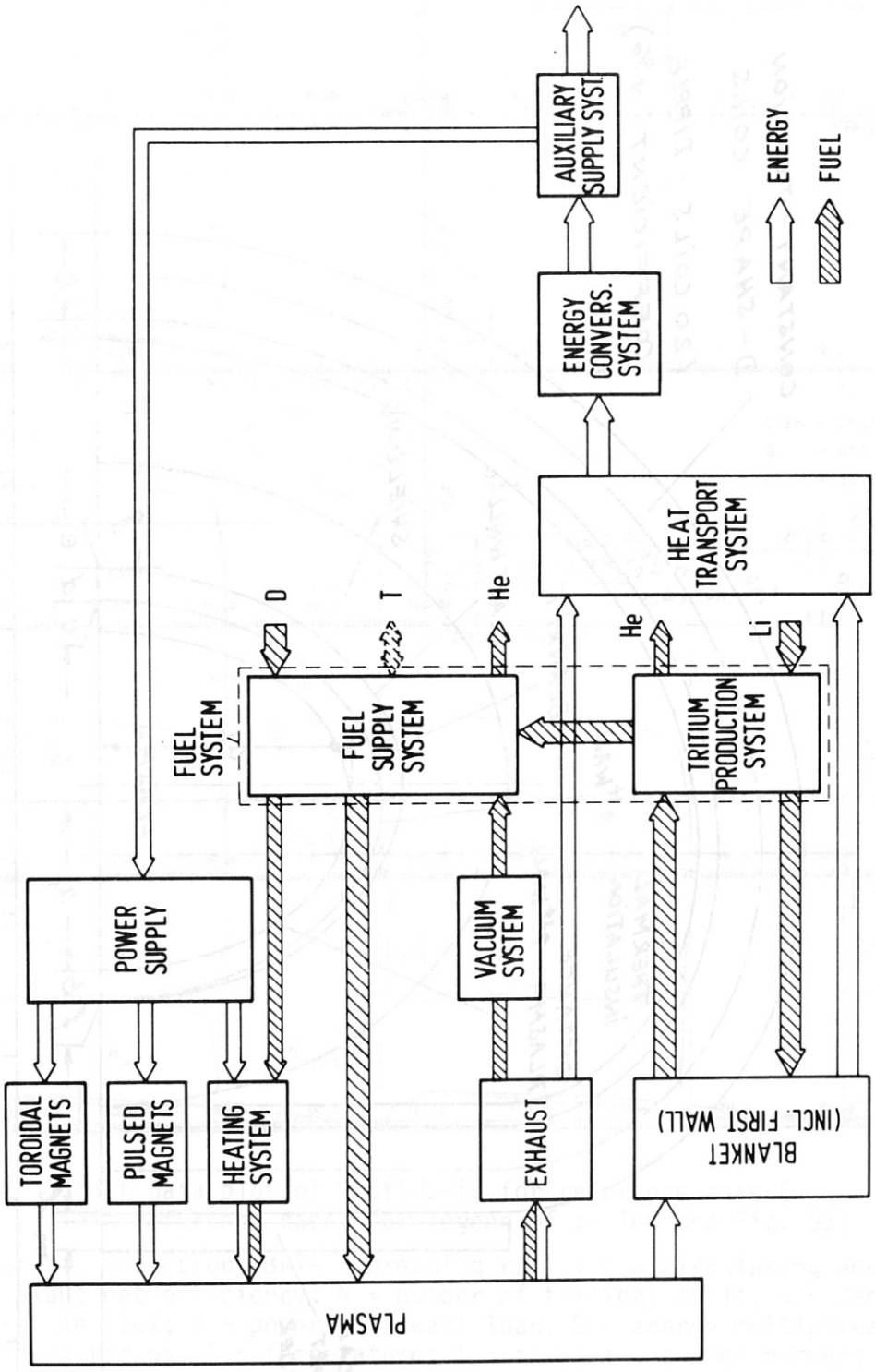

FIGURE 32 Structure of SISYFUS-TE (power plant with a Tokamak reactor; Energy balance)

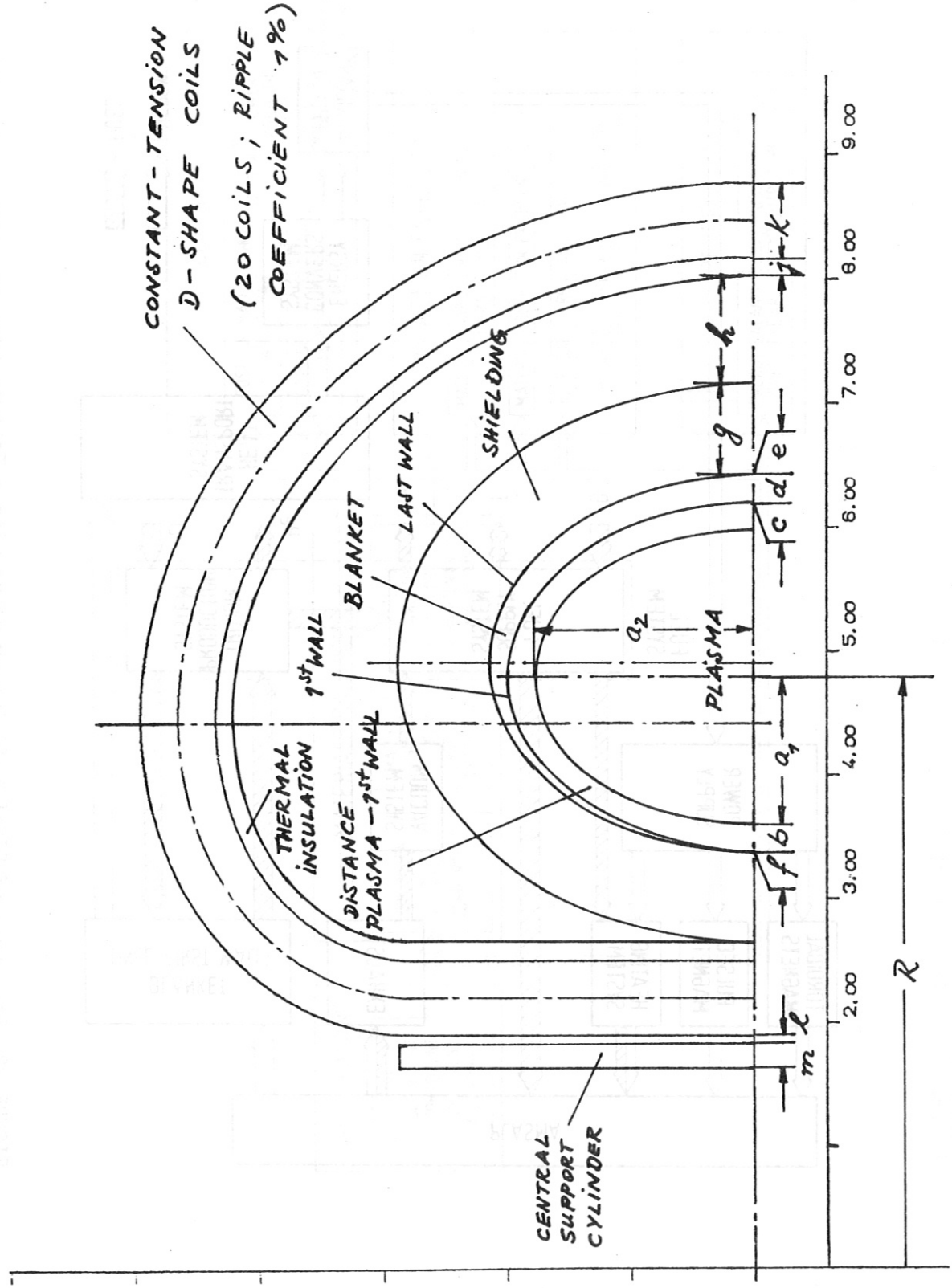

FIGURE 33 Geometry for INTOR arrangement (scale 1:50; for data see Table 1)

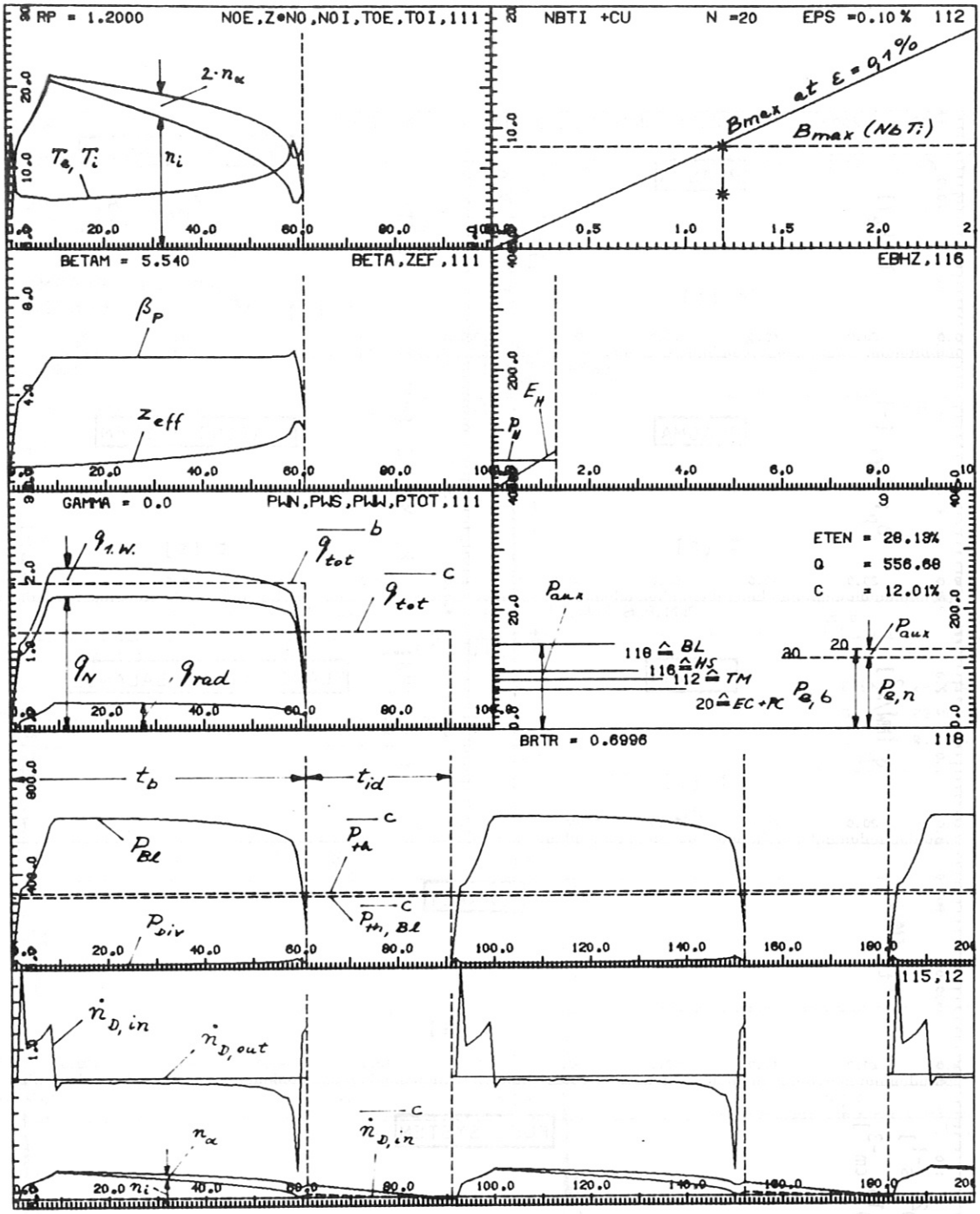

FIGURE 34 Output data plot of SISYFUS-TE for reference case C (main reference case; for legend of scales see Fig. 35)

B = magnetic induction; BRTR = breeding ratio; C = circulating energy; ETEN = plant net efficiency; N = number of toroidal coils; n = density; $\dot{n}$ = particle flux; P = power; q = wall load; Q = energy multiplication; RP = plasma radius; T = temperature; t = time; z = charge number; BETAM = β_p ; EPS = maximum strain in toroidal coil winding; GAMMA = impurity reflux coefficient; BL = blanket coolant pumps; EC = energy conversion; HS = heating system; PC = pulsed coils; TM = toroidal magnets.

Indices: α = α-particles; aux = auxiliary systems; b = burn phase; gross (for electric power output); Bl = blanket; c = cycle; D = deuterium; Div = divertor; e = electrons; H = heating; i = ions; id = idle; in = input; m = magnetic; max = maximum; N = neutrons; n = net; out = output; rad = radiation; th = thermal; tot = total.

1.W. = first wall

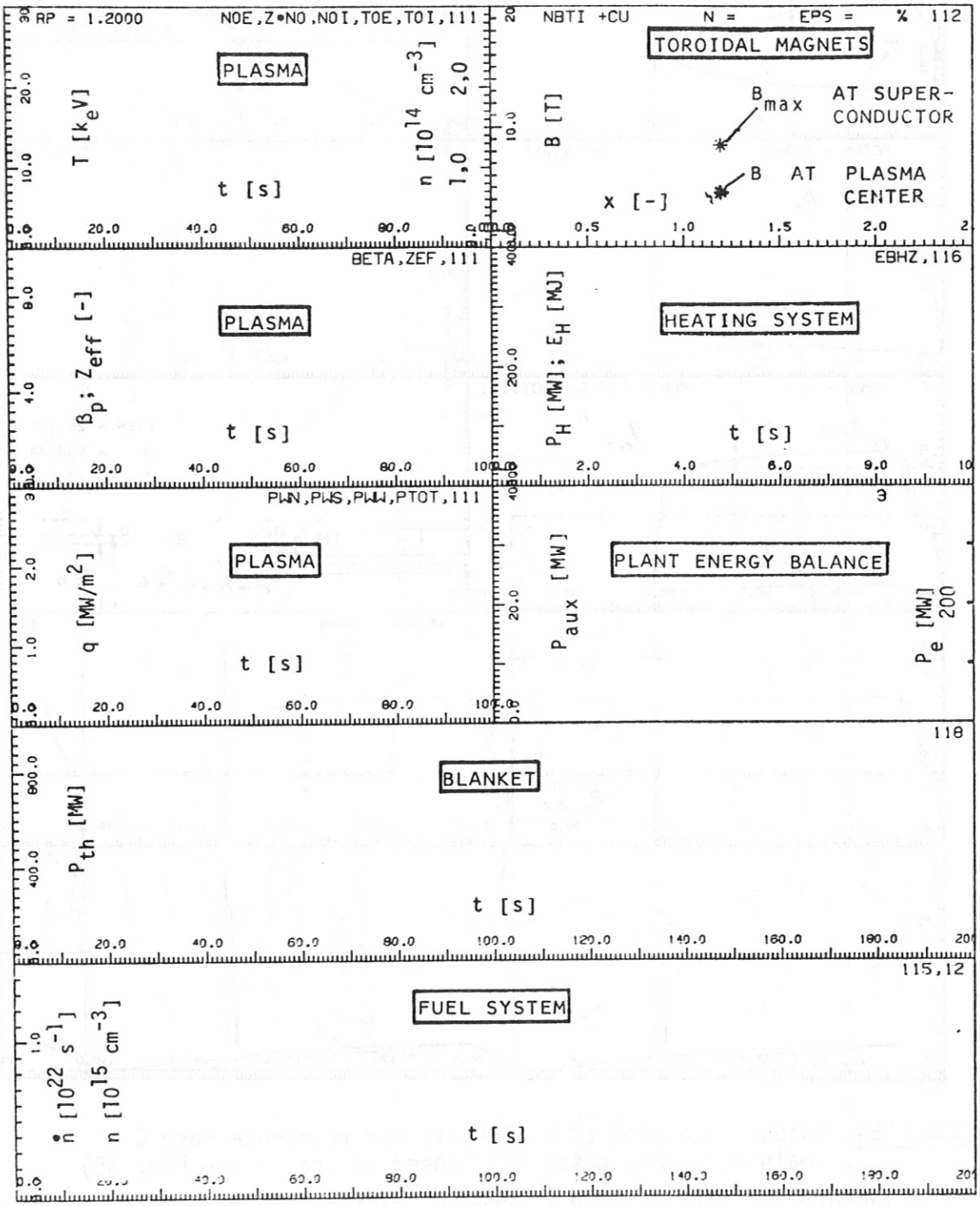

FIGURE 35 Legend of scales for output data plot of SISYFUS-TE

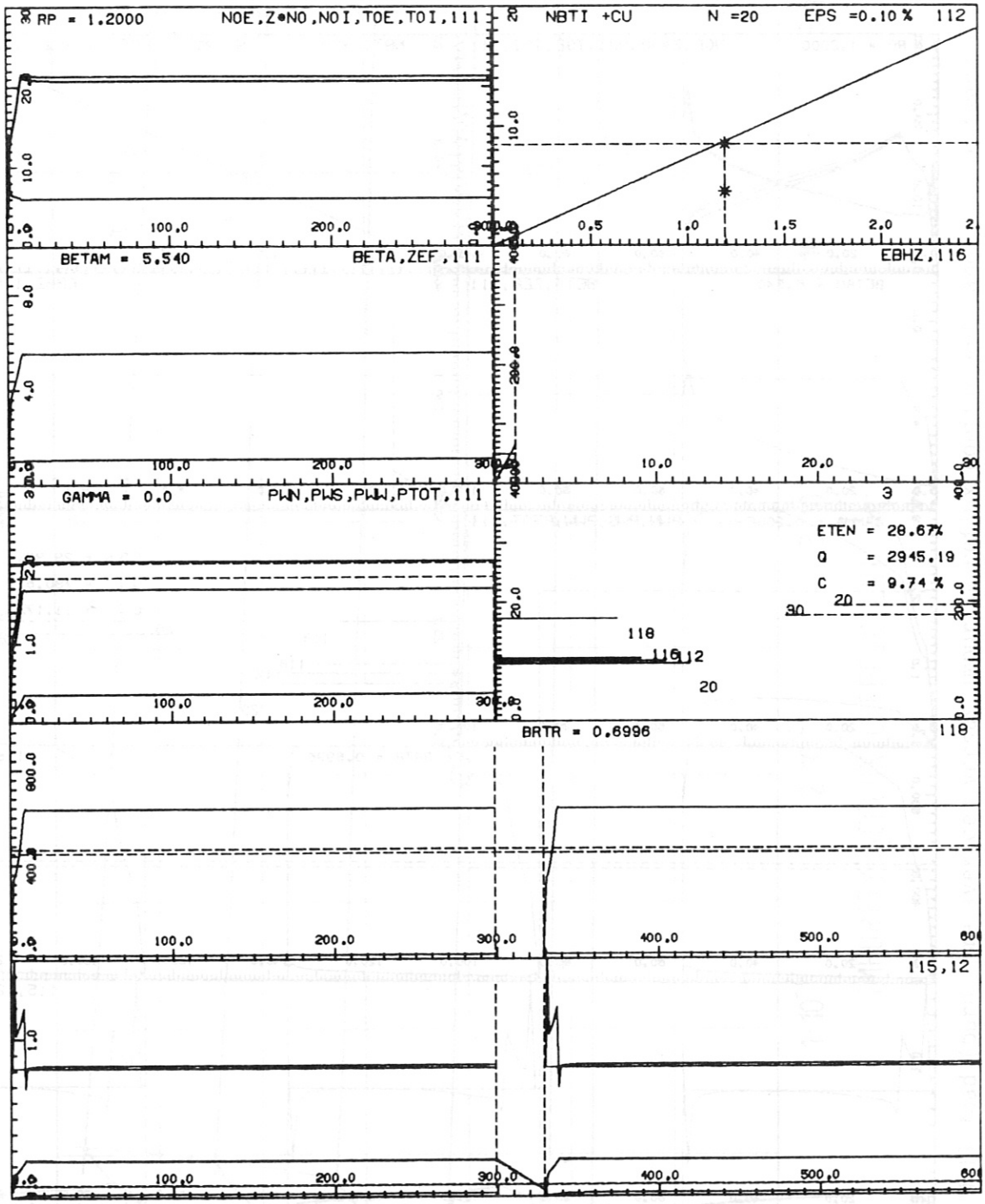

FIGURE 36 Output data plot of SISYFUS-TE for reference case A
(for legend see Figs. 34 and 35)

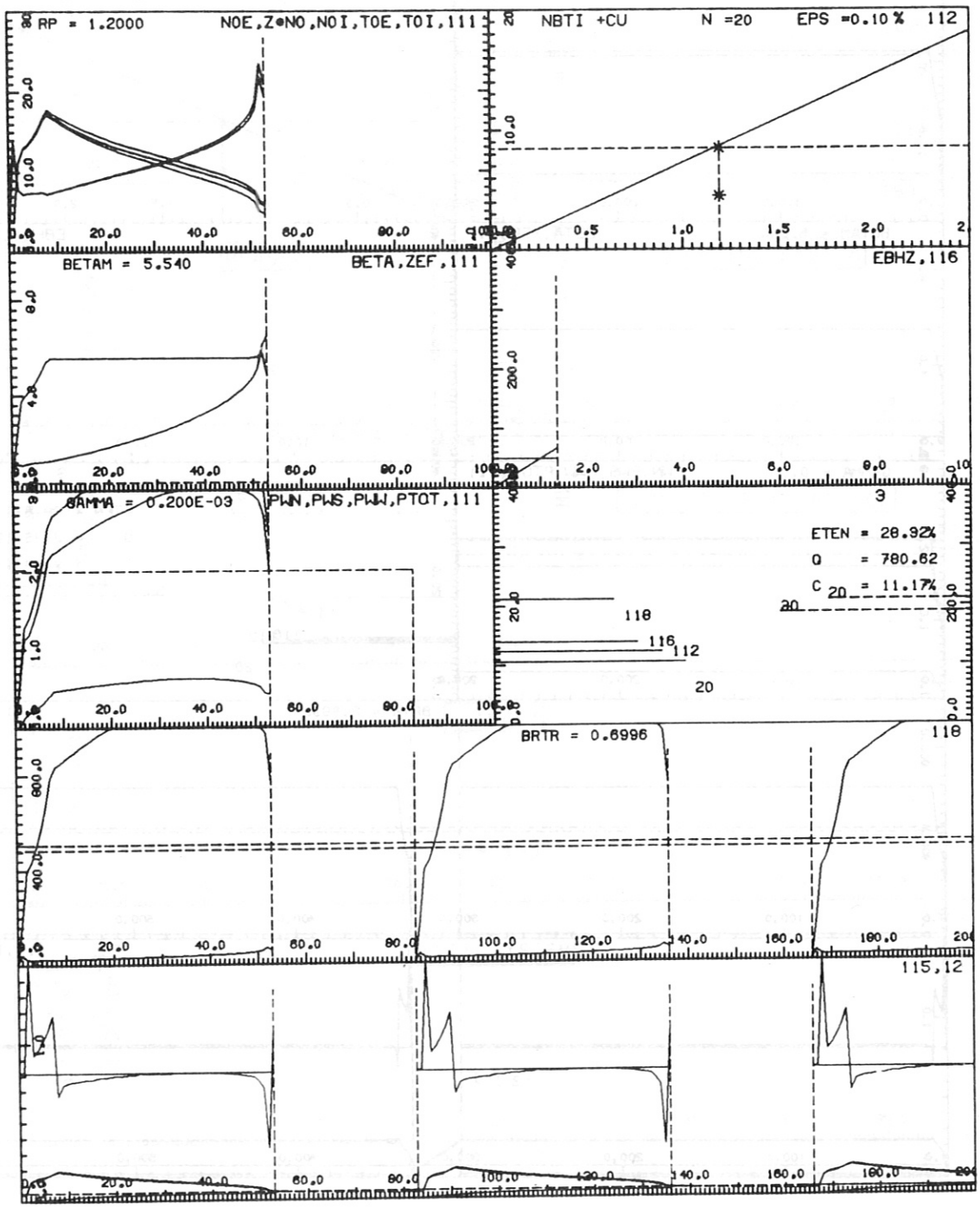

FIGURE 37 Output data plot of SISYFUS-TE for reference case B
(for legend see Figs. 34 and 35)

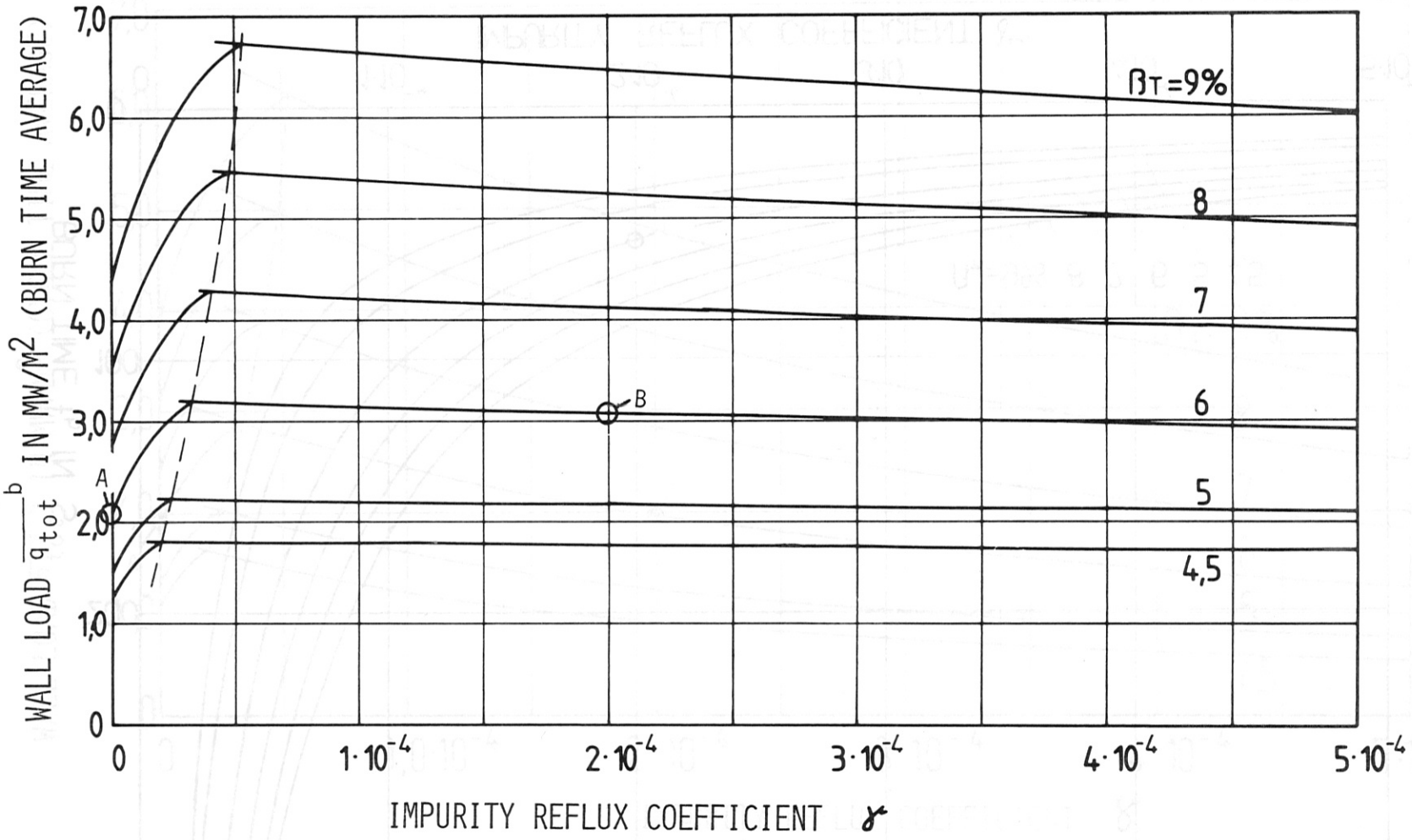

FIGURE 38 Wall load (burn time average) versus impurity reflux coefficient (anomalous outward diffusion of α -particles; t_{id} = 30 s)

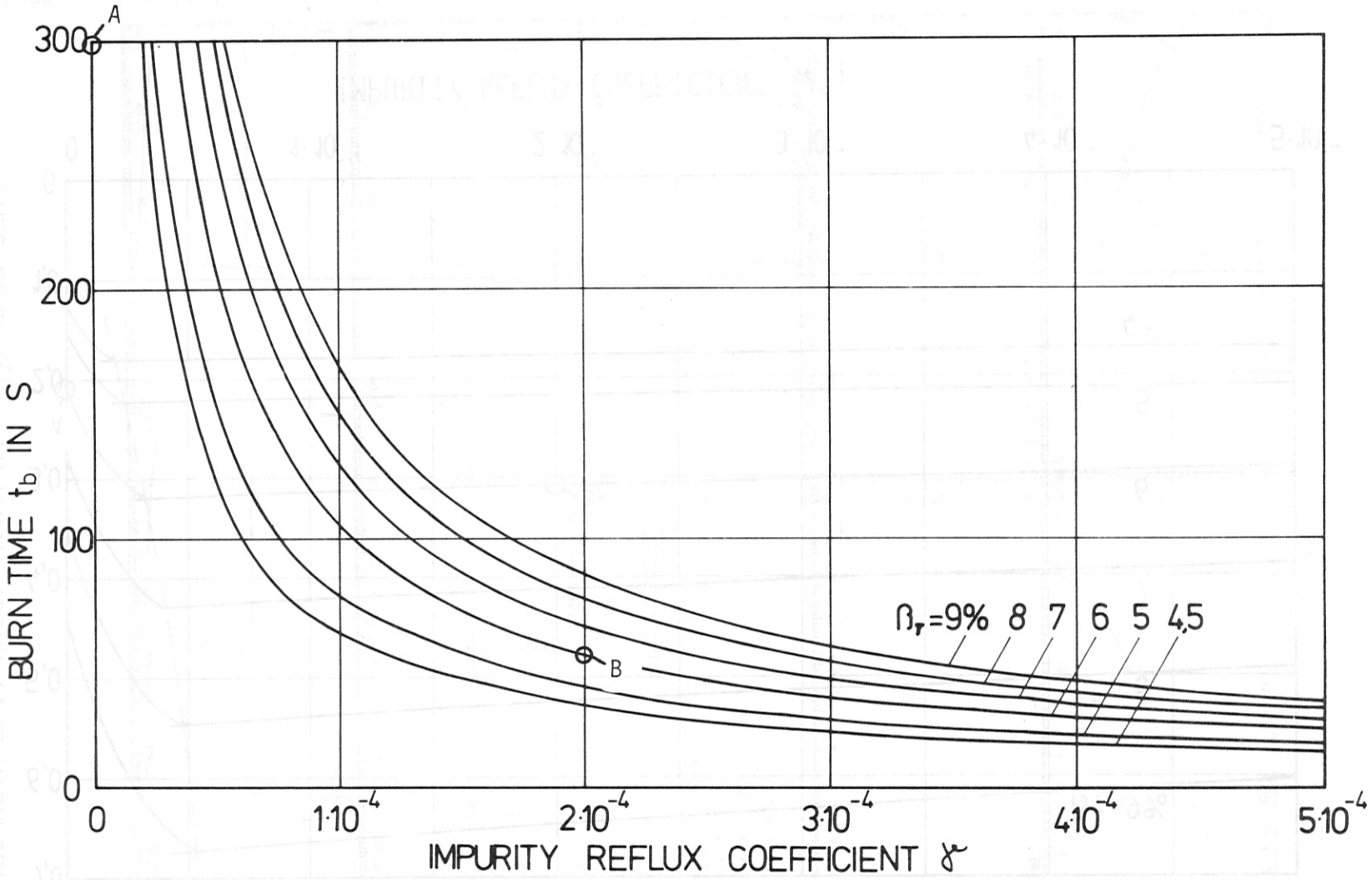

FIGURE 39 Burn time versus impurity reflux coefficient (anomalous outward diffusion of α-particles; t_{id} = 30 s)

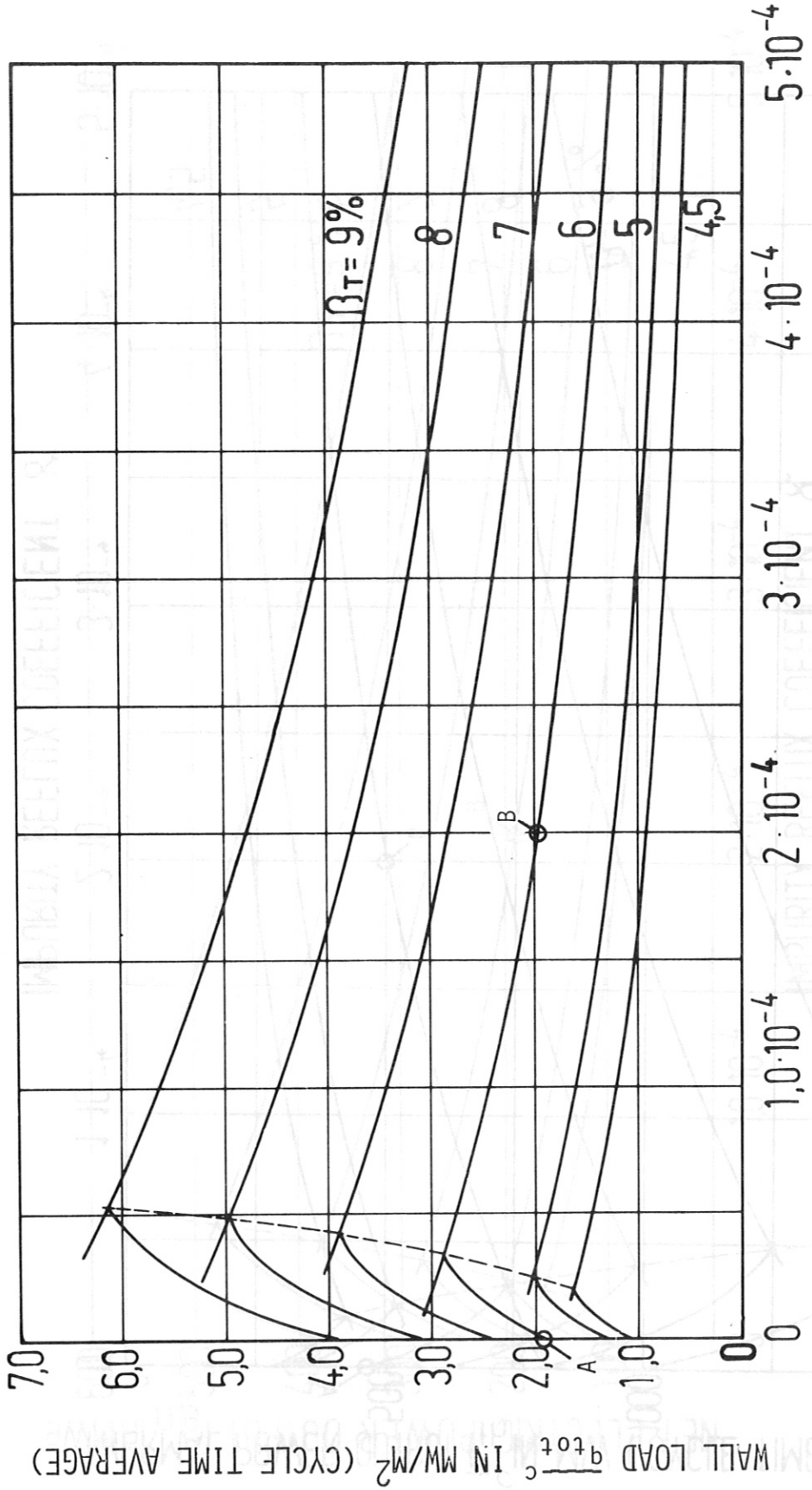

FIGURE 40 Wall load (cycle time average) versus impurity reflux coefficient (anomalous outward diffusion of α-particles; t_{id} = 30 s)

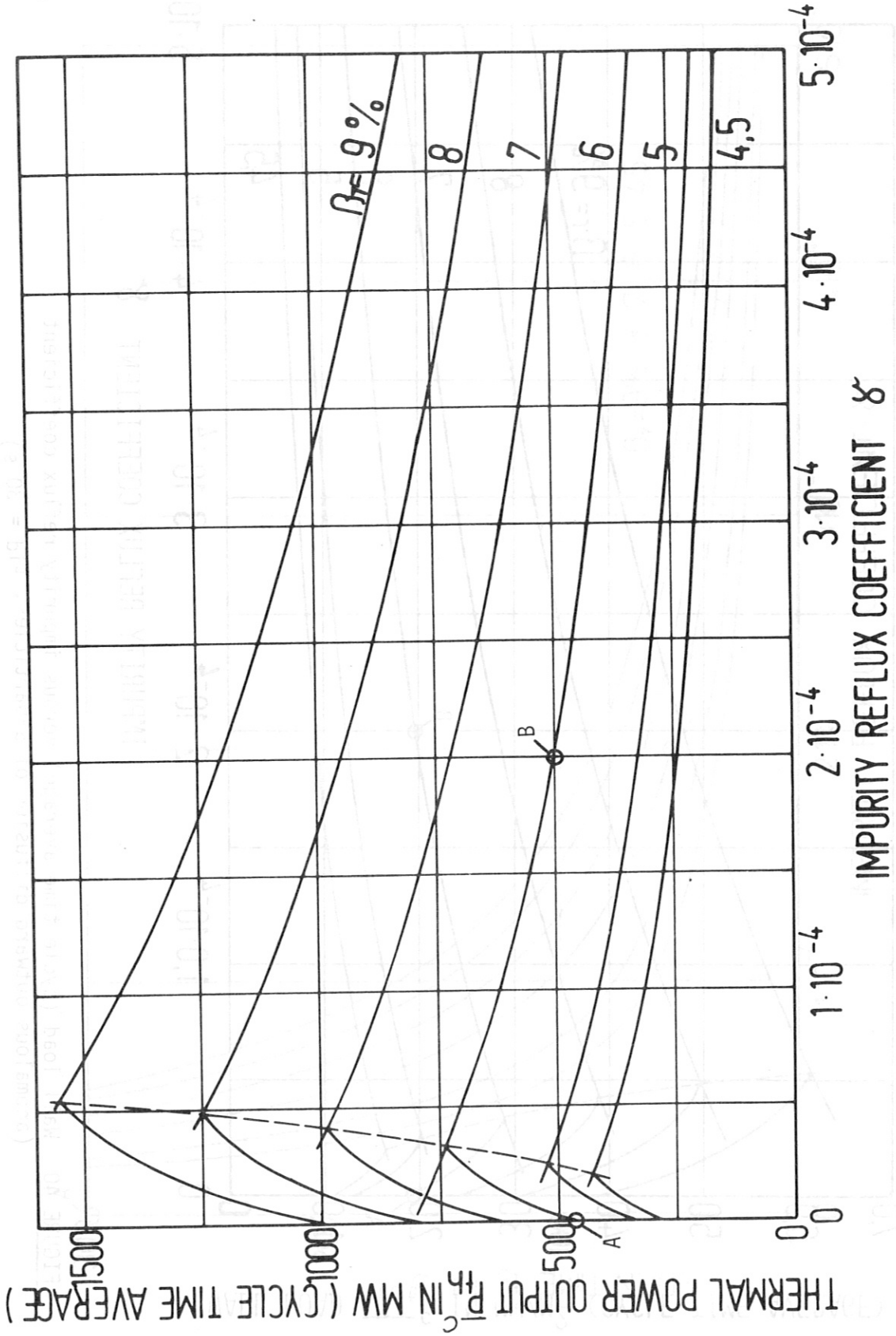

FIGURE 41 Thermal power output versus impurity reflux coefficient (anomalous outward diffusion of α-particles; t_{id} = 30 s)

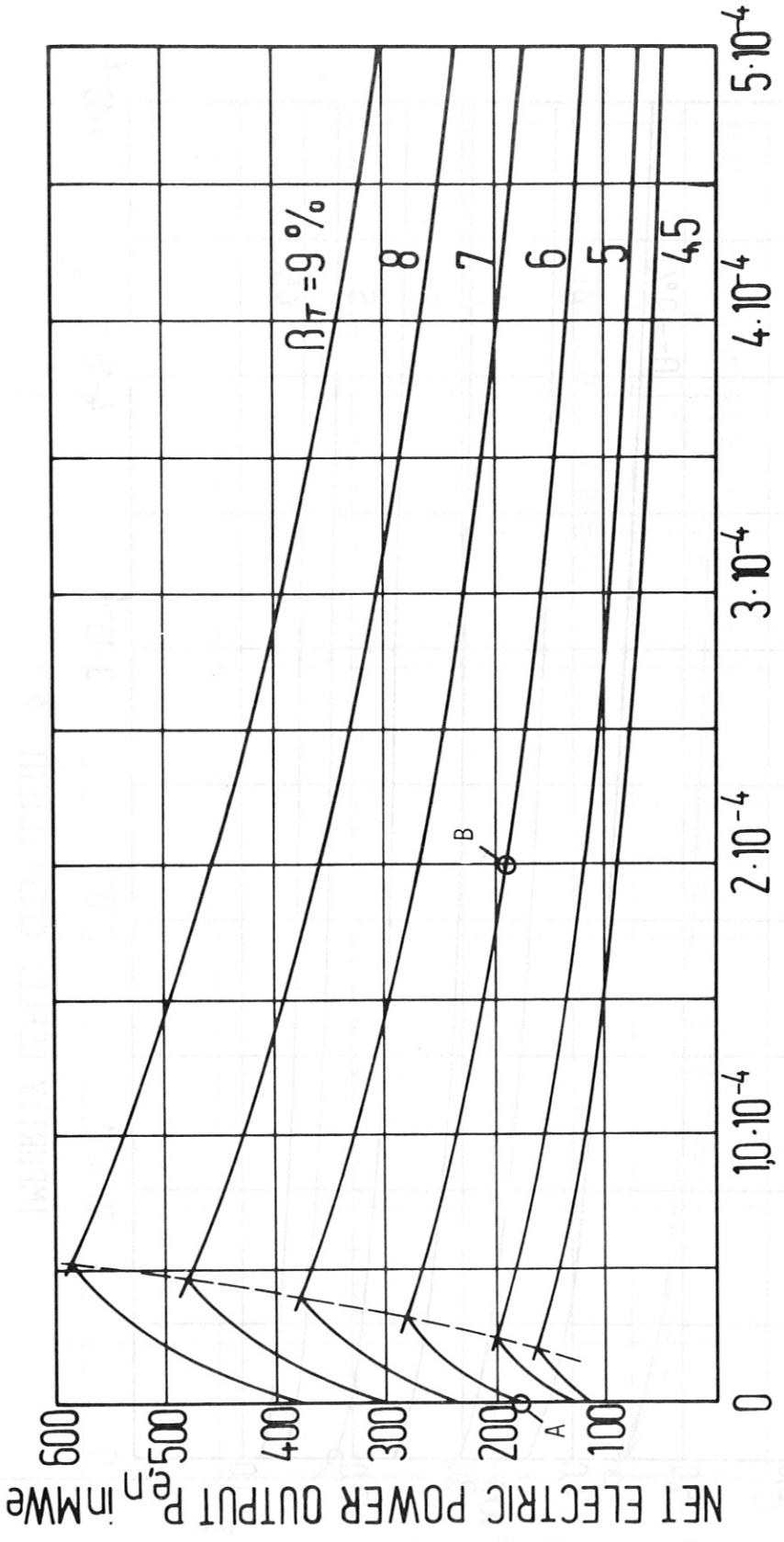

FIGURE 42 Net electric power output versus impurity reflux coefficient (anomalous outward diffusion of α-particles; t_{id} = 30 s)

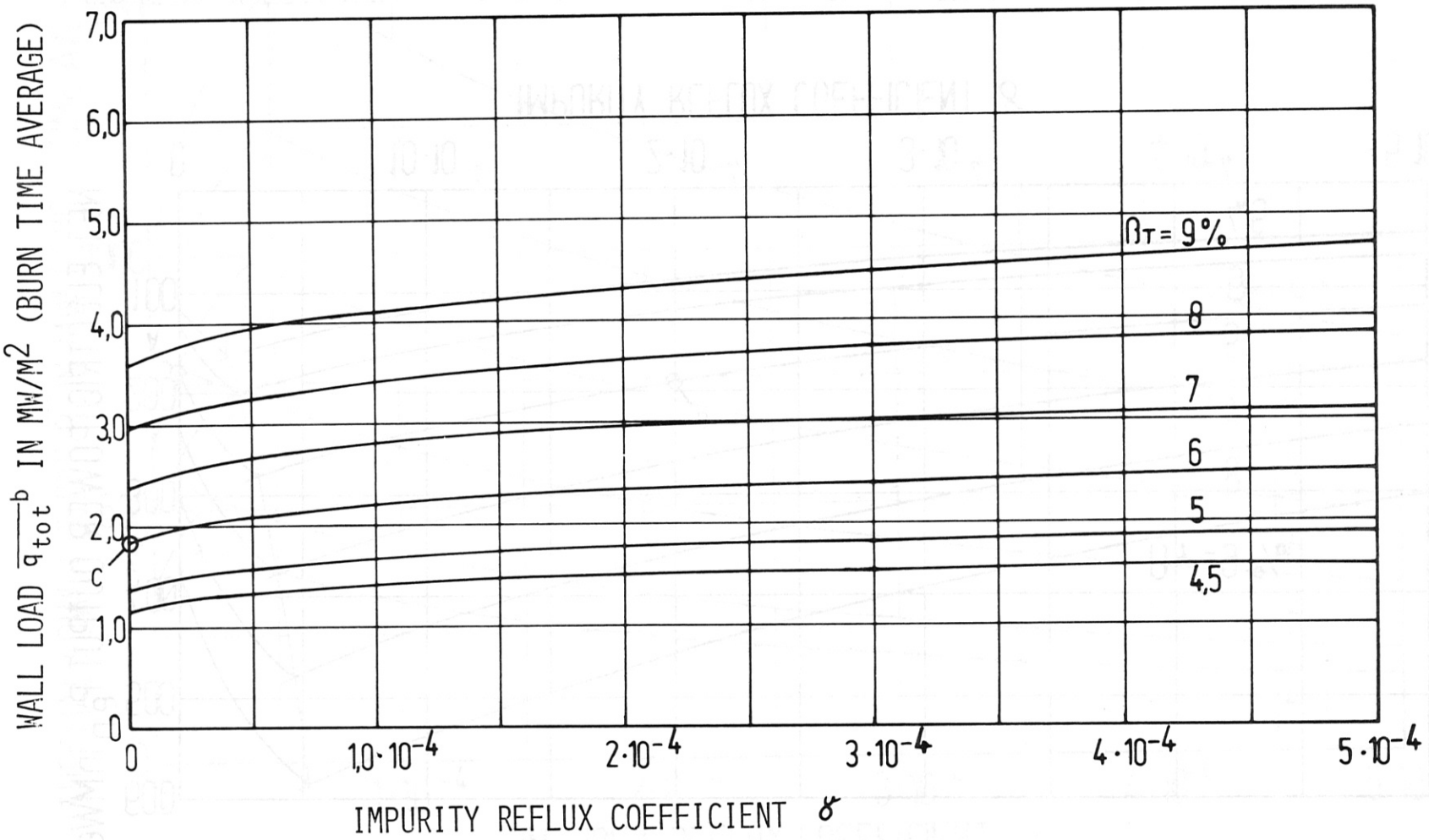

FIGURE 43 Wall load (burn time average) versus impurity reflux coefficient (α-particle accumulation; t_{id} = 30 s)

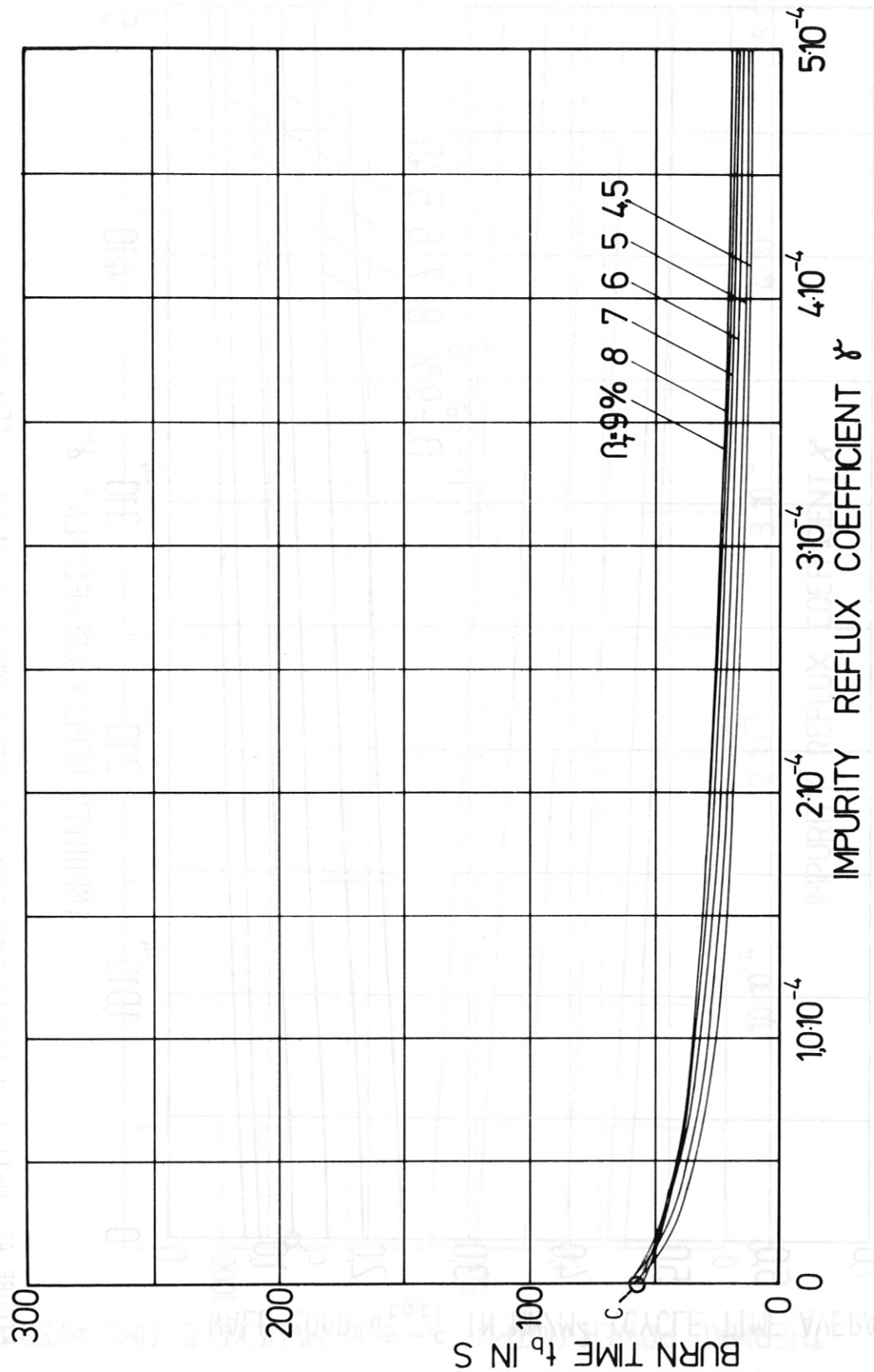

FIGURE 44 Burn time versus impurity reflux coefficient (α-particle accumulation; t_{id} = 30 s)

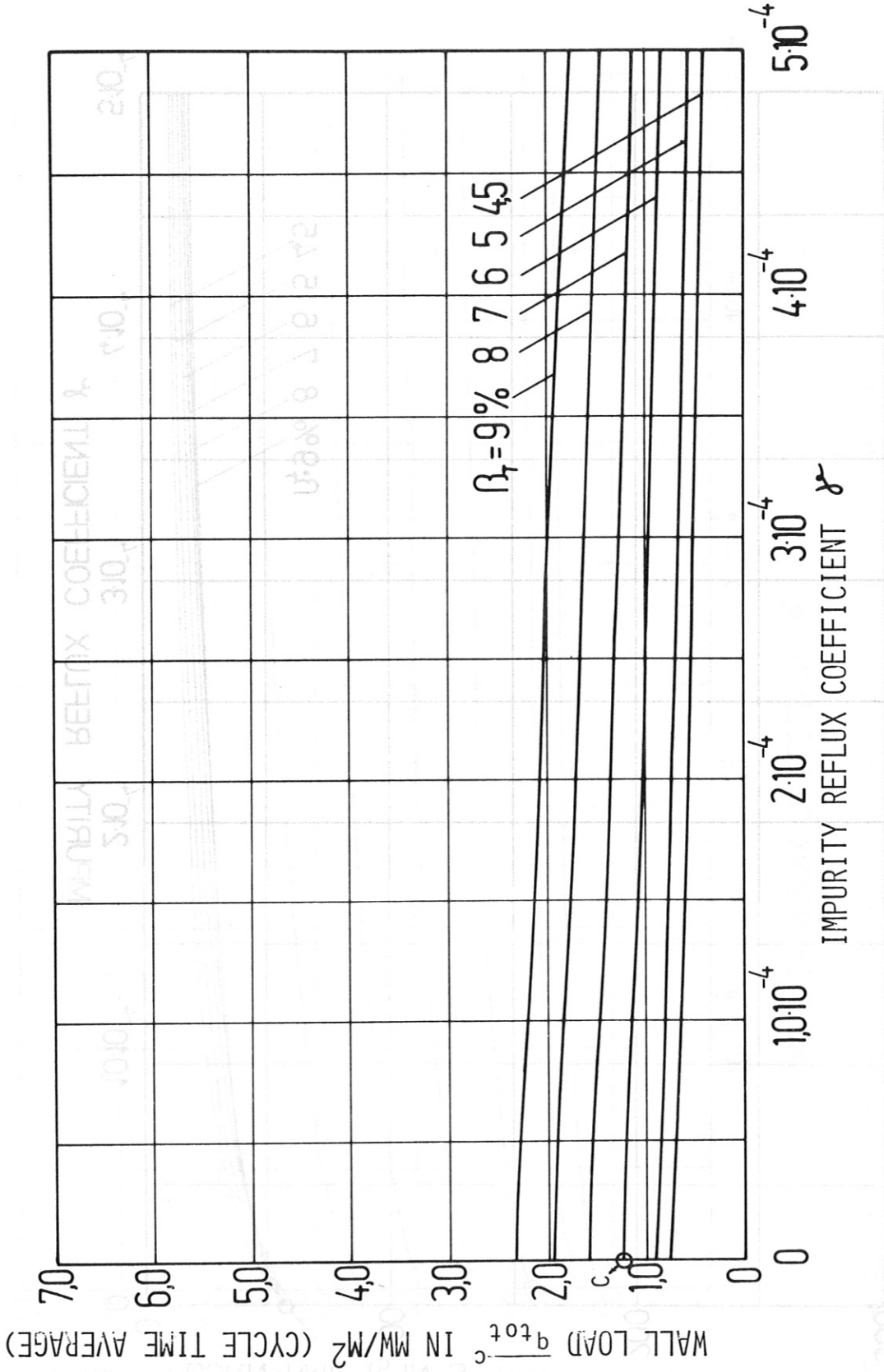

FIGURE 45 Wall load (cycle time average) versus impurity reflux coefficient (α-particle accumulation; t_{id} = 30 s)

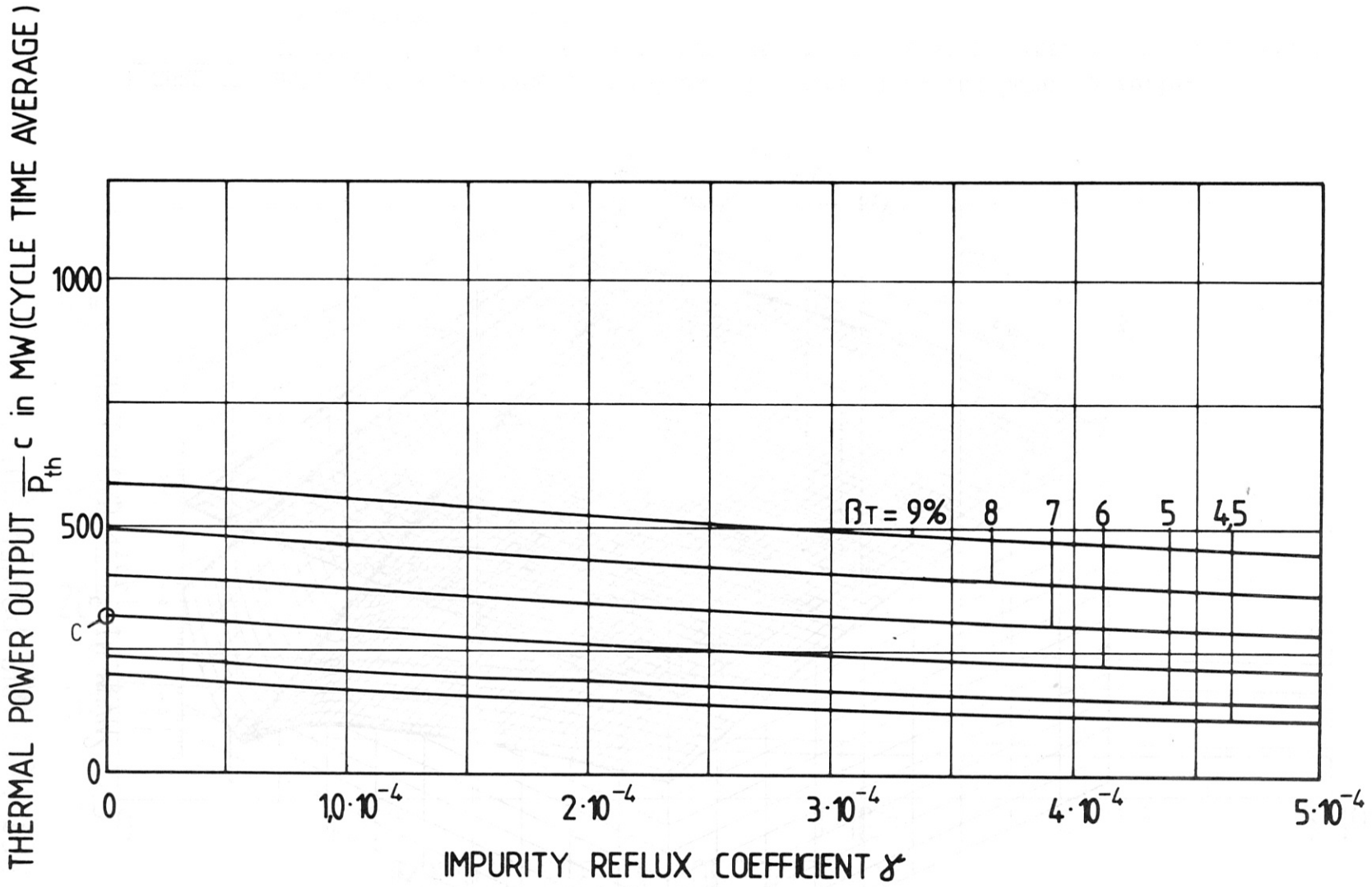

FIGURE 46 Thermal power output versus impurity reflux coefficient (α-particle accumulation; t_{id} = 30 s)

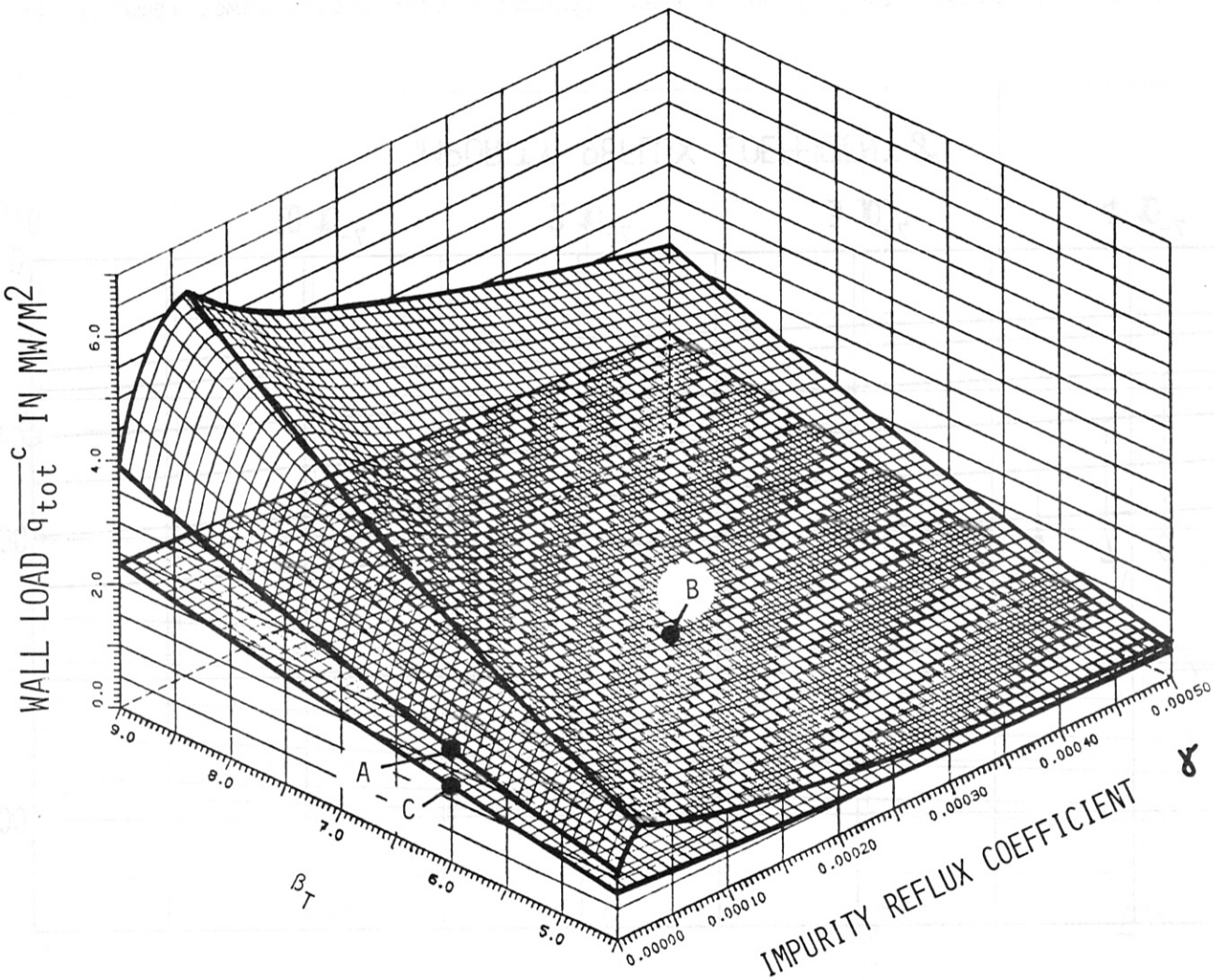

FIGURE 47 Wall load (cycle time average) as a function of β_T and impurity reflux coefficient (upper area: anomalous outward diffusion of α-particles; lower area: accumulation of α-particles)

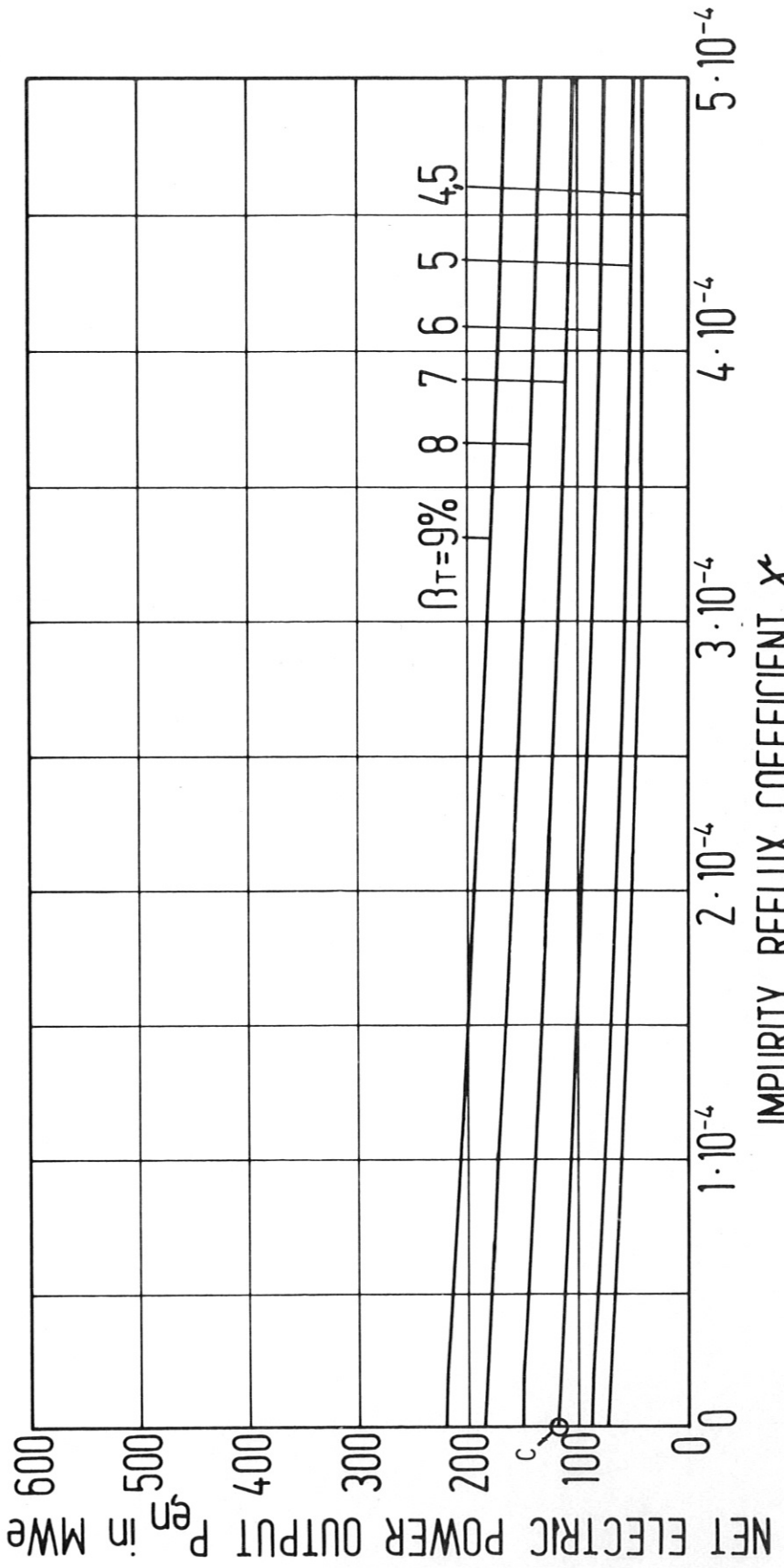

FIGURE 48 Net electric power output versus impurity reflux coefficient (α-particle accumulation; t_{id} = 30 s)